MEMBRANE FORMATION

diffusion induced demixing processes in ternary polymeric systems

8

BART REUVERS

MEMBRANE FORMATION
diffusion induced demixing processes in ternary polymeric systems

PROEFSCHRIFT

ter verkrijging van de graad van doctor
in de technische wetenschappen
aan de Universiteit Twente,
op gezag van de rector magnificus,
prof. dr. ir. H. H. van den Kroonenberg,
volgens besluit van het College van Dekanen
in het openbaar te verdedigen op
donderdag 8 januari 1987 te 16.00 uur

door

ALBERTUS JOHANNES REUVERS
geboren op 29 juni 1956
te Amersfoort

Dit proefschrift is goedgekeurd door de promotor prof.dr. C.A. Smolders
referenten: dr. F.W. Altena en dr. J.W.A. van den Berg

VOORWOORD

Bij het in dit proefschrift beschreven onderzoek ben ik geholpen en gestimuleerd door vele mensen waarvan ik er hier een paar met name wil noemen.

Marcel Mulder heeft mij als kamergenoot op een enthousiaste wijze geholpen bij het inwerken op het voor mij volkomen onbekende gebied van de membraantechnologie. In de loop van mijn onderzoek heeft in het bijzonder Frank Altena op een stimulerende wijze als onontbeerlijk klankbord gediend. Aan het experimentele werk hebben vooral Peter van Berkel, Clemens Padberg, Edeltraud Bertlein en Erik Bulten bijgedragen. Hans van den Berg, Johan Ronner en Thonie van den Boomgaard hebben geholpen de leesbaarheid en begrijpelijkheid van het proefschrift te vergroten. En last, but not least, wil ik Bartie Bruggink en Julia Ardesch noemen die de grote hoeveelheid typewerk voor hun rekening hebben genomen.

Ik wil iedereen, ook de hier niet genoemde mensen, bedanken voor hun bijdrages aan mijn onderzoek en de uitstekende werksfeer binnen de werkgroep membraanfiltratie.

CONTENTS

Chapter 2 has been published in J. Pol. Sci. Pol. Phys., 24 (1986) 793.
Chapter 3 and 4 have been submitted for publ. to J. Membr. Sci.
Chapter 6 and the Appendix of this thesis will be submitted for publ. to J. Membr. Sci.
Chapter 5 will be submitted for publ. to J. Appl. Pol. Sci.

1. INTRODUCTION

1.1. Artificial membranes

Membranes are well known as the walls of living cells. These walls act as selective barriers to molecules which are being transported through a living tissue.

Artificial permselective membranes are used, if one wishes to separate specific components from a gaseous or a liquid mixture. An ideal permselective membrane should act as an unpenetrable barrier to one or more of the components, whereas the other components should permeate the membrane without being opposed by the membrane. In reality, this ideal situation will never be reached and the permselective membrane should be considered as a barrier penetrable to all components of the mixture but at different rates. This difference is due to the specific physico-chemical properties of the membrane material in relation to the permeants. Thus a membrane can raise or lower the concentration of specific components in the mixture. The desired product(s) can be found in practise either at the feed or permeate side of the membrane.

The choice of the membrane material determines which components permeate preferentially through the membrane (the selectivity of the membrane). The effective thickness of the membrane determines the amount of permeate that results from a certain energy input into the separation process (the permeability of the membrane).

The necessary driving force for membrane separation can be obtained by pressurizing the liquid or gaseous phase at the feed side of the membrane (hyperfiltration or gas separation) or by applying a low (partial) pressure at the other side of the membrane (pervaporation).

Ultrafiltration membranes are used for the filtration of high molecular weight solutions, e.g. protein solutions. The performance of an ultrafiltration membrane is not only determined by the physico-chemical properties of the membrane material in relation to the permeants, but also by the size of the pores in the membrane.

The performance of microfiltration membranes is completely determined by their porosity. These membranes are used to filtrate suspensions or biological solutions, with particle diameters larger than 50 nm.

Apart from membrane filtration other techniques are available to separate mixtures (distillation, crystallization, adsorption, extraction, centrifugation, complexation, etc.). Every separation technique has its specific advantages, depending on the chemical and physical nature of the substances to be separated. Some general advantages of membrane filtration are the low energy consumption of the process and the possibility to perform the separation process continuously and at a moderate temperature.

Because the membrane filtration technique is in a stage of rapid development the number of realized applications is continuously increasing. Some examples of industrial applications of membranes are:

- production of process water for greenhouses from brackish ground water, or potable water;
- concentration and separation of product streams in the food industry: raw milk, skimmed milk and whey;
- waste water treatment;
- concentration and fractionation of starches and proteins;
- treatment of oil/water emulsions.
- dehydration of alcohol/water mixtures;
- separation of the gaseous mixture H_2/NH_3.

An extended survey of membrane applications is given in Desalination [1].

1.2. Preparation of synthetic membranes

Artifical membranes can be prepared from a number of different materials. The survey given below is limited to synthetic membranes and excludes inorganic membranes, dynamic membranes and liquid membranes. Synthetic membranes are made from man-made polymers.

Some preparation techniques of synthetic membranes are [2]:

- Sintering;
  a polymer powder is pressed and sintered to form a microporous membrane.
- Stretching;
  a partly crystalline film or foil is stretched, which results in the occurrence of small ruptures. The pore size in these membranes can be controlled in between 0.1 and 3 μm.

- Track etching;
  a polymer film or foil is subjected to a high energy particle radiation (metal ions) perpendicular to the film. The particles create tracks with increased reactivity. The film is then immersed in an acid bath. The etching process in the bath yields cylindrical pores with a very narrow pore radius distribution. The average pore radius can vary in between 0.02 and 10 μm.
- Extrusion of a polymer melt;
  homogeneous gas separation membranes can be obtained by extrusion of a film from a polymer melt.
- Coating;
  a thin homogeneous polymeric layer is created on top of a porous support layer by dip coating, interfacial polymerization or plasma polymerization.
- Phase inversion;
  the concept of phase inversion, introduced by Kesting [3] can be defined in the following way: by bringing a homogeneous polymer solution in a supersaturized state, demixing processes are induced rearranging the spatial distribution of polymer in the solution; the resulting spatial redistribution of polymer is then fixed by gelation or by passing across the glass point.

  The solidified polymer matrix can be suitable for all kinds of filtration processes from microfiltration to gas separation or hyperfiltration, depending on the variation of the preparation procedure.

The vast majority of the commercially available membranes is made by the phase inversion process. Phase inversion can be obtained in the following way.

- Contacting a solution film, consisting of a polymer and a solvent, with a nonsolvent vapour phase which is saturated with the solvent (precipitation from the vapour phase). The polymer solution is subjected to a nonsolvent inflow, while the solvent saturated vapour phase prevents the outflow of solvent. This technique [3,4] yields an isotrope microporous membrane.
- Contacting a solution film consisting of polymer, nonsolvent and a volatile solvent with air (precipitation by controlled evaporation). If the boiling point of the solvent lies at least 30°C below the boiling point of the nonsolvent this technique can yield hyperfiltration membranes, consisting of a very thin dense layer (skinlayer) at the upper surface of the solution film contacting the air and a relatively thick porous sublayer [5].

- Lowering the temperature of a solution consisting of polymer, solvent and nonsolvent (thermal precipitation). This technique can yield isotropic microporous membranes as well as skinned membranes [6].
- Contacting a polymer solution film with a nonsolvent bath (immersion precipitation). The polymer solution is subjected to an exchange of solvent and nonsolvent. In general, this technique yields asymmetric membranes consisting of a thin permselective skinlayer formed at the interface between the bath and the film, and a thick porous sublayer.

In this thesis the immersion precipitation process is studied. This method is widely used to prepare membranes, whereas the processes occuring during immersion precipitation, resulting in membrane morphology, are hardly understood. The objective of this study is to gain insight into mass transport and demixing phenomena occuring during the immersion precipitation process. With the aid of this knowledge, existing empirical relations between the process circumstances and the ultimate membrane morphology may be explained or improved.

1.3. Immersion precipitation

The application of the immersion precipitation technique for the preparation of asymmetric membranes has been successfully introduced by Loeb and Sourirajan [7] in 1962. The dense toplayer of their cellulose acetate membrane had permselective properties suitable to separate salt from brackish sea water, while the toplayer was thin enough (0.2-0.5 μm) for a high water flux. The relatively thick sublayer (0.1 mm) possessed an interconnective porous structure with a sufficient mechanical strength to withstand high pressures.

Loeb and Sourirajan prepared their membrane in 4 steps:

1. a homogeneous solution was prepared consisting of 22.3 weight% cellulose acetate, 66.6 weight% acetone, 10 weight% water and 1.1 weight% magnesium perchlorate;
2. the solution was cast on a glass plate as a 0.2-0.5 mm thick film and the solvent was allowed to evaporate during 3-4 minutes;
3. the solution film was immersed into a water bath at 0°C, which resulted in demixing and solidification of the film;

4. after being washed in streaming water during 24 h, the solidified film was immersed into a 75-80°C water bath for 1-2 minutes.

Since 1962, asymmetric membranes have been prepared from various types of polymers [8-11]. It turned out that the preparation procedure, applied by Loeb and Sourirajan, also resulted in the formation of asymmetric hyperfiltration or ultrafiltration membranes when the following modifications were made:

- the addition of salt or a nonsolvent to the casting solution can often be omitted;
- the evaporation step, which results in an asymmetric polymer distribution in the film before being immersed into the nonsolvent bath, is not always a necessary step to induce the formation of an asymmetric structure; one can prepare asymmetric membranes also from casting solutions which contain a solvent with a high boiling point; or asymmetric hollow fibers can be obtained with a dense toplayer at the interior, which has not been contacted with air [12];
- the coagulation bath temperature can be varied;
- the thermal treatment in a water bath, which results in a densification of the toplayer of the CA-membrane [2], can be omitted when other polymers than CA are used.

In our opinion the basic principles of membrane formation by the immersion precipitation technique can be studied in great detail by considering the following characteristics:

- three components are used: a polymer, a solvent and a nonsolvent; the latter two must be miscible in all proportions;
- a homogeneous solution is prepared from the polymer and the solvent (and eventually also the nonsolvent);
- this homogeneous solution is cast or spun as a thin flat or cylindrical film and immersed into a coagulation bath consisting of the nonsolvent (and eventually also the solvent), immediately after being cast or spun.

In this thesis the influence of the following variables on the membrane formation process and the ultimate membrane characteristics will be studied:

- the type of components used (solvent, nonsolvent and polymer);
- the initial concentration of the two (or three) components in the casting

solution;
- the initial concentration of the solvent in the coagulation bath.

Important membrane characteristics controlled by the immersion precipitation process are:
- the porosity of the toplayer. This characteristic property determines whether the membrane is suitable for ultrafiltration on the one hand or hyperfiltration, gas separation and pervaporation on the other hand. Immersion precipitation hardly ever yields membranes suitable for microfiltration. Only when an extra polymer component is added to the casting solution and solvent is added to the coagulation bath, microporous membranes can be obtained [13]. However, the effect of addition of an extra polymer component to the casting solution is beyond the scope of this thesis;
- the thickness of the toplayer. The toplayer thickness affects the permeability of the membrane;
- the porosity of the sublayer. The optimal sublayer of an asymmetric membrane can withstand high mechanical stresses and does not contribute to the membrane resistance. However, high mechanical stresses can not always be used because immersion precipitation often results in the presence of large conical voids (macrovoids) in the sublayer of the membrane [12,14-17]. These macrovoids, with a length of several microns to, in some cases, the total thickness of the membrane, can cause rupture of the skin under high operating pressures. The second condition for an optimal sublayer structure is obeyed only if the small pores in the sublayer are interconnected.

Important membrane characteristics controlled by the physico-chemical material properties of the polymer, and not by the immersion precipitation process, are:
- the chemical and temperature stability of the membrane;
- the permselectivity of hyperfiltration, gas separation and pervaporation membranes.

Chronologically, the immersion precipitation process can be split up into two parts:
- mass transfer resulting in an asymmetric polymer distribution and metastable compositions in the immersed polymer solution film;
- demixing processes responsible for the porosity of the ultimate film.

In the next two sections these parts are discussed.

1.4. Mass transfer preceding the onset of demixing

In literature it is found to be generally accepted that the asymmetric structure of membranes prepared by immersion precipitation is caused by an asymmetric polymer distribution in the immersed solution film at the very moment of onset of demixing in the film. However, there is disagreement about the origin of the asymmetric polymer distribution in the film. There are three different ways to explain the polymer distribution at the moment of onset of demixing:

a) The asymmetric polymer distribution is already present in the cast solution film, before being immersed into the coagulation bath, due to surface tension effects which cause the polymer concentration at the surface of the film to be raised. Representatives of this approach are Panar [18] and Tanny [6];

b) The asymmetric polymer distribution is a result of evaporation of the solvent from the upper layer of the cast film during the evaporation step. The duration and the conditions of the evaporation step determine to a large extent both the polymer distribution in the film at the moment of immersion of the film (Ray [19], Anderson [20] and Castellari [21]) and the properties of the ultimate membrane (Sourirajan [22], Kunst [23] and Kesting [3]). The influence of the evaporation step on membrane structure has been studied intensively for Loeb-Sourirajan type of membrane forming systems with acetone as the highly volatile solvent.

c) The asymmetric polymer distribution is a result of the ternary diffusion process in the immersed solution film. This diffusion process, that starts upon contacting the film and the bath, results in a solvent depletion from the toplayer of the film and a relative small penetration of the nonsolvent in the toplayer. The highly concentrated polymer layer at the surface of the film opposes the outdiffusing solvent molecules more strongly than the indiffusing nonsolvent molecules. Thus, the polymer concentration in the sublayer is lower than the polymer concentration in the toplayer at the moment of on-

set of demixing. Authors supporting this approach are Frommer [15], Strathmann [24], Koenhen [25], Altena [26] and Wijmans [27].

In our opinion, the polymer distribution at the liquid-gas interface of a freshly cast solution (like in opinion a) above) does not determine the polymer distribution at the moment of onset of demixing because, upon immersion of the cast solution, the polymer distribution at the liquid-liquid interface will immediately adapt to the new thermodynamic environment at this interface.

We agree with the opinion that the evaporation step (mentioned under b) can affect the asymmetric structure of the membrane under certain circumstances. However, in this thesis we prefer to investigate the influence of the ternary diffusion process in the immersed film on the polymer distribution at the moment of onset of demixing for the following reasons:

- in contrast with the evaporation step, this diffusion process is an inevitable part of the immersion precipitation process;
- until now this process has mainly been the subject of speculation or treated qualitatively, resulting in indications that this diffusion process affects the ultimate membrane structure very strongly.

In literature a few studies are reported on the rate of exchange of solvent and nonsolvent in polymer solutions contacted with a coagulation bath. Measurements have been performed on flat films (Frommer [14] and Altena [28]) but also on spinning lines (Gröbe [29] and Paul [30]). (The measurements on spinning lines were performed in order to elucidate the mechanism of synthetic fiber formation by means of 'the wet spinning process', which is also an application of immersion precipitation [31]). Unfortunately, these experiments give no information about the diffusion process that occurs during the very short period before the onset of demixing in the polymer solution.

In this thesis another approach is chosen to study the diffusion behavior in the polymer solution from the very moment of contacting the film and the bath: we will calculate this ternary diffusion behavior. Not only the diffusion behavior in the immersed polymer solution, but also the compositions which are metastable for liquid-liquid demixing (i.e. the binodal curve) are calculated. Combination of these two analyses can yield the composition profile (and, thus, the polymer distribution) in the immersed film at the very moment of onset of liquid-liquid demixing. Some preliminary work in this di-

rection has been done by Cohen [32].

Cohen recognized that the diffusion induced occurrence of liquid-liquid demixing in a polymer solution contacted with a nonsolvent bath is a process that is largely similar to the diffusion induced emulsification, which is sometimes observed upon contacting two non-equilibrated liquid phases consisting of three (or more) low molecular weight components. (The low molecular weight components are not miscible in all proportions (Ruschak [33])). Although the presence of macromolecules in a non-equilibrated system may have some special influence on the rate of diffusion and demixing, the qualitative description of the diffusion processes in two non-equilibrated liquid phases, given by Ruschak, can act as the base for a theory that predicts the composition changes in an immersed polymer solution.

Cohen also contributed to the formation of such a theory by introducing chemical potential gradients instead of concentration gradients as the driving forces for diffusion. In this way the diffusion behavior in the polymer solution is related to the concentration dependence of the chemical potentials of the components. Because the concentration dependence of the chemical potentials is also needed to analyse the stability criteria for liquid-liquid demixing [34], the approach followed by Cohen offers the possibility to analyse both the diffusion and demixing aspects of the problem as a function of the same thermodynamic quantities.

In this thesis the approach of Cohen will be followed to derive a general theory that describes the diffusion behavior and predicts the moment of onset of liquid-liquid demixing in the immersed film, as a function of thermodynamic and hydrodynamic parameters characterizing the ternary system.

1.5. Demixing processes during immersion precipitation

After immersion of the cast solution into the coagulation bath an exchange of solvent and nonsolvent occurs in the polymer solution. This diffusion process may induce thermodynamically metastable or unstable compositions in the solution, i.e. the solution can decrease its free energy of mixing by splitting up into two (or more) phases with different compositions. When these phases are liquid, the demixing process is called liquid-liquid phase separa-

tion. When one of the phases is solid and crystalline, the demixing process is called crystallization.

The mechanism of liquid-liquid demixing of a homogeneous solution depends on the degree of stability of the solution:

- when a solution is metastable, phase separation occurs through the generation and growth of stable nuclei of a new phase; these stable nuclei can only be generated by certain type of concentration fluctuations. Phase separation by means of nucleation and growth is called binodal decomposition (demixing).
- when a solution is unstable, phase separation occurs through amplification of even the smallest concentration fluctuations. This type of phase separation process is called spinodal decomposition.

-liquid-liquid phase separation in ternary membrane forming systems-

Ternary systems consisting of polymer, solvent and nonsolvent are always characterized by a liquid-liquid demixing gap; i.e. a composition range where the free energy of the system can be lowered through separation into two liquid phases. This gap can be represented in an isothermal phase diagram (Fig. 1). The boundary of this gap is called the binodal. The spinodal is situated within this gap and touches the binodal in one point, the so called critical composition. The spinodal encloses all the instable compositions; in between the spinodal and the binodal, compositions are metastable.

The dashed lines in Figure 1 represent some tielines: a composition situated on a tieline splits up in the two liquid phases connected by the tieline and situated on the binodal. From Figure 1 it can be seen that liquid-liquid demixing in ternary membrane forming systems generates a polymer lean and a polymer rich phase.

Nucleation of the polymer lean phase occurs when the metastable region is entered above the critical point, which is the case for an immersed casting solution with an appropriate polymer concentration (10-20 vol.%).

Before a spinodal composition can be reached by diffusion, the composition of the system must always cross the region in between the binodal and the spinodal (except at the critical point). In our opinion the rate of nucleation of the polymer lean phase is so high that the diffusion process can

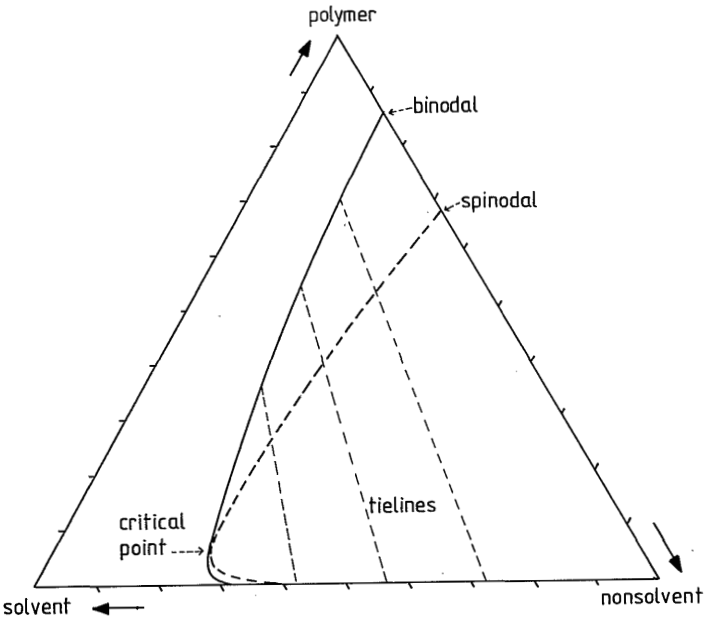

Fig. 1. Schematic representation of the isothermal phase diagram of a polymer/solvent/nonsolvent system.

never produce spinodal compositions in the immersed casting solution. This opinion is based on experiments performed in our laboratory: by quenching, metastable solutions with polymer concentrations up to 30 vol.% were obtained and investigated as to the kinetics of phase separation; the onset of demixing of these solutions was so fast that no induction times for demixing could be detected, even at a very low degree of supersaturation (0.1 % nonsolvent). This indicates that demixing occurs instantaneously upon passing the binodal.

The tiny droplets of the polymer lean phase formed during the liquid-liquid demixing process are surrounded by a polymer rich phase which solidifies through gelation or glass transition during the continuing precipitation process. Whether the droplets of the polymer lean phase do coalesce and form an interconnective structure before the solidification of the polymer rich phase takes place, strongly depends on the polymer concentration in the solution at the moment of onset of liquid-liquid demixing.

-crystallization and formation of aggregates-

Many systems consisting of polymer, solvent and nonsolvent are characterized by a composition range where agglomerates of polymer molecules are formed [35-38]. Information about the precise structure of these agglomerates is still lacking, although there are indications that crystallization plays a role during the formation process of these agglomerates. Because the exact nature of these agglomerates is still unknown, it would be premature to define them as being a phase and their mechanism of formation as being a phase separation process. Following Labudzinska [35-36], these agglomerates will be called aggregates in this thesis.

Despite the lack of information about the exact nature of these aggregates, it is clear that their formation during immersion precipitation can have a large influence on the porosity of the ultimate membrane: because it involves nucleation of a solid structure, aggregate formation (in contrast to liquid-liquid phase separation) can induce an interconnective porous structure from a highly concentrated polymer solution. Because of this effect, the occurrence of aggregate formation in a membrane forming system is attended by a decrease of the membrane sublayer resistance under operation process circumstances.

Compared to liquid-liquid phase separation, demixing by means of aggregate formation is a slow process [37]. This means that the effect of aggregate formation on the ultimate membrane morphology strongly depends on the rate of penetration into the metastable composition range during the diffusion process.

1.6. Structure of this thesis

For our experimental research we have chosen the system cellulose acetate (CA)/solvent/water. As the solvent we have used dioxane, tetrahydrofurane (THF) and acetone. Immersion precipitation performed using these systems yields a wide variety in morphological structure. In this thesis it is examined which factors are responsible for this variety in structure.

Chapter 2 gives experimental data on the demixing behavior upon cooling of CA/solvent/water systems for CA concentrations up to 40 wt.%. The rapid process of liquid-liquid phase separation is clearly distinguished from the slow

process of aggregate formation by examining the dependence of the cloud point position on the cooling rate and by structure analysis of quenched solutions.

In Chapter 3 equations and boundary conditions are derived for the isothermal diffusion processes that occur in the coagulation bath and in the polymer solution after immersion of a cast polymer solution into a coagulation bath. Mass transfer phenomena are expressed in terms of thermodynamic driving forces and frictional coefficients.

Using the equations and boundary conditions derived in Chapter 3, the composition changes in a CA-acetone casting solution, immersed into a water bath, are calculated in Chapter 4. These composition changes are calculated using experimental hydrodynamic and thermodynamic data from the three limiting binary mixtures. Using the calculated demixing gap for the system CA/acetone/water, the concentration profile at the very moment of onset of liquid-liquid demixing in the immersed solution film is predicted. The calculated and experimentally found moment of onset of liquid-liquid demixing are compared for varying casting solution compositions.

Chapter 5 is concerned with the influence of the CA polydispersity and the solvent type used on the liquid-liquid demixing behavior of CA/solvent/water systems. Experimentally obtained compositions of coexisting phases and cloud points are compared with calculated compositions of coexisting phases and binodal curves, in order to verify the expression for the free energy of a ternary system given in Chapter 3.

Using equations and boundary conditions derived in Chapter 3 and experimental frictional coefficients for the system CA/dioxane/water, the composition changes and the moment of onset of liquid-liquid demixing in an immersed film are calculated in Chapter 6, for systems with varying values of the thermodynamic interaction parameters. For various CA/solvent/water systems the time interval in between immersion of the film and onset of liquid-liquid demixing is also measured by means of light transmission measurements.

In Chapter 7 the relation between the casting solution composition, the coagulation bath compositions and the components used on the one hand, and the morphology of the ultimate membrane obtained by means of immersion precipitation on the other hand, is discussed using calculated and experimental data from this thesis and from literature.

In the Appendix of this thesis some empirical criteria for the occurrence of macrovoids in membranes are derived from experimental data. A theory is proposed which explains the formation of macrovoids during the immersion pre-

cipitation process.

1.7. References

1. Desalination, vol. 53 (1985).
2. H. Strathmann, Trennung von molekularen Mischungen mit Hilfe synthetischer Membranen. Steinkopf Verlag, Darmstadt, 1979.
3. R.E. Kesting, "Synthetic Polymer Membranes", McGraw Hill, New York, 1972.
4. R. Zsigmondy and W. Bachman, Z. Anorg. Allg. Chem., 103 (1918) 109.
5. R.E. Kesting, United States Patent, 3 884 801, May 20, 1975.
6. G.B. Tanny, J. Appl. Polym. Sci., 18 (1974) 2149.
7. S. Loeb and S. Sourirajan, Advan. Chem. Ser., 38, (1962) 117.
8. A.S. Michaels, US Patent 3651024 (1967).
9. A.S. Michaels and R.W. Baker, DBP 1792580.
10. W. Schumann and H. Strathmann, US Patent 3925211 (1975).
11. J.E. Jolley, US Patent 3172741.
12. H. Strathmann, K. Koch, P. Amar and R.W. Baker, Desalination, 16 (1975) 179.
13. I. Cabasso, E. Klein and J.K. Smith, J. Appl. Polym. Sci., 21 (1977) 165.
14. M.A. Frommer and D. Lancet, Reverse Osmosis Membrane Research, H.K. Lonsdale and H.E. Podall, Eds., Plenum Press, New York (1972) 85.
15. M.A. Frommer an R.M. Messalem, Ind. Eng. Chem. Prod. Res. Dev., 12 (1973) 328.
16. V. Gröbe and G. Mann, Faserforsch. Textiltechn., 19 (1968) 49.
17. R. Matz, Desalination, 10 (1972) 1.
18. M. Panar, H.H. Hoehn and R.R. Hebert, Macromolecules, 6 (1973) 777.
19. R.J. Ray, Thesis, Chapter 3, University of Colorado (1983).
20. J.E. Anderson and R. Ullmann, J. Appl. Phys., 44 (1973) 4303.
21. C. Castellari and S. Ottani, J. Membrane Sci., 9 (1981) 29.
22. S. Sourirajan and B. Kunst in Synthetic Membranes, S. Sourirajan, Ed., National Research Council Canada, Ottawa (1977) 129.
23. B. Kunst and Z. Vajnaht, J. Appl. Polym. Sci., 21 (1974) 2505.
24. H. Strathmann and K. Koch, Desalination 21 (1977) 241.
25. D.M. Koenhen, M.H.V. Mulder and C.A. Smolders, J. Appl. Polym. Sci., 21

(1977) 199.

26. F.W. Altena, Thesis, Twente University, Enschede, The Netherlands (1982).
27. J.G. Wijmans and C.A. Smolders, Synthetic Membranes: Science, Engineering and Applications, P.M. Bungay, H.K. Lonsdale and M.N. de Pinho, Eds., D. Reidel Publ. Comp., Dordrecht, Holland (1986).
28. F.W. Altena, J. Smid, J.W.A. van den Berg, J.G. Wijmans and C.A. Smolders, Polymer, 26 (1985) 1531.
29. H.J. Heyer and V. Gröbe, Faserforsch. Textiltechn., 18 (1967) 577; V. Gröbe and H.J. Heyer, Faserforsch. Textiltechn., 19 (1968) 33, 313, 398.
30. D.R. Paul, J. Appl. Polym. Sci., 12 (1968) 383.
31. A. Ziabicki, Fundamentals of Fibre Formation, Wiley, New York, 1976.
32. C. Cohen, G.B. Tanny and S. Prager, J. Polym. Sci., Polym. Phys. Ed., 17 (1979) 477.
33. K.J. Ruschak and C.A. Miller, Ind. Eng. Chem. Fundam., 11 (1972) 534.
34. P.J. Flory, Principles of Polymer Chemistry, Cornell Univ. Press, Ithaca (1953).
35. A. Labudzinska, A. Wasiak and A. Ziabicki, J. Polym. Sci., C16 (1967) 2835.
36. A. Labudzinska and A. Ziabicki, Kolloid Z.Z. Polym. 234 (1971) 21.
37. J.G. Wijmans, H.J.J. Rutten and C.A. Smolders, J. Polym. Sci., Polym. Phys. Ed., 23 (1985) 1941.
38. F.W. Altena, J.S. Schröder, R. van de Hulst and C.A. Smolders, J. Polym. Sci., Polym. Phys., 24 (1986) 1725.

2. DEMIXING AND GELATION BEHAVIOR OF TERNARY CELLULOSE ACETATE SOLUTIONS

By A.J. Reuvers, F.W. Altena and C.A. Smolders

2.1. Summary

The demixing behavior on cooling of ternary systems of cellulose acetate/solvent/water has been examined for CA concentrations up to 40 wt.% CA in several solvents. Cloud points have been measured as a function of cooling rate. The rapid process of liquid-liquid demixing can be discriminated from the slow process of aggregate formation by examining the dependence of the cloud point on the cooling rate and by structure analysis of quenched solutions with scanning electron microscopy. The appearance of aggregate formation depends strongly on the type of solvent. Slow cooling of ternary solutions in which acetone is the solvent leads to aggregate formation long before liquid-liquid demixing occurs.

In addition, isothermal sol-gel transitions have been measured for quenched solutions at varying gelation times. It is concluded that gelation is not always preceded by aggregate formation.

2.2. Introduction

This investigation into the demixing behavior of ternary cellulose acetate (CA) solutions has been carried out in order to obtain experimental data, which are necessary to describe the formation mechanism of asymmetric membranes produced by means of the immersion precipitation process.

Asymmetric membranes of CA can be obtained by immersing a film of a binary polymer solution into a water bath. During immersion there is a rapid exchange of solvent and nonsolvent in the polymer film, which leads to the formation of an asymmetric membrane consisting of a dense top layer and a porous substructure. Depending on the specific solvent, the top layer can vary in density and thickness [1]. These structural properties are of great relevance to the transport characteristics of the final membrane, such as the degree of selectivity and the permeability. To understand the influence of the type of

solvent used on the top layer structure we must study two characteristic features. First, we must know how the type of solvent influences the concentration profile in the film during the precipitation process. Second, we must know the demixing behavior and the kinetics of demixing as a function of the composition of the ternary system polymer/solvent/nonsolvent.

This study is concerned with the second characteristic. We have focused our attention on the ternary systems CA/solvent/water where the solvent is either dioxane, acetone, or tetrahydrofuran (THF). The solvents are miscible with water in all proportions.

We examined the three systems for the following types of demixing processes.

(1) Liquid-liquid phase separation. On cooling, a polymer solution may become metastable and may then separate into two liquid phases through nucleation and growth of one of the phases.

(2) Formation of aggregates. On cooling, the solution may become metastable and may then demix as a result of aggregation of the polymer molecules, possibly induced by crystallization. One could also call this process precipitation.

These processes can be discriminated by examining the kinetics of demixing. At a low degree of supercooling the formation of aggregates is supposed to be a slower process than liquid-liquid phase separation. Because the CA solutions studied showed a rapid gelation after the demixing process, we could also examine the type of demixing by means of structure analyses of the final product with the aid of electron microscopy.

Besides studying the nature of the demixing processes we also investigated the gelation behavior of the systems.

In the past the demixing behavior and gelation behavior of several ternary polymer solutions have been investigated [2]. Particularly, the system polyacrylonitrile (PAN)/solvent/water has been the object of intensive research [3-8]. investigations into the demixing behavior of the system CA/solvent/water have been limited to cloud point measurements for CA concentrations less than 25% for several solvents including acetone [10-12] and dioxane [9-11]. Since the kinetics of demixing was not taken into account it was not possible to judge from the results what kind of demixing process caused the turbidity.

2.3. Experimental procedures

- Materials used and preparation of the samples -

CA was obtained from Eastman Kodak with an acetyl content of 39.8% and a viscosity number 3 (ASTM). The solvents were of reagent grade and were used without further purification, except for drying on molecular sieves. The water was demineralized and ultrafiltrated.

Solutions were prepared in glass tubes, which were sealed under vacuum at liquid nitrogen temperature. Solutions for the determination of the sol-gel transitions were provided with a mercury drop of 0.1 g in the tube. Solutions used for quenching to 20°C were prepared in tubes with an inner diameter of 4 mm and a wall thickness of 1 mm. The tubes were rotated and heated at 90°C for at least 2 days to obtain homogeneous solutions.

- Determination of the cloud points -

Both the formation of aggregates and the liquid-liquid phase separation process were accompanied by very strong light scattering; sometimes the solutions became milky white. Therefore, it was sufficient to measure changes in light transmission of the samples instead of changes in light scattering under a certain angle. The light source was a helium-neon laser. The intensity of the transmitted light was monitored on a recorder and was measured as a function of the temperature at two cooling rates: 0.6 and 0.02°C/min. For a detailed description of this technique we refer to Wijmans [13].

The temperature at which the intensity of the transmitted light became less than the intensity of an homogeneous solution was called the cloud point temperature. This temperature was measured within an accuracy of 2°C in the case of aggregate formation and within an error of 0.5°C in the case of liquid-liquid-liquid phase separation. We measured the cloud point temperature as a function of the nonsolvent/solvent ratio at constant polymer concentration. Interpolation led to the composition with a cloud point temperature of 20°C. This procedure was repeated for several polymer concentrations.

- Determination of the Type of Demixing Process -

As mentioned before, the formation of aggregates is supposed to be a slower process than liquid-liquid demixing at a low degree of supercooling. If the cloud point temperature does not depend on the cooling rate we assume that liquid-liquid demixing takes place. When the cloud point temperature measured does depend on the cooling rate we assume that the turbidity is caused by aggregate formation.

As will become clear further on, in the case of CA/acetone/water solutions, in the concentration range of interest the aggregate formation was found to be so rapid that the liquid-liquid demixing gap could not be reached without aggregate formation taking place. Hence, for this system cloud point measurements could not be used to determine the exact position of the liquid-liquid demixing gap, and we had to use a special method to determine its position.

We assumed that a solution having a composition that is situated in the liquid-liquid demixing gap at 20°C is able to separate into two liquid phases upon quenching to 20°C by means of the nucleation and growth mechanism until aggregate formation and gelation in the concentrated phase stop this process. In a solution which has a composition that is situated outside the liquid-liquid demixing gap only aggregate formation occurs upon quenching to 20°C. Structure analysis with scanning electron microscopy (SEM) can reveal the difference in structure due to the different demixing processes.

Therefore, we prepared solutions with a higher nonsolvent/solvent ratio than the cloud point compositions already determined. At constant polymer concentration we prepared several solutions with varying nonsolvent/solvent ratio. After being homogenized at 90°C the solutions were quenched in a 20°C thermostate bath. The tubes were kept at this temperature for 24 h, during which aggregates were formed, which resulted in a stiff gel network. Then the tubes were broken in order to remove the gels. Samples of the gels were treated for structure analysis with SEM in two different ways.

(1) The gels were put in two successive solvent extraction baths with nonsolvent/solvent mass ratios of 50/50 and 100/0, respectively. Then they were quenched in liquid nitrogen, broken, and dried. The baths were necessary to obtain stiff gels that could be dried without destroying the structure. A thin conductive gold coating was sputtered on the fracture surface, and the samples were examined with SEM.

(2) To avoid possible structure transformations caused by the solvent ex-

traction baths and the drying process we also examined the structure of the gels without any pretreatment. The gels were quenched in liquid nitrogen, broken, and the fracture surfaces were examined at -160°C with SEM equipped with a cryo-unit. A disadvantage of this method is the possibility of destroying the structure by crystal formation and the lower conductivity of the sample surface as compared to the previously mentioned sample preparation procedure where a gold layer was applied.

- Determination of the isothermal sol-gel transition -

The ternary systems CA/dioxane/water and CA/acetone/water have been characterized with respect to their gelation behavior. We have measured the position of the sol-gel transition in the ternary diagram by means of the falling ball method [14]. A mercury drop of about 0.1 g was put in the solutions. Homogeneous fluid solutions at 90°C were quenched to 20°C, and after 25 h the tubes were turned upside down. If the mercury drop moved downward we classified the solution as a liquid. If the drop did not move we classified the solution as a gel. We repeated the experiment, with a time allowed for gelation of 100 h. After some preliminary measurements we examined about 50 different solutions with dioxane as the solvent and about 25 solutions with acetone as the solvent with compositions near the sol-gel transition.

2.4. Results

In this section we first discuss the results of the cloud point measurements of the three ternary systems of interest. For the system CA/acetone/water these results gave us no information about the actual location of the liquid-liquid demixing gap. Therefore, we used the special technique as described in the experimental section to determine the liquid-liquid demixing gap for this system. The results are described in the second part of this section. The last part of this section is devoted to the determination of the position of the sol-gel transitions in the systems CA/dioxane/water and CA/acetone/water.

- Cloud point measurements -

In Figure 1 the cloud point compositions at 20°C have been plotted for the three solvents, determined at two different cooling rates.

For the system CA/THF/water the location of the cloud point curve does not depend on the cooling rate up to 40 wt.% CA. In this case the cloud point curve discriminates between homogeneous solutions and solutions which separate into two liquid phases.

For the system CA/dioxane/water the location of the cloud point curve does not depend on the cooling rate up to 26 wt.% CA. This is in accordance with the results found by Altena [9]. Above 26 wt.% CA the location of the cloud point curve depends on the cooling rate. For a cooling rate higher than 0.6°C/min the location of the cloud point curve does not change any more. Therefore, we conclude that above 26 wt.% CA the cloud point curve at a cooling rate of 0.02°C/min is caused by aggregate formation and that the cloud point curve at a cooling rate of 0.6°C/min is caused by liquid-liquid demixing.

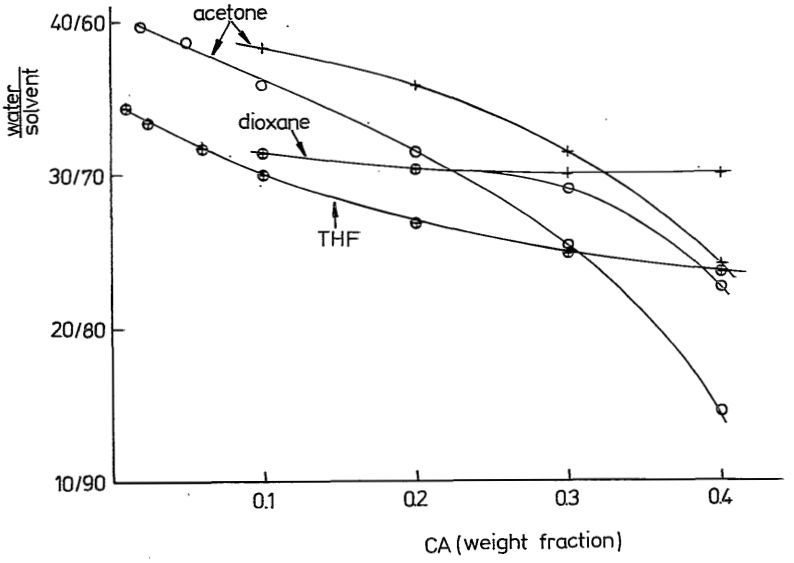

Fig. 1. Cloud point compositions for ternary CA solutions at 20°C for three solvents. Cooling rate: 0.6°C/min (+) and 0.02°C/min (0).

As we can see from Figure 1 the location of the cloud point curve for the system CA/acetone/water depends on the cooling rate for all CA concentrations considered. For a cooling rate higher than 0.6°C/min the location of the cloud point curve changes further. Therefore, we conclude that for both cooling rates the cloud points are caused by aggregate formation.

- SEM analysis -

Evidently, more rapid cooling should be carried out to be able to surpass aggregate formation and to enter the liquid-liquid phase separation gap. By carefully choosing the composition, quenching the solution to 20°C, and applying the SEM analysis technique as described in the experimental section we were able to determine at what composition liquid-liquid phase separation occurs at 20°C.

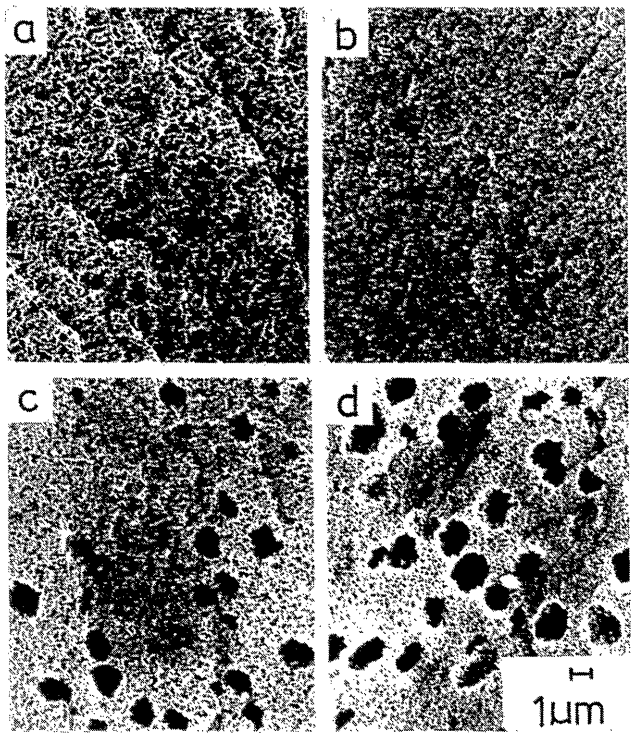

Fig. 2. SEM micrographs for 30 wt.% ternary CA solutions quenched to 20°C. Water/acetone ratio: (a) 36/64; (b) 37/63; (c) 38/62; (d) 40/60.

From the micrographs presented in Figure 2 it can be seen that in 30 wt.% CA solutions with water/acetone ratios of 40/60 and 38/62, liquid-liquid phase separation has taken place: the large voids are clearly the result of nucleation and growth of the diluted phase. The growth process was stopped because of a consecutive gelation of the concentrated phase surrounding the nuclei. It can also be seen that in the concentrated phase, aggregate formation took place. The aggregates exhibit a fibrous structure. In the solutions with a water/acetone ratio <38/62, only aggregate formation took place.

From Figure 3 we see that solutions containing 20 wt.% CA with a water/acetone ratio >38/62 are situated inside the liquid-liquid demixing gap. Comparison of Figure 3(d) and 3(b) shows that in case 3(d) the concentrated phase is denser than in case 3(b). This is to be expected since liquid-liquid phase separation is likely to lead to a higher polymer concentration in the concentrated phase when the demixing gap is entered further.

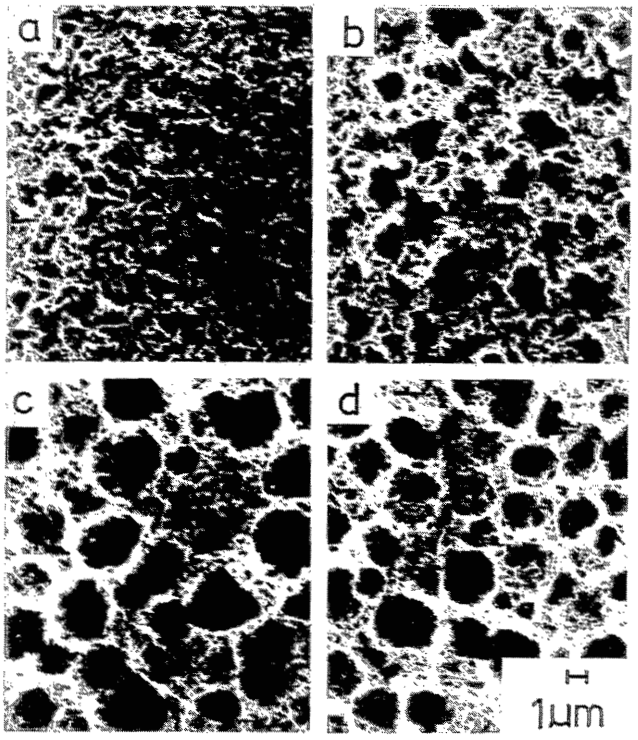

Fig. 3. SEM micrographs for 20 wt.% ternary CA solutions quenched to 20°C. Water/acetone ratio: (a) 38/62; (b) 39/61; (c) 40/60; (d) 42.5/57.5.

All micrographs shown in this paper originate from gels that have been put in two successive solvent extraction baths and have been dried before examination with the SEM, except the micrograph represented in Figure 4(a). This micrograph represents a gel analyzed using the SEM in combination with the cryo-unit. Comparison of Figure 4(a) with 4(b) leads to the conclusion that both ways of preparing the samples for SEM analysis give the same picture and therefore do not lead to serious changes of the structure.

At lower CA concentrations [Fig. 4(c) and (d)] the droplets which consist of the diluted phase have coalesced to form larger droplets before gelation of the concentrated phase took place. This can be understood since it takes more time before the aggregates in the concentrated phase form a continuous network which could oppose further coalescence.

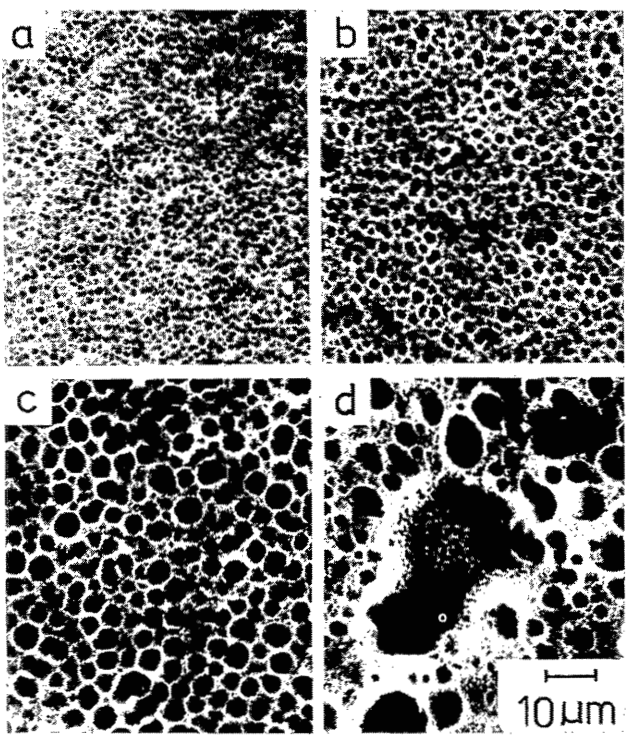

Fig. 4. SEM micrographs for ternary CA solutions quenched to 20°C. Water/acetone ratio: 42.5/57.5 wt.% CA: (a) 20 (sample prepared without solvent leaching); (b) 20; (c) 15; (d) 12.5.

From Figure 5 it can be seen that for a 10% CA solution with a water/ acetone ratio of 40/60 coalescence of the diluted phase took place, whereas a solution with a water/acetone ratio of 39/61 did not separate into two liquid phases, so that coalescence could not take place here. Again, this shows that with the combination of quenching and SEM analysis described in this paper an accurate and reliable determination of the location of the liquid-liquid demixing gap is possible.

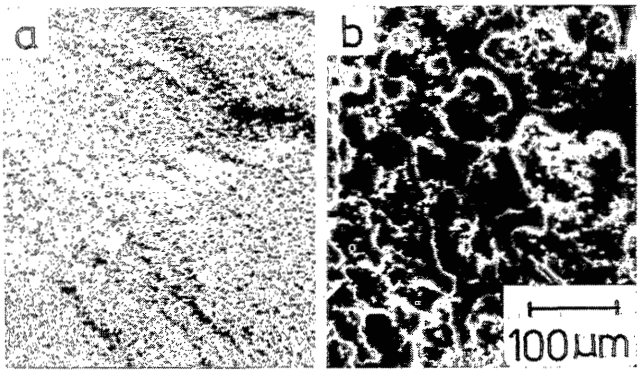

Fig. 5. SEM micrographs for 10 wt.% ternary CA solutions quenched to 20°C. Water/acetone ratio: (a) 39/61; (b) 40/60.

The results of the cloud point measurements and the SEM analysis can be combined to give isothermal (20°C) representations of ternary phase diagrams for both CA/acetone/water (Fig. 7) and CA/dioxane/water (Fig. 6).

- Sol-gel transitions -

For the system CA/dioxane/water we have determined the sol-gel transition from 10% CA until 52% CA. For the system CA/acetone/water we have determined the sol-gel transition from 10% CA until 40% CA. For all experiments done the upper limit for the CA concentration of the examined solutions is given by the fact that no homogeneous solution could be obtained within 2 days at 90°C. Longer exposure to this temperature leads to a degradation of the polymer. The results of the investigation into the location of the sol-gel transition are represented in Figures 6 and 7.

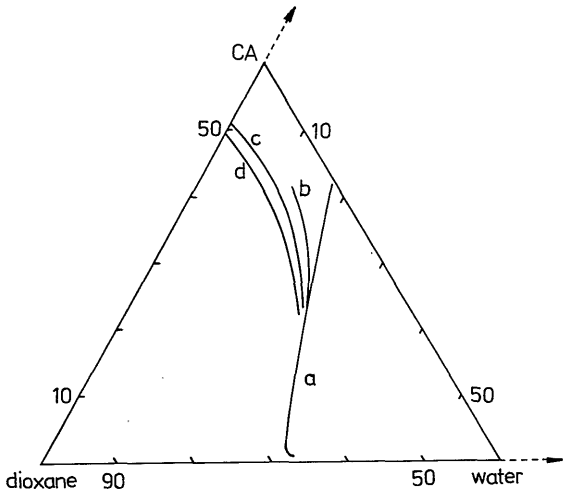

Fig. 6. Isothermal phase behavior for the system CA/dioxane/water at 20°C. (a) Liquid-liquid demixing gap (determined by cloud point measurements. (b) Cloud point curve (cooling rate: 0.02°C/min). (c) Sol-gel transition (time allowed for gelation: 25 h). (d) Sol-gel transition (time allowed for gelation: 100 h).

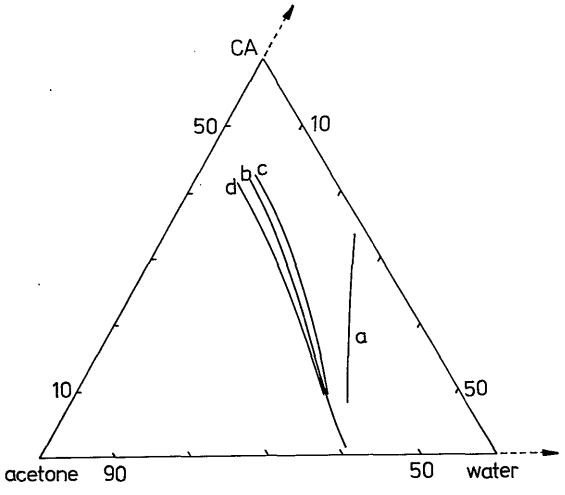

Fig. 7. Isothermal phase behavior for the system CA/acetone/water at 20°C. (a) Liquid-liquid demixing gap (determined by structure analysis). (b) Cloud point curve (cooling rate: 0.02°C/min). (c) Sol-gel transition (time allowed for gelation: 25 h). (d) Sol-gel transition (time allowed for gelation: 100 h).

It can be concluded that the time allowed for the gelation process influences the position of the sol-gel transition. The measured sol-gel transitions and sol-aggregate transitions are nonequilibrium transitions. The liquid-liquid demixing curves represent the transition between equilibrium phases because the location of these curves does not depend on the cooling rate.

2.5. Discussion

By varying the cooling rate (CA/dioxane/water) and examining the structure of quenched solutions (CA/acetone/water) we were able to discriminate between aggregate formation and liquid-liquid demixing. It was found that aggregate formation strongly depends on the kind of solvent. With acetone, aggregates are formed even at very low CA concentrations (2 wt.%). On the contrary, with THF, aggregate formation only takes place at very high CA concentrations (>40 wt.%). By cooling ternary solutions of PPO [16] and PAN [3,4] it was also found that aggregate formation sets in before liquid-liquid demixing takes place. In our opinion, the methods described in this paper could be used to determine the actual position of the liquid-liquid demixing gap for these systems. In points (1)-(3) we give some further comments.

(1) In figure 8 our results for the system CA/acetone/water are presented together with the results given by Strathmann [12], Frommer [11], and Guillotin [10]. The results given by Frommer and Guillotin are cloud points determined by titration of water. The authors do not give quantitative information about the time effects of their observations. The cloud point curve given by Strathmann is partly determined by means of titration of water. The upper and lower part of the curve given by Strathmann are determined by adding a specific amount of water to a CA solution and separating the concentrated part of the demixed solution from the diluted part. The compositions of the concentrated and diluted part form the upper and lower part of the cloud point curve given by Strathmann.

The cloud points given in the literature differ to a large extent. In our opinion this is caused by the fact that different times were allowed for the solutions to demix. In the ternary phase diagram the cloud points are situated at the left of the liquid-liquid demixing gap determined with our quenching technique. This means that the cloud points are probably caused by aggre-

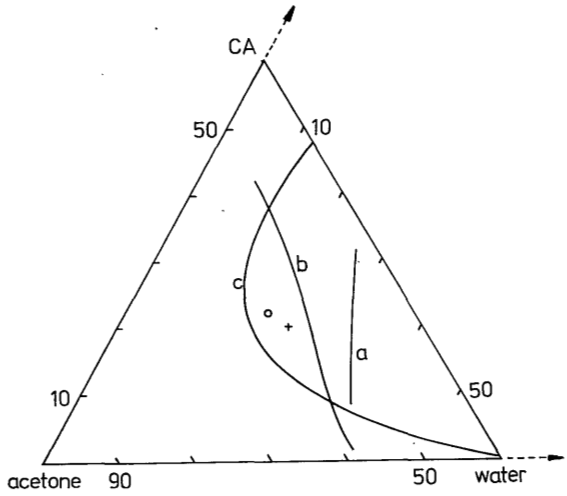

Fig. 8. Isothermal phase behavior for the system CA/acetone/water at 20°C. (a) Liquid-liquid demixing gap (this work). (b) Cloud point curve (this work, cooling rate: 0.02°C/min). (c) Cloud point curve Strathmann [12]. (o) Cloud point Guillotin [10]. (+) Cloud point Frommer [11].

gate formation and not by liquid-liqud demixing. The upper and lower parts of the cloud point curve given by Strathmann are not identical to the liquid-liquid demixing curve, as he supposes, since he ignores the influence of aggregate formation and gelation on this type of experiment.

(2) In this paper we do not intend to explain the mechanism of aggregate formation. Nevertheless, some remarks can be made on this phenomenon. We think that microcrystallites are responsible for the solid structure of the aggregates because of the following reasons.

(a) We observed a large difference between the temperature at which the aggregates are formed and gelation sets in and the temperature at which the aggregates dissolve and the structure becomes fluid. We measured that this temperature difference is 40°C for a 30 wt.% CA solution with a water/acetone ratio of 25/75. According to Tan [15] this temperature difference only occurs when microcrystallites are formed.

(b) Crystallization is a slow process in comparison with liquid-liquid demixing because of the time needed for orientation of the polymer molecules, both for nucleus formation and for growth.

(c) Aggregate formation also occurs in solutions of PPO [16] but does not occur in (even very concentrated) solutions of polysulfone. PPO is a semi-crystalline polymer just like CA; polysulfone is a completely amorphous polymer. To get more information about the role of crystallization during aggregate formation it is necessary to do DSC experiments [17].

Labudzinska [3,4] has examined the interrelation between aggregate formation and gelation for ternary solutions of PAN and PVA by means of light scattering and viscosity measurements. She concludes that gelation is not necessarily preceded by aggregate formation. This is in agreement with our observations. We observed that all examined CA/acetone/water gels were turbid, whereas clear CA/dioxane/water gels could be obtained. So we conclude that the gelation of the examined CA/acetone/water gels is always preceded by aggregate formation, while CA/dioxane/water solutions also form gels without the formation of large, strongly light scattering aggregates.

(3) In order to draw conclusions about the role of aggregate formation during the membrane formation process it is necessary to know more about the kinetics of aggregate formation at high CA concentrations. The concentration changes in the precipitating polymer film are so rapid that the slow process of aggregate formation at low CA concentrations can be easily surpassed. Liquid-liquid demixing certainly plays a role during membrane formation. This phase separation process is responsible for the formation of the porous substructure of the membrane. As already mentioned by Ziabicki [2] it is also important to know more about the kinetics of liquid-liquid demixing in ternary polymer solutions. In combination with knowledge about the diffusion behavior during membrane formation we hope to be able to say more about the thickness of the top layer of the membrane. Further investigations will be carried out on the kinetics of liquid-liquid phase separation.

2.6. Conclusions

For the interpretation of turbidity measurements it is necessary to examine the influence of the cooling rate on the location of the cloud point compositions. As long as the location of the cloud point compositions does not depend on the cooling rate we assume that liquid-liquid phase separation takes place.

For the system CA/acetone/water we used a new method to determine the liq-

uid-liquid demixing gap. By quenching homogeneous solutions to 20°C and analyzing the structure of the demixed and gelled solution by means of electron microscopy we were able to discriminate between the two demixing processes. This method can also be applied to other rapidly gelling systems. For the system examined by us this method leads to a considerable improvement of the accuracy of the phase diagram.

The authors wish to thank C.J. Padberg for performing a substantial part of the experimental work and J.W.A. van de Berg for his helpful remarks.

2.7. APPENDIX A. Demixing behavior of ternary poly(2,6-dimethyl-1,4-phenyleneoxide) solutions

The polymer poly(2,6-dimethyl-1,4-phenyleneoxide) (PPO) is a suitable membrane material because of its good chemical and physical properties. Broens et al. [18] showed that membranes with promising ultrafiltration properties are obtained if a casting solution of 10 wt.% PPO in a 78/22 (wt.%) mixture of trichloroethylene (TCE) and 1-octanol (OcOH) is immersed into a coagulation bath containing methanol (MeOH).

Wijmans [16] investigated phase separation phenomena occurring in solutions prepared from this quaternary system in order to elucidate the mechanism of membrane formation. Turbidity measurements on the quaternary system were performed at a cooling rate of 0.1°C/min. It turned out that the binary system PPO-TCE demixes at a PPO concentration of 32 wt.%. At lower PPO concentrations a certain amount of OcOh and/or MeOH had to be added to the binary system to induce demixing of the solution upon cooling to 25°C. From the shape of the cloud point curve, Wijmans concluded that crystallization is responsible for the turbidity increase at high PPO concentrations and liquid-liquid demixing for the turbidity increase at high nonsolvent concentrations.

In this chapter we have shown that the rapid process of liquid-liquid demixing can be distinguished from the slow process of aggregate formation (or crystallization) by examination of the kinetics of demixing. To verify the conclusions of Wijmans, the position of the liquid-liquid demixing gap is determined for the systems PPO/TCE/MeOH and PPO/TCE/OcOH in the following way.

At 5, 10 and 20 wt.% PPO, series of homogeneous solutions were prepared,

with nonsolvent/solvent ratios equal to and higher than the nonsolvent/solvent ratios at the cloud point compositions determined by Wijmans. PPO was taken from the batch used by Wijmans [16]; $\bar{M}_n$ = 21,000; $\bar{M}_w$ = 56,000. Homogeneous solutions at 90°C were quenched in a 25°C thermostate bath, and the time interval beween the moment of quenching and the onset of turbidity (the induction time t') was measured. Turbidity was detected by visual observation.

For PPO/TCE/MeOH solutions containing 5 or 10 wt.% PPO, t' was always too small to be measurable. This means that liquid-liquid demixing is responsible for the onset of turbidity.

For PPO/TCE/MeOH solutions containing 20 wt.% PPO and for all PPO/TCE/OcOH solutions, t' slowly decreased with increasing nonsolvent concentration and t' suddenly dropped to zero at a certain nonsolvent concentration. This is schematically represented in Figure A1.

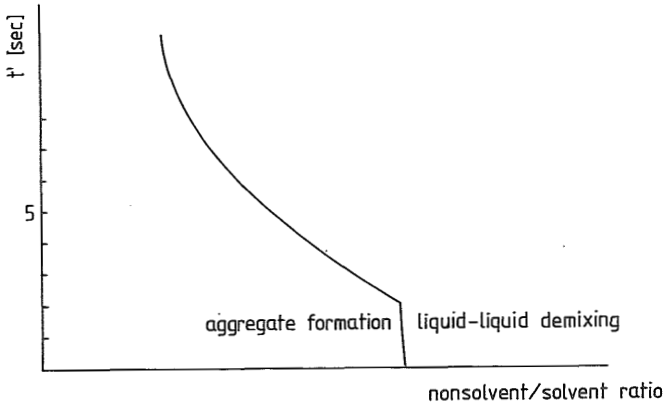

Fig. A1. Schematic representation of the induction times for demixing of quenched PPO/TCE/OcOH solutions with a varying nonsolvent/solvent ratio.

In our opinion the sharp transition in Figure A1 is caused by the fact that crystallization (or aggregate formation) is responsible for the onset of turbidity at the left hand side of this transition, whereas liquid-liquid demix-

ing is responsible for the onset of turbidity at the right hand side of the transition.

In Figure A2 the liquid-liquid demixing gaps, thus determined, are shown together with the cloud point curves determined by Wijmans. It can be seen that for the system PPO/TCE/MeOH, liquid-liquid demixing is responsible for the cloud point curve at high MeOH concentrations. This is in agreement with the conclusion of Wijmans. For the system PPO/TCE/OcOH however, crystallization is responsible for the complete cloud point curve, from high PPO concentrations until high OcOH concentrations. This is not in agreement with Wijmans' conclusions.

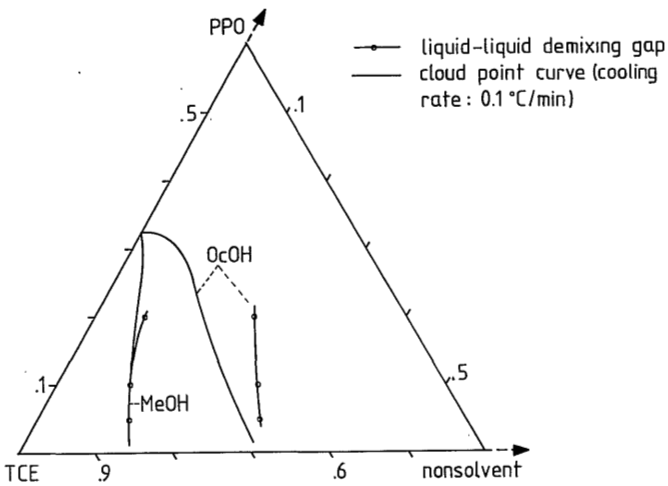

Fig. A2. Isothermal phase behavior for PPO/TCE/nonsolvent systems at 25°C, using MeOH and OcOH as nonsolvent respectively. The cloud point curves have been taken from Wijmans [16]. The liquid-liquid demixing gaps have been measured by means of quenching experiments.

We have stated before in this chapter that the shape of the cloud point curve, measured at one cooling rate only, gives not always enough information for drawing conclusions about the position of the liquid-liquid demixing gap, as has typically been done earlier by Wijmans. This statement is now confirmed by the kinetic measurements performed for the systems PPO/TCE/MeOH and PPO/TCE/OcOH.

2.8. References

1. R. Bloch and M.A. Frommer, Desalination, 7 (1970) 259.
2. A. Ziabicki, Fundamentals of Fibre Formation, Wiley, New York, 1976.
3. A. Labudzinska, A. Wasiak, and A. Ziabicki, J. Polym. Sci., C16 (1967) 2835-2844.
4. A. Labudzinska and A. Ziabicki, Kolloid Z. Z. Polym., 243 (1971) 21-27.
5. J. Bisschops, J. Polym. Sci., 12 (1954) 583-597.
6. J. Bisschops, J. Polym. Sci., 17 (1955) 89-98.
7. P. Lagerkvist, and P. Flodin, J. Polym. Sci., Polym. Lett. Ed., 19 (3) (1981) 125-130.
8. H. Strathmann and H.D. Saier, Proceedings of the 4th International Symposium on Fresh Water from the Sea, 4 (1973) 381-394.
9. F.W. Altena and C.A. Smolders, Macromol., 15 (1982) 1491-1497.
10. M. Guillotin, C. Lemoyne, C. Noël, and L. Monnerie, Desalination, 21 (1977) 165.
11. M.A. Frommer and D. Lancet, Reverse Osmosis Membrane Research, H.K. Lonsdale and H.E. Podall, Eds., Plenum, New York, 1972, p. 85.
12. H. Strathmann, P. Scheible, and R.W. Baker, J. Appl. Polym. Sci., 15 (1971) 811.
13. J.G. Wijmans, J. Kant, M.H.V. Mulder and C.A. Smolders, Polymer, 26 (1985) 1539.
14. D.R. Paul, J. Appl. Polym. Sci., 11 (1967) 439.
15. H.M. Tan, B.H. Chang, E. Baer, and A. Hiltner, Eur. Polym. J., 19 (1983) 1021.
16. J.G. Wijmans, H.J.J. Rutten and C.A. Smolders, J. Polym. Sci. Polym. Phys. Ed., 23 (1985) 1941.
17. F.W. Altena, J.S. Schröder, R. van de Hulst and C.A. Smolders, J. Polym. Sci., Polym. Phys., in press.
18. L. Broens, D.M. Koenhen and C.A. Smolders, Desalination, 22 (1977) 205.

3. A MODEL TO DESCRIBE THE MASS TRANSFER DURING IMMERSION PRECIPITATION

By A.J. Reuvers, J.W.A. van den Berg and C.A. Smolders

3.1. Summary

Equations and boundary conditions are derived for the isothermal diffusion processes in the coagulation bath and in the polymer solution after immersion of a cast (ternary) polymer solution into a (binary) coagulation bath.

This mass transfer is expressed in terms of thermodynamic driving forces and frictional coefficients. The frictional coefficients in the ternary system are assumed to be interrelated through the Onsager reciprocal relations and to be related to the measurable frictional coefficients defined in the three limiting binary composition ranges.

In combination with knowledge about the demixing processes, that can take place in the polymer solution (liquid-liquid phase separation or solid like aggregate formation), this model makes it possible to calculate the polymer concentration profile in the immersed film at the moment of demixing of the polymer solution as a function of several process parameters. The calculated concentration profile and its relation to the asymmetric structure of the ultimate membrane are presented in Chapter 4.

3.2. Introduction

The preparation of asymmetric polymeric membranes by means of immersion precipitation of a casting solution, started with the development of reverse-osmosis membranes by Loeb and Sourirajan [1] in 1962. Since then different kinds of asymmetric membranes have been prepared by means of immersion precipitation. The immersion precipitation process is also used to prepare the supporting layer of composite membranes.

It is possible to vary the membrane properties to a great extent, from typical reverse osmosis behavior to microfiltration behavior, by changing the process parameters during membrane formation or by adding extra components to the casting solution or to the coagulation bath.

The basic process of immersion precipitation can be carried out with three components. Solvent and polymer are used to prepare the casting solution and nonsolvent is used as the coagulation bath.

The formation process of the membrane can be split up into three parts:

1. Composition changes in the polymer solution before immersion into a coagulation bath, by evaporation;
2. Composition changes in the polymer solution after immersion into a coagulation bath prior to possible demixing processes;
3. Demixing processes which take place when the composition of the polymer solution becomes metastable.

Binary diffusion during the time in between casting and immersion of the polymer solution (the evaporation step) has been investigated by a number of authors [2-5]. In general they conclude that the asymmetric structure in case of Loeb-Sourirajan-type CA membranes is caused by the evaporation of acetone, which leads to an increase of the polymer concentration in the toplayer of the polymer solution. We agree that the duration of the evaporation step influences the membrane structure when volatile solvents are used. However, when non volatile solvents are used or when no evaporation step is carried out (which is the case for the innerside of a wet spun hollow fiber membrane) asymmetric membranes can also be obtained. This means that the ternary diffusion process which starts after immersion of the polymer solution into a nonsolvent bath mainly determines the asymmetric structure of the membrane.

The mass transfer in the still homogeneous polymer solution, after immersion into a nonsolvent bath has not been a subject of much investigation until now. The most far-reaching theoretical investigation has been carried out by Cohen, Tanny and Prager [6]. They showed that after immersion of the castting solution in a coagulation bath the polymer concentration at the interface of the casting solution and the coagulation bath increases strongly. With their diffusion model they also examined whether the exchange of solvent and nonsolvent could lead to instable compositions in the polymer solution. Only if this is the case, according to Cohen et al., porous membranes can be formed as a result of liquid-liquid demixing.

The third important feature of the membrane formation process is the type of demixing processes that can occur in the immersed polymer solution after diffusion has led to a metastable composition. These demixing processes create the pores in the sublayer and determine the structure of the toplayer of

the membrane.

Much research has been done into the demixing processes that occur in Loeb-Sourirajan-type CA membranes. The results of these investigations have been summarized by Lonsdale [7]. The general conclusion is that the polymer precipitates in the nonsolvent and that gelation occurs by coagulation. We prefer to call this demixing process aggregate formation. Within our group we have found that aggregate formation takes place in several membrane forming systems [8,9] and that this can lead to very different structures. We discriminate this demixing process from liquid-liquid phase separation. We have shown that both demixing processes occur in membrane forming systems and that they can be distinguished by examining the kinetics of demixing [9]. Especially at a low degree of supersaturation, aggregate formation is a slow process compared to liquid-liquid phase separation, probably because some orientation of the polymer molecules is required for the formation of aggregates.

In order to understand how these demixing processes influence the membrane structure it is necessary to examine experimentally the structure induced by demixing as a function of composition, and it is necessary to know the composition profile in the polymer film as a function of time after immersion of the film into the coagulation bath prior to the demixing processes. In this paper we will show how the composition change in the film prior to demixing can be described as a function of several process parameters. Our work has been inspired by the model of Cohen et al. [6].

3.3. The diffusion model: correspondence to and difference from the model of Cohen et al.

Cohen, Tanny and Prager describe the ternary diffusion process in the immersed polymer solution by means of two phenomenological diffusion equations. They use the chemical potential gradients as the driving forces instead of the concentration gradients. In this way it is possible to describe the ternary diffusion process as a function of binary thermodynamic parameters and binary frictional coefficients, even in the metastable region in between the binodal and the spinodal. It is assumed that the compositions at both sides of the interface between the polymer solution and the coagulation bath are always at equilibrium. The diffusion equations are described using polymer fixed position coordinates and the diffusion coefficients are defined i- -

polymer fixed frame of reference. So far we will copy the model of Cohen et al. To simplify their model Cohen et al. adopt a few assumptions. We will briefly discuss why we omit these simplifications from our model or adopt different assumptions.

Wijmans [10] clearly showed that it is not allowed to use the steady-state approximation of Cohen et al. to describe the diffusion during membrane formation. Therefore, we will not adopt the steady-state assumption. We will give the exact solution of the diffusion equations.

Furthermore, Cohen et al. neglect the frictional forces acting between solvent and nonsolvent by omitting the cross terms in the diffusion equations. We will not do so, and we will show that this omission can lead to erroneous results.

The two above mentioned simplifications enabled Cohen et al. to calculate composition paths without knowing the influence of the polymer concentration on the frictional forces acting between polymer and solvent and between polymer and nonsolvent. However, in our model we have to know the dependence of these frictional forces on polymer concentration.

Cohen et al. use constant thermodynamic interaction parameters in their expressions for the chemical potentials. From results of Altena [11] it can be concluded that the Flory-Huggins interaction parameter shows a strong concentration dependence for many solvent-water mixtures. Therefore we will use concentration dependent interaction parameters in our expressions for the chemical potentials.

Cohen et al. assume that the composition of the coagulant at the boundary of the casting solution remains equal to the bulk composition of the original bath. However, even if the coagulation bath is well stirred, there will be a stagnant layer in the vicinity of the interface. We will assume that only diffusion takes place in the coagulation bath. When the coagulation bath is stirred this assumption is still valid during the very important first seconds after immersion of the polymer solution.

Cohen et al. assume that liquid-liquid demixing can occur only when an instable spinodal composition has been reached. In our opinion liquid-liquid demixing takes place when the binodal has been passed and a metastable composition with even a very low degree of supersaturation has been reached.

3.4. The phenomenological equations describing the diffusion in the polymer solution

In this section we will derive the phenomenological equations describing the diffusion in the polymer solution. We will show that the diffusion equations of Cohen et al. lack a factor (the polymer volume fraction) and that the recent criticism of McHugh and Yilmaz [12] on the continuity equations, used by Cohen, is unfounded.

We will index the components as follows: nonsolvent (1), solvent (2) and polymer (3). For a complete list of symbols we refer to the end of this paper.

De Groot and Mazur [13] derive the following relation between fluxes $\underline{J}_i^c$ and thermodynamic driving forces X_j in a ternary system:

$$\underline{J}_i^c = \sum_{j=1}^{2} L_{ij} X_j \qquad i = 1,2 \tag{1}$$

The superscript c refers to a mass flux [kg/m²s].
Because of the exchange of solvent and nonsolvent after immersion of the film, the interface between the polymer solution and the coagulation bath will move. Hartley and Crank [14] suggest that this moving boundary problem can be simplified by defining the fluxes relative to a polymer fixed frame of reference:

$$\underline{J}_i^c = c_i(\underline{v}_i - \underline{v}_3), \tag{2}$$

where c_i is the concentration of component i [kg/m³].
For these fluxes the thermodynamic driving forces in eqn. (1) are given by [13]:

$$X_j = -\frac{\delta \mu_j}{\delta x}, \tag{3}$$

where μ_j is the chemical potential of component j per kg j and x is the cartesian spatial position coordinate perpendicular to the membrane surface.
We assume that the phenomenological coefficients, L_{ij}, obey the Onsager reciprocal relations [13]:

$$L_{12} = L_{21} \tag{4}$$

In order to obtain differential equations describing the ternary diffusion process the flux equations (1) have to be combined with the continuity equations.

The continuity equations in terms of volume fluxes [m/s] relative to the cell fixed frame of reference are

$$\frac{\delta \tilde{J}_i^{\phi}}{\delta x} = - \frac{\delta \phi_i}{\delta t} \qquad i = 1,2,3 \tag{5}$$

where $\phi_i = c_i \bar{v}_i$ is the volume fraction of component i and where $\bar{v}_i$ is the partial specific volume of component i. The tilde ~ denotes that $\tilde{J}_i$ is a flux relative to the laboratory fixed frame of reference.

$$\tilde{J}_i^{\phi} = \phi_i v_i \quad (= c_i \bar{v}_i v_i) \tag{6}$$

We will assume that the partial specific volumes are constant. In that case the volume and laboratory fixed frames of reference are equal and it can be derived (from the Gibbs-Duhem equation that relates the X_j's to each other) [6] that J_i^{ϕ} and $\tilde{J}_i^{\phi}$ are related as follows:

$$J_i^{\phi} = \tilde{J}_i^{\phi} - (\phi_i/\phi_3)\tilde{J}_3^{\phi} \qquad i = 1,2 \tag{7}$$

where J_i^{ϕ} refers to a volume flux relative to the polymer fixed frame of reference.
Combination of eqns. (5) and (7) yields

$$\frac{\delta J_i^{\phi}}{\delta x} = -\phi_3 \frac{\delta(\phi_i/\phi_3)}{\delta t} - \tilde{J}_3^{\phi} \frac{\delta(\phi_i/\phi_3)}{\delta x} \qquad i = 1,2 \tag{8}$$

As suggested by Crank [14] we introduce a new position coordinate m (see figure 1) in order to eliminate $\tilde{J}_3^{\phi}$ from eqn. (8).

$$m(x,t) = \int_0^x \phi_3(\xi,t)d\xi \tag{9}$$

$$\delta m(t = \text{constant}) = \phi_3 \delta x(t = \text{constant}).$$

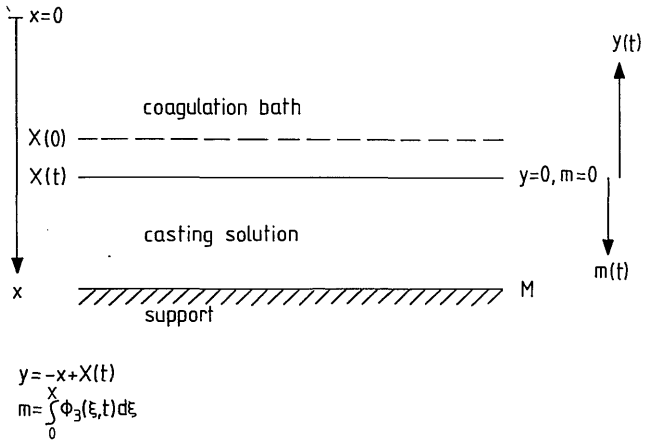

Fig. 1. Schematic representation of the cast polymer solution layer, the coagulation bath and the position coordinates used.

A detailed description will be given of the way in which eqn. (8) is transformed by the transition from x to m position coordinates. In our opinion, McHugh [12] performs this transformation in a wrong way which leads to their erroneous continuity equations.

In the following equations the subscripts to the derivatives refer to constant parameters.

$$\phi_3 \frac{\delta(\phi_i/\phi_3)}{\delta t}/m = \phi_3 \frac{\delta(\phi_i/\phi_3)}{\delta t}/x + \phi_3 \frac{\delta(\phi_i/\phi_3)}{\delta x}/t * \frac{\delta x}{\delta t}/m \tag{10}$$

$$\phi_3 \frac{\delta x}{\delta t}/m = \underline{\tilde{J}}_3^{\phi} \tag{11}$$

$$\frac{\delta \underline{J}_i^{\phi}}{\delta x}/t = \phi_3 \frac{\delta \underline{J}_i^{\phi}}{\delta m}/t \tag{12}$$

By substituting eqn. (10), (11) and (12) in eqn. (8) we find

$$\frac{\delta \underline{J}_i^{\phi}}{\delta m}\Big/t = -\frac{\delta(\phi_i/\phi_3)}{\delta t}\Big/m \qquad i = 1,2 \tag{13}$$

These continuity equations are in agreement with the equations of Wijmans [10] who examined the mass balance in a 'polymer fixed' volume element. They are also in agreement with the equations proposed by Crank [14] to simplify a moving boundary problem.

We now wish to combine the flux eqn. (1) with the continuity eqn. (13) in order to eliminate the fluxes. First we have to substitute the mass fluxes $\underline{J}_i^c$ in eqn. (1) by volume fluxes $\underline{J}_i^{\phi}$

$$\underline{J}_i^{\phi} = -\sum_{j=1}^{2} \bar{v}_i L_{ij} \frac{\delta \mu_j}{\delta x} \qquad i = 1,2 \tag{14}$$

The transition to m position coordinates according to eqn. (9) transforms eqn. (14) into

$$\underline{J}_i^{\phi} = -\sum_{j=1}^{2} \bar{v}_i \phi_3 L_{ij} \frac{\delta \mu_j}{\delta m} \qquad i = 1,2 \tag{15}$$

We see that this transformation leads to the appearance of ϕ_3 in the flux equations, the term that is missing in the flux equations of Cohen et al.

Now we can combine the flux eqn. (15) and the continuity eqn. (13):

$$\frac{\delta(\phi_i/\phi_3)}{\delta t} = \frac{\delta}{\delta m}\left\{ \sum_{j=1}^{2} \bar{v}_i \phi_3 L_{ij}(\phi_1,\phi_2) \frac{\delta \mu_j}{\delta m} \right\} \qquad i = 1,2 \tag{16}$$

These ternary diffusion equations describe the concentration changes as a function of time and place in the immersed polymer solution, if the appropriate boundary and initial conditions are used.

The phenomenological coefficients L_{ij} (defined in the polymer fixed frame of reference) are concentration dependent. We will show how these ternary coefficients can be related to binary frictional coefficients which in turn can be related to measurable diffusion and sedimentation coefficients.

The expressions for the chemical potentials as a function of the composition are given in appendix A.

3.5. The equations describing the binary diffusion in the coagulation bath

We assume that the polymer concentration in the coagulation bath, after immersion of the polymer solution, can be neglected. Fick's second law describes the binary diffusion process

$$\frac{\delta \phi_i}{\delta t} = \frac{\delta}{\delta x} \left\{ D(\phi_i) \frac{\delta \phi_i}{\delta x} \right\} \tag{17}$$

$D(\phi_i)$ is the diffusion coefficient defined in the volume (laboratory) fixed frame of reference.
In the preceding section it has been shown that by the introduction of the position coordinate m in the polymer solution, the moving boundary between the coagulation bath and the solution can be fixed to the position m=o.

For the coagulation bath we introduce a new position coordinate y in order to describe the diffusion behavior in this bath relative to the interfacial boundary (see Figure 1).

$$y = -x + X(t) \tag{18}$$

where X(t) is the position of the boundary between the polymer solution and the coagulation bath, measured in position coordinates x.

The transformation to position coordinates y, according to eqn. (18), converts eqn. (17) into

$$\frac{\delta \phi_i}{\delta t} = \frac{\delta}{\delta y} \left\{ D(\phi_i) \frac{\delta \phi_i}{\delta y} \right\} - \frac{\delta \phi_i}{\delta y} \frac{\delta X(t)}{\delta t} \tag{19}$$

$$\frac{\delta X(t)}{\delta t} = \underline{J}_1^{\phi}(y=0) + \underline{J}_2^{\phi}(y=0) \tag{19a}$$

We will use these equations to describe the diffusion in the unstirred coagulation bath.

3.6. The initial and boundary conditions

At the very moment of immersion of the cast film into the coagulation bath, we consider the film and the bath to be completely homogeneous. This leads to the following initial conditions,

$$\begin{aligned} &y > 0: \ \phi_i^{(c)}(y,0) = \phi_i^{(c)} \qquad i = 1,2 \\ &0 \leqq m \leqq M: \ \phi_i^{(s)}(m,0) = \phi_i^{(s)} \qquad i = 1,2,3 \end{aligned} \tag{20}$$

The superscripts (c) and (s) refer to the coagulation bath and the polymer solution respectively. M is the total volume of polymer per unit area of casting solution.

From the moment of contact between the film and the bath, two different kinds of concentration profiles are possible in the area of contact between the bath and the film:

1. A concentration profile consisting of a boundary layer between two liquid phases and on both sides of this boundary layer steep concentration gradients which become smoother in the course of time.
2. A concentration profile consisting of one steep concentration gradient which becomes smoother in the course of time.

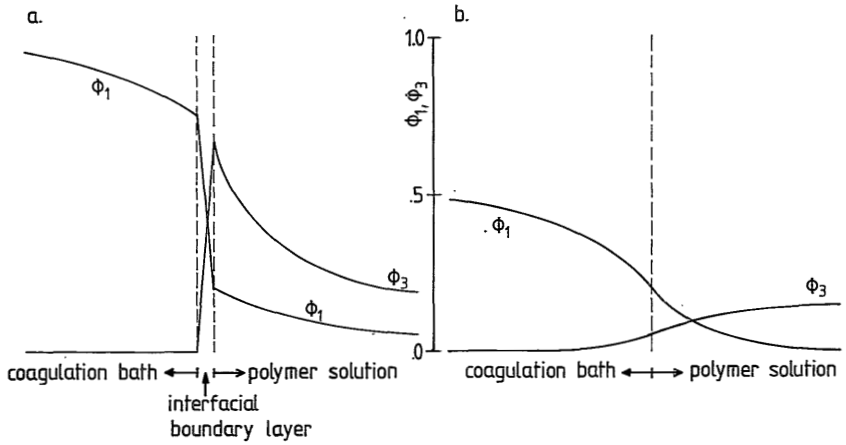

Fig. 2. The two possible kinds of concentration profiles in the contact area between the bath and the solution after immersion of a polymer solution into a coagulation bath. a. Concentration profile with an interfacial boundary layer. b. Concentration profile without an interfacial boundary layer.

Both kinds of concentration profiles are shown in Figure 2.

In Chapter 4 of this thesis we will show that situation 1) correctly describes the actual concentration profile, if the initial solvent concentration in the coagulation bath does not exceed a certain limiting value (i.e. the criterion for demixing conditions must be fulfilled). We will assume that the thickness of the interfacial boundary layer is equal to zero.

One of the principles of irreversible thermodynamics is the existence of a state of local equilibrium even when no equilibrium exists on a macroscopic scale. This means that at the boundary of the two phases considered (the coagulation bath and the polymer solution) the following boundary conditions exist:

$$\mu_i^{(c)}(y=0,t) = \mu_i^{(s)}(m=0,t) \qquad i = 1,2,3 \tag{21}$$

When we consider the ternary phase diagram, eqn. (21) means that at any time the boundary compositions in the film and in the coagulation bath are situated on the binodal and are connected by a tieline. The boundary conditions (21) make it necessary to calculate the tielines using expressions for μ_i as a function of composition. It will be shown that $\phi_3^{(c)}(y=0,t)$ can be neglected if $\phi_2^{(c)}$ does not exceed a certain limiting value.

The other conditions at the boundary of the two phases are

$$\underline{J}_i^{\phi}(y=0,t) = -\underline{J}_i^{\phi}(m=0,t) \qquad i = 1,2 \tag{22}$$

At m=M the boundary conditions are given by

$$\frac{\delta\phi_i}{\delta m} = 0 \qquad i = 1,2 \tag{23}$$

We consider the coagulation bath as being infinitely thick.

Our calculations are only valid as long as the diffusion gradients in the film and in the bath are not disturbed by demixing processes or by convection.

3.7. $mt^{-1/2}$ dependent solutions

In this section we will show that the solution of the equations describing the diffusion in the polymer film is a function of $mt^{-1/2}$ and that the interfacial boundary compositions are constant during a certain period after immersion of the polymer film.

We will start to assume that the interfacial boundary compositions are constant as long as the polymer film can be treated as infinitely thick and the convection in the coagulation bath can be neglected. We will show that these assumptions yield the one and only solution of the equations, obeying the boundary conditions.

The introduction of a new variable $\ell = mt^{-1/2}$ [15] enables us to transform eqn. (16) into

$$\frac{\delta(\phi_i/\phi_3)}{\delta\ell} = -\frac{2}{\ell}\frac{\delta}{\delta\ell}\left\{\sum_{j=1}^{2}\bar{v}_i\phi_3 L_{ij}(\phi_1,\phi_2)\frac{\delta\mu_j}{\delta\ell}\right\} \qquad i = 1,2 \tag{24}$$

Regarding the boundary and initial conditions it follows that the composition in the polymer solution is a function of ℓ, if the above mentioned assumptions hold. Under the same circumstances it can be shown that

$$J_i^{\phi}(m=0,t) = \frac{\delta}{\delta t}\int_o^M \left\{\frac{\phi_i(m,t)}{\phi_3(m,t)} - \frac{\phi_i(m,o)}{\phi_3(m,o)}\right\}dm$$

$$= \frac{1}{2}t^{-1/2}C_i \qquad i = 1,2 \tag{25}$$

the constant C_i being given by

$$C_i = t^{-1/2}\int_o^M \left\{\frac{\phi_i(m,t)}{\phi_3(m,t)} - \frac{\phi_i(m,o)}{\phi_3(m,o)}\right\}dm$$

The rate of movement of the boundary (19a) is given by

$$\frac{\delta X(t)}{\delta t} = -\underline{J}_1^{\phi}(m=0,t) - \underline{J}_2^{\phi}(m=0,t) = -\frac{1}{2}t^{-1/2}(C_1+C_2) \tag{26}$$

We can rewrite the diffusion equation for the coagulation bath by introducing the new variable $\ell' = yt^{-1/2}$:

$$\frac{\delta\phi_i}{\delta\ell'} = \frac{2}{\ell'}\left\{(C_1+C_2)\frac{\delta\phi_i}{\delta\ell'} - \frac{\delta}{\delta\ell'}(D(\phi_i)\frac{\delta\phi_i}{\delta\ell'})\right\} \qquad (27)$$

It follows that the composition in the coagulation bath is a function of ℓ' as long as our assumption holds that no convection takes place and the boundary composition is constant. This implies that

$$\underline{J}_i^{\phi}(y=0,t) = \frac{\delta}{\delta t}\int_0^Y \{\phi_i(y,t) - \phi_i(y,o)\}dy + \frac{\delta X(t)}{\delta t}\phi_i(t=o)$$

$$= \frac{1}{2}t^{-1/2}C_i' \qquad i = 1,2 \qquad (28)$$

where C_i' is given by

$$C_i' = t^{-1/2}\int_0^Y \{\phi_i(y,t) - \phi_i(y,0)\}dy - \{C_1+C_2\}\phi_i(t=0),$$

and Y is a position in the coagulation bath on a constant distance from the interfacial boundary, where the original composition remains unchanged.
If the solvent concentration in the coagulation bath is not too high it is always possible to find a pair of constant boundary compositions obeying condition (21) which yield such C_i's and C_i''s that boundary condition (22) is obeyed.

Thus we have shown that the assumption mentioned at the beginning of this section yields a solution of the diffusion equations that obeys the boundary conditions mentioned in the previous section. Because these boundary conditions restrict the number of solutions of the diffusion equations to only one solution, we can conclude that this unique solution yields constant interfacial boundary compositions under the special circumstances mentioned in the assumption. Besides we have shown that the composition in the film is a function of $mt^{-1/2}$ as long as the composition at m=M remains unchanged and no convection takes place in the coagulation bath. These conclusions simplify the solution of our diffusion problem considerably.

3.8. Ternary phenomenological coefficients L_{ij} simplified to functions of binary frictional coefficients R_{ij}

For the solution of eqn. (16) we need expressions for the phenomenological coefficients L_{ij}. It is possible in principle to obtain the values of L_{ij} by measuring ternary diffusion coefficients as a function of composition. In combination with expressions for the chemical potentials the L_{ij}'s can then be calculated. However, the measurement of ternary diffusion coefficients is a time consuming job. We prefer the parameters in our model to be more easily measurable. Therefore we want to obtain expressions for the ternary L_{ij}'s as a function of binary parameters. These parameters are binary diffusion or sedimentation coefficients, which can be easily obtained.

For the derivation of expressions for L_{ij} as a function of these binary coefficients it is helpful to introduce frictional coefficients R_{ij} which are defined by the Stefan-Maxwell flux equations [16,17]:

$$\frac{\delta \mu_i}{\delta x} = -\sum_{j=1}^{3} R_{ij} c_j (\underline{v}_i - \underline{v}_j) \qquad i = 1,2,3 \tag{29}$$

$\underline{v}_i$ and $\underline{v}_j$ are the average velocities of component i and j with respect to the laboratory fixed frame of reference. Unlike L_{ij} the frictional coefficients R_{ij} are not depending on the choice of frame of reference.

Dunlop [16] shows that eqn. (29) can be reduced to the following form:

$$\frac{\delta \mu_1}{\delta x} = -R_{13} c_3 (\underline{v}_1 - \underline{v}_3) - R_{12} c_2 (\underline{v}_1 - \underline{v}_2) \tag{30}$$

$$\frac{\delta \mu_2}{\delta x} = -R_{21} c_1 (\underline{v}_2 - \underline{v}_1) - R_{23} c_3 (\underline{v}_2 - \underline{v}_3)$$

We assume that $R_{12} = R_{21}$ [16,17] (31)

Because $\delta \mu_i / \delta x$ is the driving force per kg i, $R_{ij} c_j (\underline{v}_i - \underline{v}_j)$ is the frictional force acting between component i and j per kg i.

The references [16,17] work with moles where we work with kg's. This means that their R_{ij}'s differ a factor $M_i * M_j * 10^{-6}$ from the R_{ij}'s defined above. (M_i = molecular weight component i [g mol^{-1}]).

We will first derive the relation between the L_{ij}'s and the R_{ij}'s. Rearrangement of eqn. (30) yields the following expressions:

$$c_i(\underline{v}_i-\underline{v}_3) = -\sum_{j=1}^{2} \frac{\beta_{ij}}{\alpha} \frac{\delta\mu_j}{\delta x} \qquad i = 1,2 \tag{32}$$

where $\beta_{12} = \beta_{21} = c_1c_2R_{12}$, $\beta_{11} = c_1(c_1R_{12}+c_3R_{23})$, $\beta_{22} = c_2(c_2R_{12}+c_3R_{13})$ and $\alpha = c_3(c_2R_{12}R_{23}+c_1R_{12}R_{13}+c_3R_{13}R_{23})$.

When we compare eqn. (32) with eqn. (1) to (3):

$$c_i(\underline{v}_i-\underline{v}_3) = -\sum_{j=1}^{2} L_{ij} \frac{\delta\mu_j}{\delta x} \qquad i = 1,2$$

It is clear that the relation between the phenomenological and the frictional coefficients is given by

$$L_{ij} = \frac{\beta_{ij}}{\alpha} \qquad i = 1,2,\ j = 1,2 \tag{33}$$

This result is in agreement with the expression derived by Spiegler [18].

In the three limiting binary composition ranges eqn. (30) yields the following relations, for $\phi_i+\phi_j = 1$:

$$\frac{\delta\mu_i}{\delta x} = -c_jR_{ij}(\phi_j)(\underline{v}_i-\underline{v}_j) \qquad i = 1,\ j = 2 \text{ or } 3;\ i = 2,\ j = 1 \text{ or } 3. \tag{34}$$

In the next section we will show how the binary frictional coefficients in eqn. (34) are related to binary diffusion or sedimentation coefficients. However, we will first express the ternary frictional coefficients as a function of the binary coefficients $R_{ij}(\phi_j)$. This can be done by adopting a few assumptions concerning the concentration dependence of the ternary frictional coefficients.

For $R_{12}(\phi_1,\phi_2)$ we adopt the assumption that this coefficient is a function of the ratio $\phi_1/\phi_1+\phi_2$. We assume that the presence of the polymer influences the frictional force per m^3 acting between the components 1 and 2. However, the magnitude of the frictional force per kg 1 remains proportional to c_2 at constant ratio $\phi_1/\phi_1+\phi_2$ and varying ϕ_3.

$$R_{12}(\phi_1,\phi_2) = \underset{\phi_3=0}{R_{12}(\phi_1')}, \text{ where } \phi_1' = \frac{\phi_1}{\phi_1+\phi_2} \tag{35}$$

Because of the reciprocal relation (31),

$$R_{21}(\phi_1,\phi_2) = R_{12}(\phi_1,\phi_2) \tag{35a}$$

For the concentration dependence of R_{13} and R_{23} we adopt a different assumption. We assume that these frictional coefficients depend on the polymer volume fraction only. We consider the polymer to act as a porous plug whose permeability for component 1 or 2 is not influenced by the presence of the other low molecular weight component. Thus, we assume that the permeability of the plug is only influenced by the polymer volume fraction.

$$R_{i3}(\phi_i,\phi_3) = \underset{\phi_i+\phi_3=1}{R_{i3}(\phi_3)} \tag{36}$$

In Figure 3 the assumptions (35) and (36) are visualized in a ternary diagram.

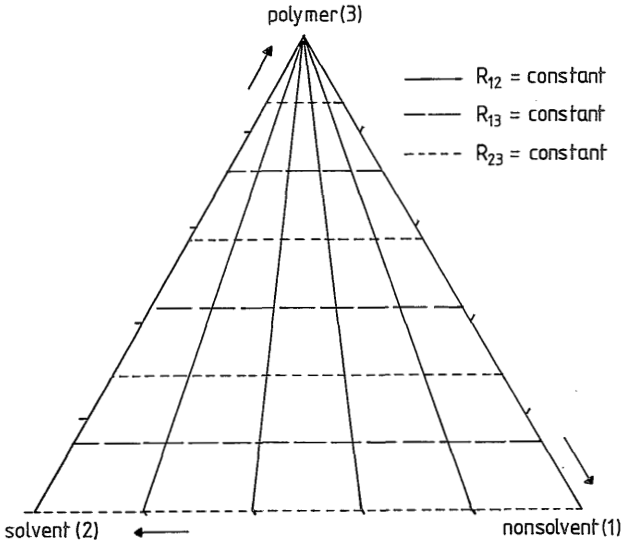

Fig. 3. Lines connecting compositions with equal ternary frictional coefficients R_{ij} according to eqn. (35) and (36).

3.9. Binary frictional coefficients $R_{ij}(\phi_j)$ as a function of binary diffusion or sedimentation coefficients

The binary frictional coefficient R_{ij} can be related to the binary phenomenological coefficient $(L_i)_j$ defined as follows:

$$\underline{J}_i^c = c_i(\underline{v}_i - \underline{v}_j) = -(L_i)_j \frac{\delta\mu_i}{\delta x} \tag{37}$$

Combination of eqns. (37) and (34) yields the following relation:

$$R_{\substack{ij \\ \phi_i+\phi_j=1}} = \frac{\bar{v}_j\phi_i}{\bar{v}_i\phi_j(L_i)_j} \tag{38}$$

In appendix B the following relation between the binary diffusion coefficient D and $(L_i)_j$ has been derived:

$$(L_i)_j = D/(\phi_j \frac{d\mu_i}{dc_i}).$$

Substitution of this expression in eqn. (38) yields the following expression for the binary frictional coefficient:

$$R_{\substack{ij \\ \phi_i+\phi_j=1}} = \frac{\bar{v}_j\phi_i}{D} \frac{d\mu_i}{d\phi_i} \tag{39}$$

In Chapter 4 of this thesis we will use this expression for the calculation of the binary coefficient R_{12}.

The binary coefficient $(L_i)_j$ can also be expressed as a function of the sedimentation coefficient s_j. This relation has been derived for the coefficients $(L_2)_3$ and s_3 in appendix C:

$$(L_2)_3 = \frac{1}{\bar{v}_2(\rho\bar{v}_2-1)} s_3(\phi_3) \tag{40}$$

When we substitute this expression in eqn. (38) we obtain the following ex-

pression for the binary coefficient R_{23}:

$$R_{23}\Big|_{\phi_1=0} = \frac{\phi_2\bar{v}_3(\rho\bar{v}_2-1)}{\phi_3}\,\frac{1}{s_3(\phi_3)} \qquad (41)$$

Thus we can obtain the binary coefficient R_{23} by measuring the sedimentation coefficient of the polymer in the solvent as a function of the concentration. In Chapter 4 of this thesis we will show the results for the system CA-acetone.

It is very difficult to determine R_{13} by means of diffusion or sedimentation measurements because the polymer can be dissolved in the nonsolvent only in a very small concentration range. Even if we could determine R_{13} it is doubtful whether this quantity would describe the friction between nonsolvent and polymer correctly in the presence of an excess amount of solvent. It will appear that mainly in this composition range the ternary diffusion process in a membrane forming system takes place. Thus we have to estimate R_{13}. We will estimate $R_{13}(\phi_3)$ by relating this coefficient to $R_{23}(\phi_3)$. For a proper estimation of $R_{13}(\phi_3)$ it is helpful to derive the relation between R_{13} and R_{23} in the hypothetical case that in a binary system the resistance force per m^3 exerted by the polymer on the nonsolvent equals the resistance force exerted by the polymer on the solvent at the same volume fraction of polymer:

The binary flux equations are given by (see eqn. (37)):

$$\underline{J}_i^{\phi} = -\{\bar{v}_i^2\,(L_i)_3\}*\{\frac{1}{\bar{v}_i}\frac{\delta\mu_i}{\delta x}\} \qquad i = 1,2 \qquad (42)$$

where μ_i is the chemical potential per kg i and $\{\frac{1}{\bar{v}_i}\frac{\delta\mu_i}{\delta x}\}$ is the driving force per m^3. It can be concluded that in our hypothetical case

$$\bar{v}_1^2\,(L_1)_3 = \bar{v}_2^2\,(L_2)_3 \qquad (43)$$

From eqn. (38) and (43) it follows that

$$R_{13} = (\bar{v}_1/\bar{v}_2)R_{23}, \qquad (44)$$

In reality the resistance forces exerted by the polymer on the solvent and the nonsolvent will differ, especially because the sizes of the two low molecular weight components differ. Therefore we will use the following expression for R_{13} in our model calculations:

$$R_{13} = C(\bar{v}_1/\bar{v}_2)R_{23},$$

where C may be constant, or depending on ϕ_3.

3.10. Conclusions

A set of general diffusion equations (eqn. 16) and boundary conditions have been derived for the mass transport in a ternary polymer solution after immersion into a coagulation bath and prior to possible demixing processes.

Additionally, expressions for the binary diffusion in the coagulation bath, relative to the moving boundary between the polymer film and the coagulation bath have been derived (eqns. (19) and (19a)).

As long as the composition at the bottom of the polymer solution remains unchanged, the composition changes in the polymer solution are a function of $mt^{-1/2}$ only. This means that during this period, all compositions existing in the polymer solution can be described by a constant composition trajectory.

The relation between the ternary phenomenological coefficients L_{ij} and the ternary frictional coefficients R_{ij} is given by eqn. (33). We have simplified the ternary frictional coefficients to functions of binary frictional coefficients, eqns. (35) and (36). The frictional coefficient describing the interaction between solvent and nonsolvent is related to the binary diffusion coefficient, eqn. (39). The frictional coefficient describing the interaction between solvent and polymer is related to the sedimentation coefficient, eqn. (41). The frictional coefficient describing the interaction between nonsolvent and polymer must be estimated.

In Chapter 4 of this thesis we will calculate the composition profiles in a cellulose acetate-acetone solution after immersion into water. We will use experimental, concentration dependent, sedimentation and diffusion coefficients in the expressions for R_{ij}. In the expressions for the chemical poten-

tials, eqn. (A2,3,4), we will use experimental concentration dependent Flory Huggins parameters.

An experimental method will be presented to verify the results of the calculations and to estimate the value of R_{13}.

3.11. APPENDIX A. Equilibrium thermodynamics for a three component system

For the expression of the Gibbs free energy of mixing we use the Flory-Huggins theory for polymer solutions [19], extended to systems with three components by Tompa [20]

$$\frac{\Delta G_m}{RT} = n_1 \ln\phi_1 + n_2 \ln\phi_2 + n_3 \ln\phi_3 + g_{12}(u_2) n_1 \phi_2 + \chi_{13} n_1 \phi_3 + g_{23}(v_2) n_2 \phi_3, \quad \text{(A1)}$$

where n_i is the number of moles i and χ_{13} is the nonsolvent polymer interaction parameter; g_{12} is the solvent-nonsolvent interaction parameter which is assumed to be a function of u_2, with $u_2 = \phi_2/(\phi_2+\phi_1)$. g_{23} is the solvent-polymer interaction parameter which is assumed to be a function of $v_2 = \phi_2/(\phi_2+\phi_3)$.

In fact eqn. (A1) is valid only in the case of concentration gradients equal to zero. However, we will neglect the influence of the steep concentration gradients at the boundary between polymer solution and coagulation bath, on the local free energy.

From eqn. (A1) we derive the following equations for the chemical potentials of the components in the mixture:

$$\Delta\mu_1^+/RT = \ln\phi_1 - s\phi_2 - r\phi_3 + (1+g_{12}\phi_2+\chi_{13}\phi_3)(1-\phi_1) - sg_{23}\phi_2\phi_3 - \phi_2 u_2(1-u_2)\frac{dg_{12}}{du_2} \quad \text{(A2)}$$

$$s\Delta\mu_2^+/RT = s\ln\phi_2 - \phi_1 - r\phi_3 + (s+g_{12}\phi_1+sg_{23}\phi_3)(1-\phi_2) - \chi_{13}\phi_1\phi_3 + \phi_1 u_2(1-u_2)\frac{dg_{12}}{du_2} + s\phi_3 v_2(1-v_2)\frac{dg_{23}}{dv_2} \quad \text{(A3)}$$

$$r\Delta\mu_3^+/RT = r\ln\phi_3 - \phi_1 - s\phi_2 + (r+g_{23}s\phi_2+\chi_{13}\phi_1)(1-\phi_3)$$
$$-g_{12}\phi_1\phi_2 - s\phi_2 v_2(1-v_2)\frac{dg_{23}}{dv_2} \qquad (A4)$$

The chemical potentials are expressed per kmole of segments of component 1; s and r are the ratios of the molar volumina:

$$s = \frac{\bar{v}_1 M_1}{\bar{v}_2 M_2}, \qquad r = \frac{\bar{v}_1 M_1}{\bar{v}_3 M_3}$$

We use the expressions (A2) and (A3) in the diffusion equations for the polymer solution. For the boundary condition we have to evaluate all three expressions for the chemical potentials. The conditions for liquid-liquid equilibrium (at the boundary) are:

$$\Delta\mu_i^+ \text{ (diluted phase)} = \Delta\mu_i^+ \text{ (concentrated phase)} \quad (i=1,2,3) \qquad (A5)$$

Altena [11] describes how the binodal and the tielines, connecting the coexisting phases in a ternary diagram, can be calculated.

3.12. APPENDIX B. The relation between the binary coefficients $(L_i)_j$ and D

The binary diffusion coefficient D is measured relative to the laboratory fixed frame of reference, which is equal to the volume fixed frame of reference in the case of constant partial volumes $\bar{v}_i$.
The relation between D and $\tilde{L}_i$ is given by

$$\underline{\tilde{J}}_i^c = c_i\underline{v}_i = -D\frac{\delta c_i}{\delta x} = -\tilde{L}_i\frac{\delta\mu_i}{\delta x} \qquad (B1)$$

where $\tilde{L}_i$ is the phenomenological coefficient defined in the volume fixed frame of reference.
From eqn. (B1) it can be derived that

$$\frac{D}{d\mu_i/dc_i} = \tilde{L}_i \tag{B2}$$

The relation between the coefficient $(L_i)_j$, defined in the component j fixed frame of reference, and D is derived as follows:

$$-(L_i)_j \frac{\delta\mu_i}{\delta x} = c_i(\underline{v}_i - \underline{v}_j) = \frac{c_i}{\phi_j}\{(1-\phi_i)\underline{v}_i - \underline{\tilde{J}}_j^{\phi}\} =$$

$$\frac{c_i}{\phi_j}\{(1-\phi_i)\underline{v}_i + \underline{\tilde{J}}_i^{\phi}\} = \frac{c_i\underline{v}_i}{\phi_j} = -\frac{\tilde{L}_i}{\phi_j}\frac{\delta\mu_i}{\delta x} \tag{B3}$$

From eqn. (B2) and (B3) it follows that

$$(L_i)_j = D/(\phi_j \frac{d\mu_i}{dc_i}) \tag{B4}$$

3.13. APPENDIX C. The relation between the binary coefficient $(L_2)_3$ and the sedimentation coefficient s_3

s_3 is related to a phenomenological coefficient Q, defined below [21]:

$$s_3 = Q\frac{\rho\bar{v}_2}{c_3}(1+c_3/c_2)(1-\rho\bar{v}_3) \tag{C1}$$

where $s_3 = \underline{v}_3/g$, with $\underline{v}_3$ the average velocity of component 3 relative to the laboratory fixed frame of reference, and g the centrifugal field strength. $\rho = c_2 + c_3$, the solution density.
In the absence of a centrifugal field Q is defined as follows [21]:

$$\underline{J}_3^{*c} = -Q(1+c_3/c_2)\frac{\delta\mu_3}{\delta x} \tag{C2}$$

where $\underline{J}_3^{*c}$ is the mass flux of component 3 relative to the mass fixed frame of reference.
Conversion of Q from the mass fixed frame of reference to the polymer fixed frame of reference yields the following relation between Q and $(L_2)_3$:

$$(L_2)_3 = \frac{\rho c_2 (1 - c_3/c_2)}{c_3^2} Q$$

When we substitute this relation in expression (C1) we obtain

$$(L_2)_3 = \frac{1}{\bar{v}_2(\rho\bar{v}_2 - 1)} s_3(\phi_3) \qquad (C3)$$

3.14. List of symbols

$\bar{v}_i$ Partial volume of component i ($m^3\ kg^{-1}$)

ϕ_i Volume fraction of component i

c_i Concentration of component i ($kg\ m^{-3}$)

ρ Solution density = $\sum_i c_i$ ($kg\ m^{-3}$)

M_i Molecular weight of component i ($g\ mol^{-1}$)

χ_{ij} Flory-Huggins interaction parameter

g_{ij} concentration dependent Flory-Huggins interaction parameter

s $\bar{v}_1 M_1 / \bar{v}_2 M_2$

r $\bar{v}_1 M_1 / \bar{v}_3 M_3$

μ_i Chemical potential of component i ($J\ kg^{-1}$)

μ_i^+ Chemical potential of component i ($J\ kmol^{-1}$)

R Gas constant ($J\ K^{-1}\ kmol^{-1}$)

s_i Sedimentation coefficient of component i

L_{ij} Ternary phenomenological coefficient, defined in polymer fixed frame of reference, eqn. (1-3)

$(L_i)_j$ Binary phenomenological coefficient, defined in polymer fixed frame of reference, eqn. (37)

$\bar{L}_i$ Binary phenomenological coefficient, defined in volume fixed frame of reference, eqn. (B1)

Q Binary phenomenological coefficient, defined in mass fixed frame of reference, eqn. (C2)

D Binary mutual diffusion coefficient, defined in volume fixed frame of reference, eqn. (B1)

$\underline{v}_i$ average velocity of component i relative to the laboratory fixed frame of reference

$\underline{J}_i$ Flux of component i, relative to the polymer fixed frame of reference

$\underline{\tilde{J}}_i$ Flux of component i, relative to the volume fixed frame of reference

$\underline{J}_i^*$ Flux of component i, relative to the mass fixed frame of reference

$\underline{J}_i^\Phi$ Volume flux of component i ($m\ s^{-1}$)

$\underline{J}_i^C$ Mass flux of component i ($kg\ m^{-2}\ s^{-1}$)

R_{ij} Frictional coefficient describing the interaction between the components i and j (defined in eqn. (29))

C_i Constant defined in eqn. (25)

C_i' Constant defined in eqn. (28)

x Cartesian spatial position coordinate perpendicular to the membrane surface (m)

X Position of the interface between the film and the coagulation bath (m)

m Position coordinate of the polymer fixed reference frame, defined in eqn. (9) (m)

y Position coordinate relative to X(t) (m)

M Total volume of polymer per unit area of polymer film (m)

l $mt^{-1/2}$

l' $yt^{-1/2}$

3.15. References

1. S. Loeb and S. Sourirajan, Advan. Chem. Ser., 38 (1962) 117.
2. J.E. Anderson and R. Ullman, Mathematical analysis of factors influencing the skin thickness of asymmetric reverse osmosis membranes, J. Appl. Phys., 44:10 (1973) 4303.
3. C. Castellari and S. Ottani, Preparation of reverse osmosis membranes. A numerical analysis of asymmetric membrane formation by solvent evaporation from cellulose acetate casting solutions, J. Membrane Sci., 9 (1981) 29.
4. M. Ataka and K. Sasaki, Gravimetric analysis of membrane casting solutions, J. Membrane Sci., 11 (1982) 11.
5. R.J. Ray, Interfacial instabilities arising from excess intermolecular potential gradients: application to asymmetric membrane morphology. Thesis, University of Colorado, Chapter 3, (1983).
6. C. Cohen, G.B. Tanny and S. Prager, Diffusion-controlled formation of

porous structures in ternary polymer systems, J. Polym. Sci., Pol. Phys. Ed., 17 (1979) 477.

7. H.K. Lonsdale, Properties of cellulose acetate membranes, Desalination by reverse osmosis, U. Merten, Ed., M.I.T. Press, Cambridge, Mass., (1966) 93.
8. J.G. Wijmans, H.J.J. Rutten and C.A. Smolders, Phase separation phenomena in solutions of poly (2,6-dimethyl-1,4-phenyleneoxide) in mixtures of trichloroethylene, 1-octanol and methanol: relationship to membrane formation, J. Polym. Sci., Pol. Phys. Ed., 23 (1985) 1941.
9. A.J. Reuvers, F.W. Altena and C.A. Smolders, Demixing and gelation behavior of ternary cellulose acetate solutions, J. Polym. Sci., Pol. Phys. Ed., 24 (1986) 793.
10. J.G. Wijmans, F.W. Altena, C.A. Smolders, Diffusion during the immersion precipitation process, J. Polym. Sci., Pol. Phys. Ed., 22 (1984) 519.
11. F.W. Altena and C.A. Smolders, Calculation of liquid-liquid phase separation in a ternary system of a polymer in a mixture of a solvent and a nonsolvent, Macromolecules, 15 (1982) 1491.
12. A.J. McHugh and L. Yilmaz, The diffusion equations for polymer membrane formation in ternary systems, J. Pol. Sc., Phys. Ed., 23 (1985) 1271.
13. S.R. de Groot and P. Mazur, Non-equilibrium thermodynamics, Amsterdam: North-Holland Publ. Co. (1962).
14. G.S. Hartley and J. Crank, Some fundamental definitions and concepts in diffusion processes, Trans. Far. Soc., 45 (1949) 801.
15. J. Crank, The mathematics of diffusion, Clarendon Press, Oxford (1975), 104.
16. P.J. Dunlop, Frictional coefficients for binary and ternary isothermal diffusion, J. Phys. Chem., 68,1 (1964) 26.
17. R.W. Laity, An application of irreversible thermodynamics to the study of diffusion. J. Phys. Chem., 63 (1959) 80.
18. K.S. Spiegler, Transport processes in ionic membranes, Trans. Far. Soc., 54 (1958) 1409.
19. P.J. Flory, Principles of polymer chemistry, Cornell Univ. Press, Ithaca (1953), 541.
20. H. Tompa, Polymer solutions, Butterworths, London (1956) 182.
21. P.F. Mijnlieff and W.J.M. Jaspers, Solvent permeability of dissolved polymer material. Its direct determination from sedimentation measurements, Trans. Far. Soc., 67 (1971) 1837.

4. THE MECHANISM OF FORMATION OF MEMBRANES PREPARED FROM THE SYSTEM CELLULOSE ACETATE/ACETONE/WATER

By A.J. Reuvers and C.A. Smolders

4.1. Summary

Using equations and boundary conditions derived in Chapter 3, we have performed calculations on the ternary diffusion processes that occur in a cellulose-acetate (CA)-acetone casting solution immersed into a water bath.

We have derived the necessary concentration dependent thermodynamic and hydrodynamic parameters from experimental data on the three limiting binary mixtures.

Calculations show that immersion of the polymer solution into the coagulation bath results in an instantaneous increase of the polymer concentration at the surface of the solution.

For a CA-acetone casting solution the thickness of this concentrated surface layer will increase until the onset of liquid-liquid demixing by means of nucleation and growth of the diluted phase, that fixes the asymmetric polymer distribution in the film. The moment of onset of the demixing process depends on the thickness of the film.

However, addition of a certain minimum amount of water to the casting solution results in an instantaneous onset of liquid-liquid demixing upon immersion, yielding a membrane with a very thin skin layer.

The model calculations have been confirmed by light transmission measurements performed on immersed casting solutions.

4.2. Introduction

In Chapter 3 equations and boundary conditions have been derived, describing the diffusion processes that occur after immersion of a cast polymer solution into a nonsolvent bath, prior to possible demixing processes.

In this Chapter we will apply this formalism to a ternary system for which enough parameters are known. We will describe the diffusion processes in a

polymer solution consisting of cellulose acetate (CA) and acetone, immersed into a water bath. This system contains three of the basic components from which Loeb-Sourirajan-type membranes are prepared. Thus, the calculations presented in this paper may serve as a base when considering the mechanism of formation of these type of membranes.

We will calculate composition paths representing composition changes as a function of time or place for different coagulation bath or casting solution compositions.

The attention will be focussed on the position of the composition path relative to the position of the binodal in the ternary phase diagram. When the composition becomes metastable somewhere in the polymer solution, i.e. when the composition path crosses the binodal curve, nuclei of the polymer poor phase are formed which may grow out to be the pores in the ultimate membrane.

The moment at which this liquid-liquid demixing process will occur in the casting solution can be calculated with our diffusion model and measured by means of light transmission experiments performed on immersed casting solutions. Thus, we have a simple method at our disposal to test the diffusion model.

Besides the influence of liquid-liquid demixing we will also discuss the influence of aggregate formation on the ultimate membrane structure.

Before we present the values of the parameters used in our model calculations, we will give a short summary of the equations, relations and boundary conditions derived in Chapter 3.

The equations that describe the ternary diffusion in the polymer solution are given by:

$$\frac{\delta(\phi_i/\phi_3)}{\delta t} = \frac{\delta}{\delta m}\left\{\sum_{j=1}^{2} \bar{v}_i \phi_3 L_{ij} \frac{\delta \mu_j}{\delta m}\right\} \qquad i = 1,2 \qquad (1)$$

where $\bar{v}_i$ and ϕ_i are the partial specific volume and the volume fraction of component i respectively; μ_j is the chemical potential of component j and m is a special position coordinate described in Chapter 3. The subscripts 1, 2 and 3 refer to nonsolvent, solvent and polymer, respectively.

For a complete list of symbols we refer to Chapter 3.

The ternary coefficients L_{ij} have been expressed as a function of ternary

frictional coefficients R_{ij}:

$$L_{ij} = \frac{\beta_{ij}}{\alpha}, \tag{2}$$

where $\beta_{12} = \beta_{21} = c_1 c_2 R_{12}$, $\beta_{11} = c_1(c_1 R_{12} + c_3 R_{23})$, $\beta_{22} = c_2(c_2 R_{12} + c_3 R_{13})$ and $\alpha = c_3(c_2 R_{12} R_{23} + c_1 R_{12} R_{13} + c_3 R_{13} R_{23})$.

c_i is the concentration of component i in (kg/m^3).

The ternary frictional coefficient R_{12} has been related to the mutual diffusion coefficient D and the chemical potential μ_1 in the binary solvent-nonsolvent mixture:

$$R_{12}(\phi_1,\phi_2) = \underset{\phi_3=0}{R_{12}(\phi_1')} = \frac{\bar{v}_2 \phi_1'}{D(\phi_1')} \frac{d\mu_1}{d\phi_1'}, \text{ where } \phi_1' = \frac{\phi_1}{\phi_1+\phi_2} \tag{3}$$

The ternary frictional coefficient R_{23} has been related to the binary sedimentation coefficient s_3:

$$R_{23}(\phi_2,\phi_3) = \underset{\phi_1=0}{R_{23}(\phi_3)} = \frac{(1-\phi_3)\bar{v}_3(\rho\bar{v}_2-1)}{\phi_3} \frac{1}{s_3(\phi_3)}, \tag{4}$$

where ρ is the density of the binary polymer-solvent mixture.

The frictional coefficient R_{13} has been related to R_{23}:

$$R_{13} = C(\bar{v}_1/\bar{v}_2)R_{23} \tag{5}$$

We will assume C to be a constant that has to be estimated.

The binary diffusion in the coagulation bath is described by the following equation:

$$\frac{\delta\phi_i}{\delta t} = \frac{\delta}{\delta y}\left\{D(\phi_i)\frac{\delta\phi_i}{\delta y}\right\} - \frac{\delta\phi_i}{\delta y}\frac{\delta X(t)}{\delta t}, \tag{6}$$

where y is a special position coordinate relative to the moving interface between bath and film and X(t) is the position of this interface.

The boundary conditions at this interface are as follows:
- The chemical potentials are equal at both sides of the interface for all three components.
- The fluxes of component 1 and those of component 2 are equal at both sides of the interface.

In the next sections the values of the parameters used in the diffusion equations will be given. These parameters are:
- the binary thermodynamic interaction parameters $g_{12}(\phi_2)$, $g_{23}(\phi_2)$ and χ_{13} from which the chemical potentials are derived;
- the mutual diffusion coefficient $D(\phi_1)$ for acetone-water mixtures and the sedimentation coefficient $s_3(\phi_3)$ for CA in acetone;
- the molecular weights M_i and the constant partial volumes $\bar{v}_i$ for i = 1, 2 and 3.

4.3. Thermodynamic interaction parameters g_{12}, g_{23} and χ_{13} derived from experimental data.

In appendix A of Chapter 3, expressions for the chemical potentials μ_1, μ_2 and μ_3 are presented. In this section we will present the values of the thermodynamic interaction parameters for the binary mixtures acetone-water, CA-acetone and CA-water.

The concentration dependent parameter $g_{12}(\phi_2)$, representing the interaction between water and acetone, has been calculated from literature data [1] on the excess free energy G^E in the following way [2]:

$$g_{12}(\phi_2) = \frac{1}{x_1\phi_2}\left[x_1\ln(x_1/\phi_1) + x_2\ln(x_2/\phi_2) + G^E/RT\right], \qquad (7)$$

where x_1 represents the mole fraction of water in the mixture.

The calculated values for g_{12} are strongly concentration dependent as can be seen in Figure 1. We will describe $g_{12}(\phi_2)$ for acetone-water at 25°C as follows:

$$g_{12} = 0.979 + 1.127 \exp(-2.306\ \phi_1) + 0.292 \exp(-12.564\ \phi_1) \qquad (8)$$

The concentration dependent parameter g_{23} for CA-acetone mixtures, determined by means of osmotic pressure measurements, has been given by Altena [3]:

$$g_{23} = 0.645 - 0.11\ \phi_2 \quad (25°C) \qquad (9)$$

g_{23} appears to be less strongly concentration dependent than g_{12}.

We describe the thermodynamic interaction between water and CA with a constant parameter χ_{13}, measured by means of swelling experiments [4]:

$$\chi_{13} = 1.4 \quad (25°C)$$

These binary parameters will be used in the expressions for the chemical potentials of the ternary system CA/acetone/water.

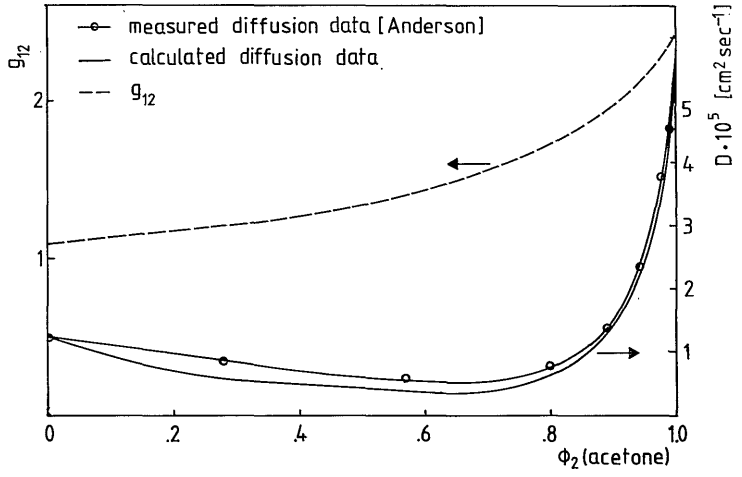

Fig.1. Concentration dependence of the thermodynamic interaction parameter g_{12} and the mutual diffusion coefficient D for the binary system acetone-water at 25°C.

4.4. The liquid-liquid demixing gap

The ternary system CA/acetone/water is not miscible in all proportions. It is possible to calculate the binodal and spinodal curve using the expressions for the chemical potentials described in appendix A of Chapter 3 and the thermodynamic interaction parameters described in the previous section.
We have calculated the binodal and spinodal curve assuming the CA to be monodisperse, with M_3 equal to 27,000.

In Figure 2 the calculated binodal and tielines are shown in a phase diagram together with the measured position of the liquid-liquid demixing gap [5]. It can be concluded that the measured position of the demixing gap and the calculated position of the binodal curve are in good agreement. This implies that the chemical potentials in this ternary system are well described by expressions with binary concentration dependent interaction parameters. We use these expressions for the chemical potentials not only for the calculation of the position of the demixing gap, but also in the diffusion equations (1) and for the calculation of the interfacial boundary compositions.

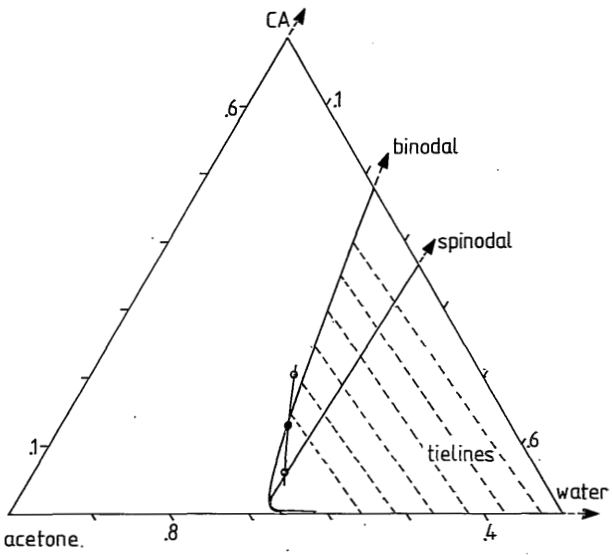

Fig. 2. Isothermal phase diagram for the system CA/acetone/water.
-O-: measured position of the liquid-liquid demixing gap at 20°C [4]. The binodal and the spinodal are calculated using interaction parameters measured at 25°C.

4.5. The binary frictional coefficient R_{12} derived from experimental diffusion data.

In the introduction of this paper the relation between R_{12} and the mutual diffusion coefficient for water-acetone mixtures is given by equation (3):

$$R_{12}(\phi_1) = \frac{\bar{v}_2\phi_1}{D(\phi_1)} \frac{d\mu_1}{d\phi_1} \qquad (\phi_3=0)$$

The chemical potential μ_1 (per kg of component 1) is given by:

$$\frac{M_1}{RT} \Delta\mu_1 = \ln\phi_1 + (1-\phi_1)\{1-s+(1-\phi_1)(g_{12}+\phi_1 \frac{dg_{12}}{d\phi_1})\}, \qquad (10)$$

where s is equal to $\bar{v}_1M_1/\bar{v}_2M_2$. The interaction parameter g_{12} is given by expression (8).

For mixtures of acetone and water we will assume R_{12} to be independent on $\phi_1/\phi_1+\phi_2$ and to be equal to $R_{12}(\phi_1=1)$ in our model calculations. From equations (3) and (10) it can be derived that

$$R_{12}(\phi_1) = R_{12}(\phi_1=1) = \frac{\bar{v}_1RT}{M_2D(\phi_1=1)} \qquad (11)$$

As a consequence of the assumption that R_{12} is constant, D must be given by:

$$D(\phi_1) = \frac{\bar{v}_2M_2\phi_1}{\bar{v}_1RT} \frac{d\mu_1}{d\phi_1} D(\phi_1=1) \qquad (12)$$

We will compare the diffusion coefficients calculated according to equation (12) with the measured values presented by Anderson [6]. Both the measured and the calculated values of $D(\phi_1)$ for the system acetone-water at 25°C are shown in Figure 1. The calculated diffusion coefficients approximately correspond to the measured diffusion coefficients. Hence we can conclude that expression (11) is a reasonable approximation for $R_{12}(\phi_1)$. From Figure 1 it follows that $D(\phi_1=1) = 1.25 * 10^{-9}$ m²/sec.

Expression (12) will be used in the equation that describes the diffusion process in the coagulation bath.

4.6. The binary frictional coefficient R_{23} derived from sedimentation measurements.

The relation between R_{23} and the sedimentation coefficient $s_3(\phi_3)$ is given by equation (4):

$$R_{23}(\phi_3) = \frac{(1-\phi_3)\bar{v}_3(\rho\bar{v}_2-1)}{\phi_3} \frac{1}{s_3(\phi_3)} \qquad (\phi_1=0)$$

We have performed sedimentation experiments for solutions of CA in acetone in order to obtain values for R_{23} as a function of ϕ_3. The experiments have been performed with a Beckman-Spinco model E Analytical Ultra Centrifuge. The sedimentation coefficients have been determined from the displacement of the maximum of the concentration gradient curve.

The CA used, obtained from Eastman Kodak, had an acetyl content of 39.8% and a viscosity number 3 (ASTM); $\bar{M}_n$ = 27,000, $\bar{M}_w$ = 54,000.

The partial volume of CA in acetone has been calculated from the slope of the solution density versus concentration plot.

The partial volume appears to be independent on concentration within the experimental concentration range (up to ϕ_3=0.12) and has a value of $0.7 * 10^{-3}$ m^3kg^{-1} at 20°C.

In Figure 3(a) the sedimentation coefficient is shown as a function of the volume fraction of polymer.

In order to transform expression (4) into a form comparable to expression (11) we introduce the variable $F(\phi_3)$:

$$F(\phi_3) = \frac{RT\phi_3}{M_2(\rho\bar{v}_2-1)(1-\phi_3)} s_3(\phi_3) \qquad (13)$$

When we substitute $F(\phi_3)$ into expression (4) R_{23} is given by:

$$R_{23}(\phi_3) = \frac{\bar{v}_3 RT}{M_2 F(\phi_3)} \qquad (14)$$

Thus R_{12} can be compared with $R_{23}(\phi_3)$ by comparing $D(\phi_1=1)$ with $F(\phi_3)$. From figure 3(b) it follows that $F(\phi_3)$ depends strongly on concentration. A linear relationship between log $F(\phi_3)$ and ϕ_3 exists for $0.05 < \phi_3 < 0.12$. Therefore, we will approximate $F(\phi_3)$ for $\phi_3 > 0.05$ with the following expression:

$$F(\phi_3) = 1.66 * 10^{(-8-5.17\ \phi_3)} \ m^2/sec. \qquad (15)$$

For $\phi_3 \to 1$, $F(\phi_3) = 1.1 * 10^{-13}$ m²/sec according to this expression. It can be shown that in this limiting case $F(\phi_3)$ must be equal to the self diffusion coefficient of acetone in CA. G.S. Park [7] has measured the self diffusion coefficient of acetone in CA for $0.15 < \phi_2 < 0.25$. Extrapolation of the data of Park to $\phi_2 \to 0$ yields a self diffusion coefficient of $2 * 10^{-14}$ m²/sec. This value is approximately in accordance with the value of $F(\phi_3=1)$. The validity of expression (15) is hereby confirmed.

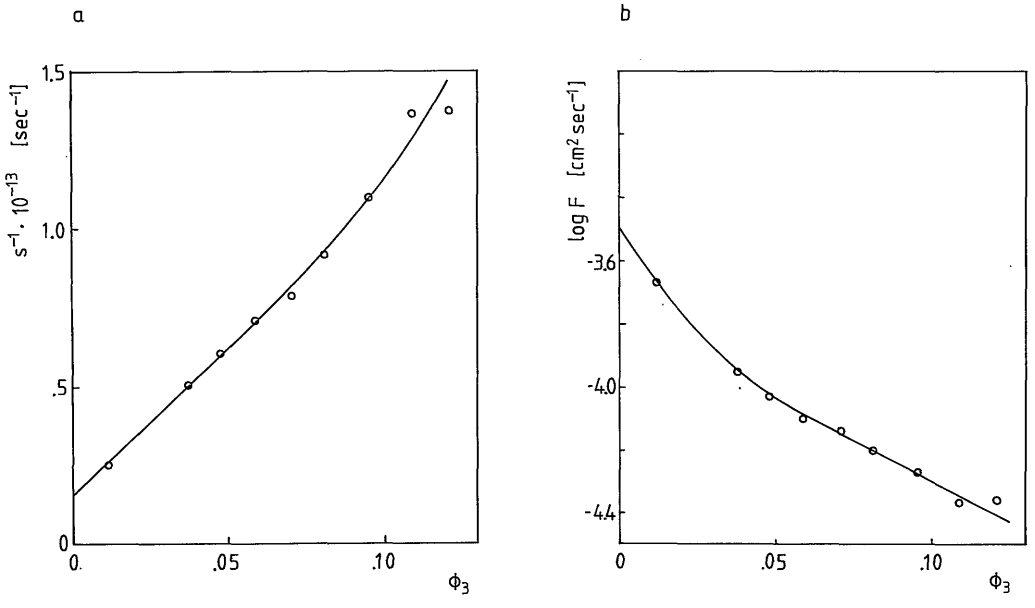

Fig. 3. a. Concentration dependence of the sedimentation coefficient s for CA in acetone at 20°C; b. Concentration dependence of F, a variable proportional to the frictional coefficient R_{23} (see eqn. 14).

4.7. Influence of the various frictional coefficients on the rate of diffusion.

Knowing the experimental values for the binary frictional coefficients, it is interesting to examine whether the frictional force between solvent and nonsolvent can be neglected compared to the frictional force exerted by the polymer on the low molecular weight components as proposed by Cohen [8].

The obscure influence of the various binary frictional coefficients on the rate of diffusion can be elucidated when we adopt the following simplifications concerning the thermodynamics of the ternary system:

$$g_{12} = g_{23} = \chi_{13} = 0$$

$$\bar{v}_1 M_1 = \bar{v}_2 M_2$$

Moreover, we assume that $R_{13} = (\bar{v}_1/\bar{v}_2)R_{23}$ (The constant C in expression (5) is taken 1).

Let us consider a ternary solution with gradients in the solvent and nonsolvent concentration, but without a gradient in the polymer volume fraction. The above mentioned assumptions make it possible to describe the diffusion process in this solution with the following equation, derived from eqn. (1):

$$\frac{\delta\phi_i}{\delta t} = \frac{\delta}{\delta x}\left\{\frac{F(\phi_3)\ D(\phi_1=1)}{(1-\phi_3)\ F(\phi_3) + \phi_3\ D(\phi_1=1)}\right\}\frac{\delta\phi_i}{\delta x}, \qquad i = 1 \text{ or } 2 \qquad (16)$$

This equation describes a kind of binary diffusion process in a polymer matrix of which the density can be chosen. The diffusion coefficient for this process, D' is given by the term between brackets.

$D(\phi_1=1) = 1.25 * 10^{-9}$ m²/sec and $F(\phi_3)$ is represented by expression (15).

We will calculate the value of $D'(\phi_3)$ for $\phi_3=0.15$. This polymer volume fraction is approximately equal to a CA weight fraction in acetone of 0.25, which is the usual CA content in a Loeb-Sourirajan-type casting solution. For $\phi_3=0.15$ it follows that $D' = 1.36 * 10^{-9}$ m²/sec.

When the frictional force acting between solvent and nonsolvent is neglected ($D(\phi_1=1) \to \infty$) as proposed by Cohen et al. [8] it follows that $D' = 18.6 * 10^{-9}$ m²/sec.

When the frictional forces acting between polymer and the low molecular weight components are neglected ($F \rightarrow \infty$) it follows that $D' = 1.47 * 10^{-9}$ m^2/sec.

From these results it can be concluded that for the system CA/acetone/water the frictional force acting between solvent and nonsolvent may not be neglected (as proposed by Cohen [8]) if one wishes to describe the diffusion behavior at a polymer volume fraction of 0.15.

4.8. Calculated composition paths valid for a short period after immersion

In this section we will present calculated composition changes in an immersed CA solution during the period over which the bottom composition of the film remains unchanged. In Chapter 3 we have shown that during this period the interfacial boundary compositions remain constant.

First, we will give a short description of the iterative procedure followed for the calculation of concentration profiles in the film as a function of time, for certain initial compositions of the coagulation bath and the polymer solution:

- The diffusion equations for the semi infinitely thick film (eqn. (1)) are solved for a randomly chosen interfacial boundary composition which is situated on the binodal in the phase diagram.
- The fluxes of solvent and nonsolvent at the interfacial boundary of the polymer solution are calculated with eqn. (25) of Chapter 3.
- These fluxes are used to calculate the rate of movement of the interfacial boundary, $\delta X/\delta t$ (eqn. (26), Chapter 3).
- $\delta X/\delta t$ is used to solve the diffusion equation for the coagulation bath (eqn.(6)), for the interfacial boundary composition that is in equilibrium (connected through a tie-line) with the interfacial boundary composition of the film.
- The solvent flux at the interfacial boundary of the bath is calculated with eqn. (28) of Chapter 3 and compared with the solvent flux at the other side of the boundary, calculated before.
- This procedure is repeated by choosing other interfacial boundary compositions until the calculated solvent fluxes at both sides of the interface are equal.

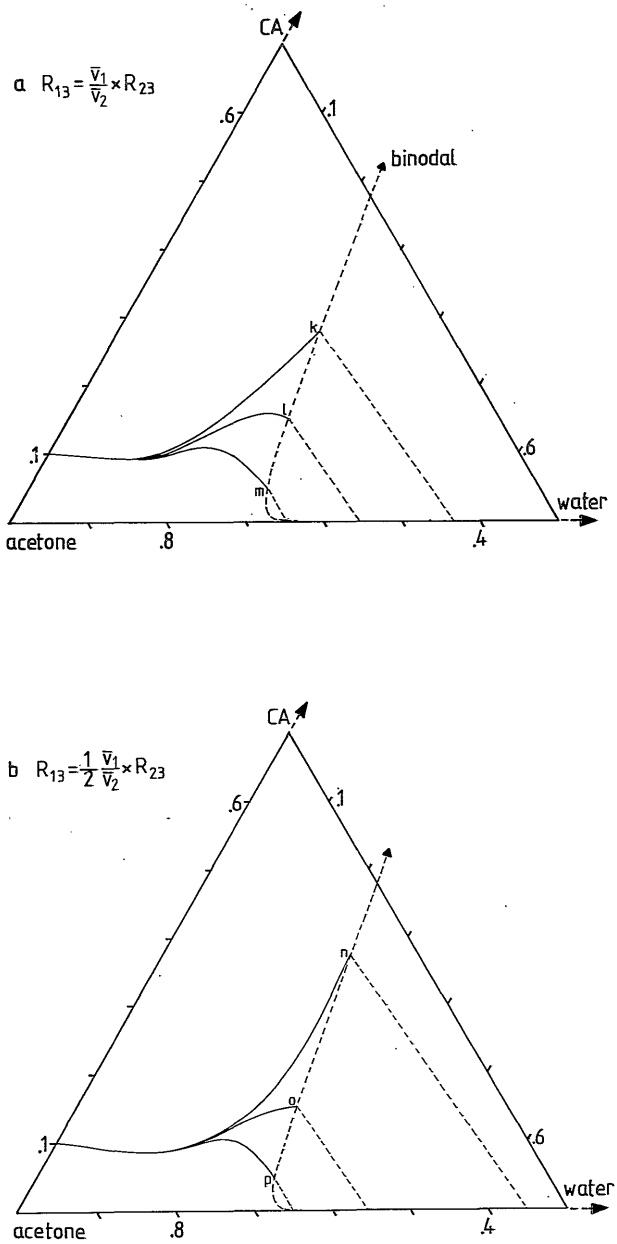

Fig. 4. Calculated composition paths for 10 vol.% CA solutions immersed into coagulation baths with different initial compositions. The index at the interfacial boundary composition refers to the corresponding initial bath concentration shown in Figure 5.

Because we wish to examine whether metastable compositions are reached somewhere in the polymer solution we will represent the calculated composition changes in the film in a ternary phase diagram. This can be carried out by representing the composition changes by means of 'composition paths'.

In this section we consider the film to be infinitely thick. Under these circumstances, the composition change in the film is a function of $mt^{-1/2}$ and the composition path can be interpreted in two different ways:

- The path shows the succession of compositions at a fixed position in the film from the initial composition to the composition for $t \rightarrow \infty$.
- The path shows the succession of compositions at a fixed moment from the bottom of the film to the interfacial boundary.

The derivation of the composition paths from the calculated concentration profiles goes along with a loss of information about the concentration distribution in the film as a function of time. However, in a following section we will show a calculated composition profile.

For our calculations we assume the initial polymer volume fraction in the film to be equal to 0.1. This corresponds with a CA weight fraction in acetone equal to 0.17.

In Figure 4 compositions paths are shown for different initial compositions of the coagulation bath, calculated using two different expressions for the unknown parameter R_{13}. Which path belongs to which initial concentration follows from Figure 5, where the boundary composition of the film is shown as a function of the initial composition of the coagulation bath. The corresponding boundary compositions are equally indexed in both figures. The tielines in Figure 4 connect the interfacial boundary compositions of the film and the coagulation bath.

An increase of the initial acetone concentration in the bath goes along with a decrease of the polymer concentration at the interfacial boundary of the film. At a certain initial solvent concentration in the bath the two-phase system cannot exist any further and the interfacial boundary layer will disappear. This means that the polymer starts to dissolve in the coagulation bath.

However, the polymer will also dissolve in the coagulation bath if this contains exactly or a little more than the amount of solvent necessary to create an interfacial boundary layer. For example, if the polymer concentration at the boundary of the film is equal to 5%, the polymer concentration at

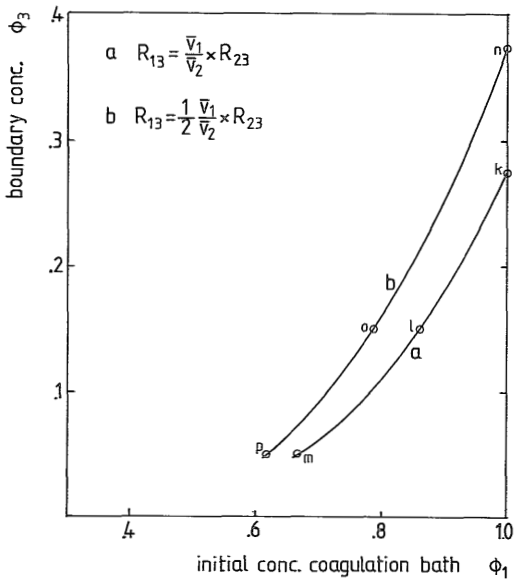

Fig. 5. Polymer concentration at the interfacial boundary in the immersed film as a function of the initial water concentration in the coagulation bath. The indices at the different boundary compositions refer to the corresponding composition paths shown in Figure 4.

the boundary of the bath will be 0.1%, which means transfer of polymer from the film. In Chapter 5 we will show that this concentration is in fact considerably higher than 0.1% because of the polydispersity of the polymer.

We will now consider the case in which the coagulation bath consists of pure water at the start of each experiment. A varying amount of water is added to the casting solution while the polymer volume fraction is kept constant at 0.1.

In Figure 6 composition paths are shown which describe the composition change in the film during the time the bottom composition of the film remains unchanged. The unknown parameter R_{13} has been varied in the same way as in Figure 4 and 5.

Figure 6 shows that the polymer concentration at the interfacial boundary increases with increasing water content of the casting solution. However, most striking is the fact that an increasing water content of the casting

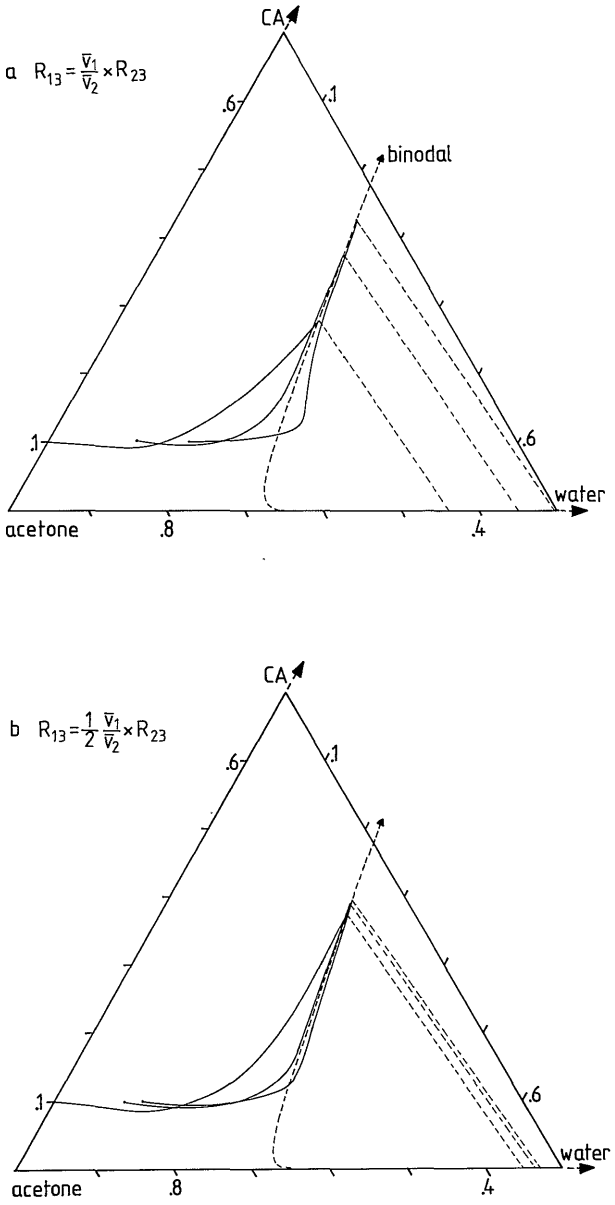

Fig. 6. Calculated Composition paths for films of 10 vol.% CA solutions immersed into pure water coagulation baths, for different water/acetone ratios in the casting solution:
a. ϕ_1/ϕ_2 = 0/100, 12.5/87.5, 20/80; b. ϕ_1/ϕ_2 = 0/100, 10/90, 12.5/87.5.

solution causes the composition path to shift towards the binodal. At a certain water content of the casting solution the composition path even crosses the binodal, which means that immediately after immersion of the film into the bath a metastable composition is reached just beneath the interfacial boundary in the film.

Earlier we have performed quenching experiments in our laboratory on metastable solutions with a degree of supersaturation of about 0.1% water. Up to a polymer concentration of 30 vol.%, these experiments yield induction times for liquid-liquid demixing which are so small that they can not be detected experimentally. Therefore, we assume that liquid-liquid demixing by means of nucleation and growth of the diluted phase takes place immediately after entering the metastable composition region.

When the composition path does not cross the binodal liquid-liquid demixing can not take place; this situation persists at least as long as the composition at the bottom of the film remains unchanged.

Thus the time it takes before liquid-liquid demixing occurs somewhere in the immersed film will increase from zero, at zero water content, to a measurable period Δt upon adding a certain critical amount of water to the casting solution. According to our calculations (see Fig. 6) this will happen at a water/acetone ratio:

$$\frac{12.5}{87.5} < \frac{\phi_1}{\phi_2} < \frac{20}{80} \quad \text{for } R_{13} = (\bar{v}_1/\bar{v}_2)R_{23},$$

$$\frac{10}{90} < \frac{\phi_1}{\phi_2} < \frac{12.5}{87.5} \quad \text{for } R_{13} = 0.5(\bar{v}_1/\bar{v}_2)R_{23}.$$

In the next section we will show how this critical value of ϕ_1/ϕ_2 can be determined experimentally. Comparison of this measured value of ϕ_1/ϕ_2 with the calculated value of ϕ_1/ϕ_2 for different expressions for R_{13}, enables us to obtain a satisfactory expression for R_{13}.

4.9. Light transmission experiments

Light transmission experiments on immersed casting solutions have been performed in order to measure the time it takes before liquid-liquid demixing occurs somewhere in the film.

The experimental setup for these measurements is shown in Figure 7. The membrane is cast on a small glass plate. The glass plate is turned upside down and placed on four points of support in a transparent water bath as quickly as possible. The water level in the bath is just in between the top and bottom of the glass plate to prevent troublesome light scattering at the water surface.

The cast film must be positioned at the lower side of the glass plate for the system CA/acetone/water, because this geometry prevents convection in the coagulation bath because of the large density difference between acetone and water. We recall that we wish to compare the results of these measurements with model calculations where only mass transfer by diffusion is considered.

Above the coagulation bath, a simple desk lamp acts as a light source. After immersion of the cast film in the coagulation bath, the light transmittance is measured and recorded as a function of time. The appearance of optical inhomogenities in the film, as a result of liquid-liquid demixing, causes the light transmittance to decrease.

After the coagulation process a small piece of membrane with a certain surface area, positioned above the detector, is cut out, dried and weighed. In combination with the known volume fraction of polymer in the cast solution the thickness of the immersed film at t=0 can be calculated.

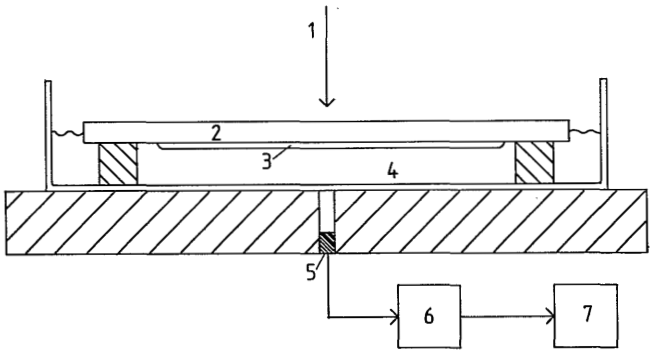

Fig. 7. Measurement of the light transmission through an immersed polymer solution; 1. lightsource; 2. glass plate; 3. polymer solution; 4. coagulation bath; detector; 6. amplifier; 7. recorder.

We have performed these measurements on CA casting solutions containing a variable amount of water and a constant volume fraction of polymer (ϕ_3=0.1). We are especially interested in the critical value of ϕ_1/ϕ_2 in the casting solution where a transition exists from delayed onset of liquid-liquid demixing to instantaneous onset of liquid-liquid demixing. The onset of liquid-liquid demixing in the immersed film is accompanied with a strong decrease in light transmittance.

Experimental results for films with an initial thickness of 220 µm are shown in Figure 8. The onset of liquid-liquid demixing is instantaneous for a water/acetone ratio in the casting solution equal to or larger than 12.5/87.5, while it is delayed for ϕ_1/ϕ_2 equal to or smaller than 10/90. Consequently, the critical value of ϕ_1/ϕ_2 lies in between 10/90 and 12.5/87.5.

When this result is compared with the critical values of ϕ_1/ϕ_2 calculated in the previous section for two different expressions for R_{13}, it can be concluded that the experimental critical value of ϕ_1/ϕ_2 agrees with the critical value of ϕ_1/ϕ_2 calculated with $R_{13} = 0.5(\bar{v}_1/\bar{v}_2)R_{23}$.

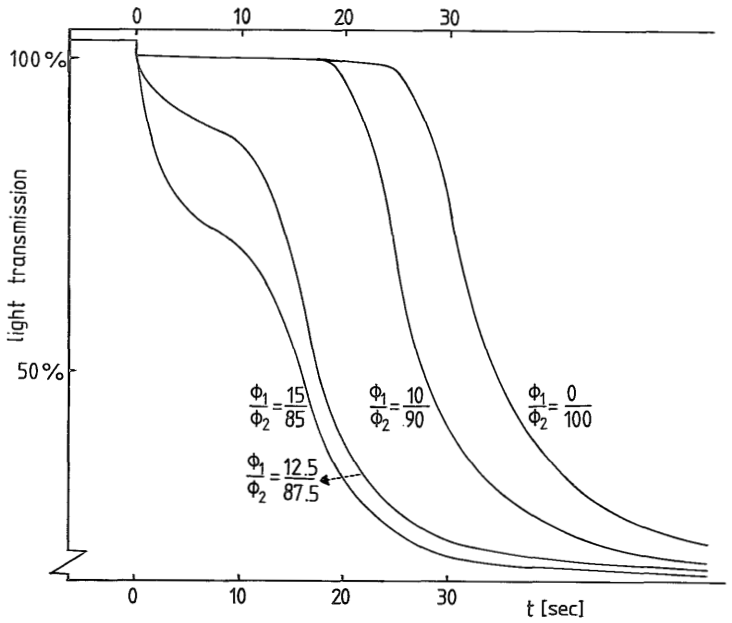

Fig. 8. Percentual light transmission through 10 vol.% CA solutions immersed into a pure water bath for different water/acetone ratios in the casting solution at 25°C. At t=0 the film and the bath are contacted with each other; initial film thickness: 220 µm.

The measurements performed on casting solutions with a water/acetone ratio smaller than the critical value, have been repeated for different film thicknesses. It has been observed that the delay time for the onset of liquid-liquid demixing is proportional to the square of the initial film thickness. From this observation two conclusions can be drawn:

- According to our model the composition path in a ternary phase diagram does not shift as long as the bottom composition of the film remains unchanged and no convection takes place in the bath. The measurements show that under these circumstances the composition path indeed does not cross the binodal, which is in agreement with the model.
- As soon as the bottom composition of the film starts to change, the composition path in the ternary phase diagram starts to shift and it may cross the binodal after a certain time.

In the previous section we have calculated compositon paths which describe composition changes that occur during the time the bottom composition of the film remains unchanged. In the next section we will present calculated composition paths which approximately describe the composition changes that occur during a longer period of immersion of a film with an initial thickness of 200 μm. We will compare the model calculations with the observation that the delay time for the onset of liquid-liquid demixing is equal to 20 seconds for an initially 200 μm thick, water-free film immersed into a pure water bath.

4.10. Calculated composition paths approximately valid for a longer period of immersion

After a certain period of immersion of a film with finite thickness the bottom composition of the film will change. As soon as this happens it cannot be argued any further that the interfacial boundary composition of the film remains constant.

Considering the final result of the precipitation process it is clear that the polymer concentration at the interface will increase. Depicted in a ternary diagram, the boundary composition will shift upwards along the binodal until no solvent is left. The change of composition at the interface is a severe complication of the calculation procedure.

We will approximate the change of the composition in the film for a longer

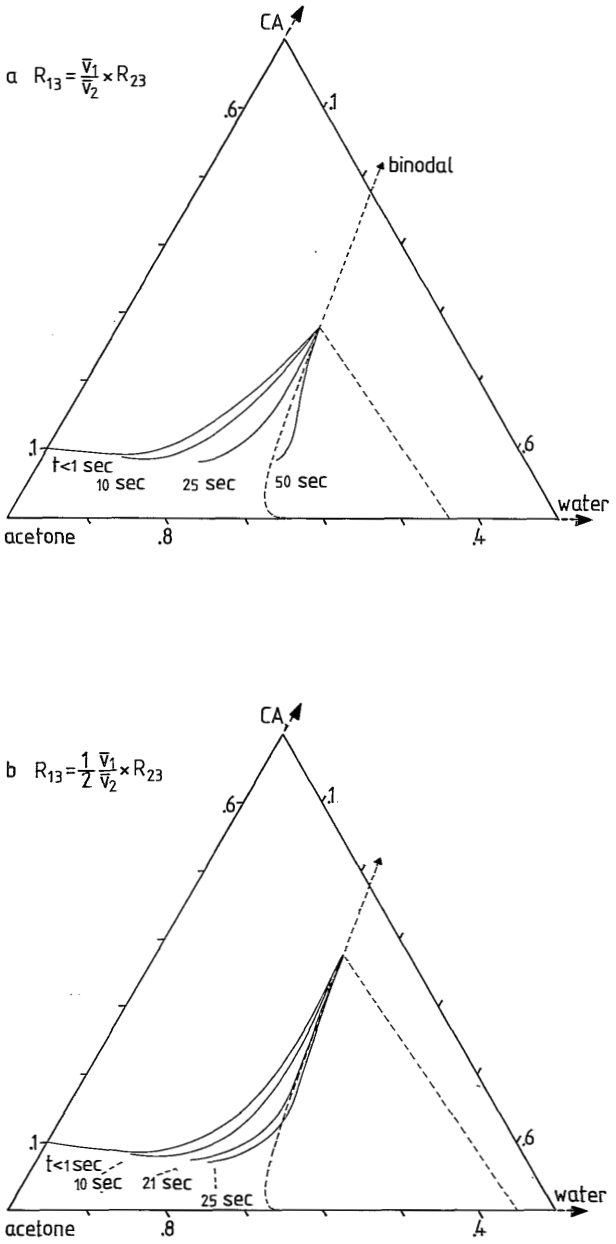

Fig. 9. Approximated change of the composition path at different immersion times for a 10 vol.% CA solution immersed into a pure water bath; initial film thickness: 200 µm.

period of immersion by assuming the interfacial boundary composition to remain constant. The approximation becomes worse of course when the bottom composition in the film differs more from the initial composition.

In Figure 9 the calculated change of the composition path is shown for an initially 200 μm thick water-free film, immersed into a pure water bath. The calculations have been performed using two different expressions for R_{13}.

With $R_{13} = (\bar{v}_1/\bar{v}_2)R_{23}$ the composition path enters the liquid-liquid demixing gap about 40 seconds after immersion of the film. With $R_{13} = 0.5(\bar{v}_1/\bar{v}_2)R_{23}$ the calculated delay time for the onset of demixing is about 22 seconds. In the previous section it has been shown that light transmission measurements yield a delay time of 20 seconds for the onset of liquid-liquid demixing in an initially 200 μm thick film. Again this is in accordance with the calculated result for $R_{13} = 0.5(\bar{v}_1/\bar{v}_2)R_{23}$.

Although the calculated delay time is only an approximation because we assumed the interfacial boundary composition to remain constant, this approximation is confirmed by Figure 6(b), which shows that the presence of a considerable amount of water in the casting solution hardly influences the interfacial boundary composition.

Thus the light transmission measurements have provided us two independent experimental checks, which indicate that our diffusion model correctly describes the composition changes in an CA/acetone (/water) solution immersed into a water (-acetone) bath, if we choose R_{13} to be equal to $0.5(\bar{v}_1/\bar{v}_2)R_{23}$. The fact that we have to choose R_{13} to be smaller than $(\bar{v}_1/\bar{v}_2)R_{23}$ seems reasonable because the smaller water molecules will penetrate the 'polymer network' easier than the acetone molecules, assuming that in the ternary solution the water molecules do not form clusters like in pure water.

4.11. Model calculations in relation to membrane formation and the ultimate membrane structure

In the previous sections we have shown that a reasonable assumption for our model is: $R_{13} \sim 0.5(\bar{v}_1/\bar{v}_2)R_{23}$. For this value of R_{13} the actual composition profile is shown in Figure 10 for an initially water-free film immersed into a pure water bath. The volume fraction of polymer and water are shown as a function of the distance from the interface between the bath and the film (x'). Because the diffusion equations have been solved using the position co-

ordinate m, it was necessary to convert the solution using the expression:

$$x' = \int_0^m \phi_3^{-1}(\xi)d\xi$$

Composition profiles at 1 second and 21 seconds after immersion of the film are shown. These profiles correspond to the composition paths shown in Figure 9(b).

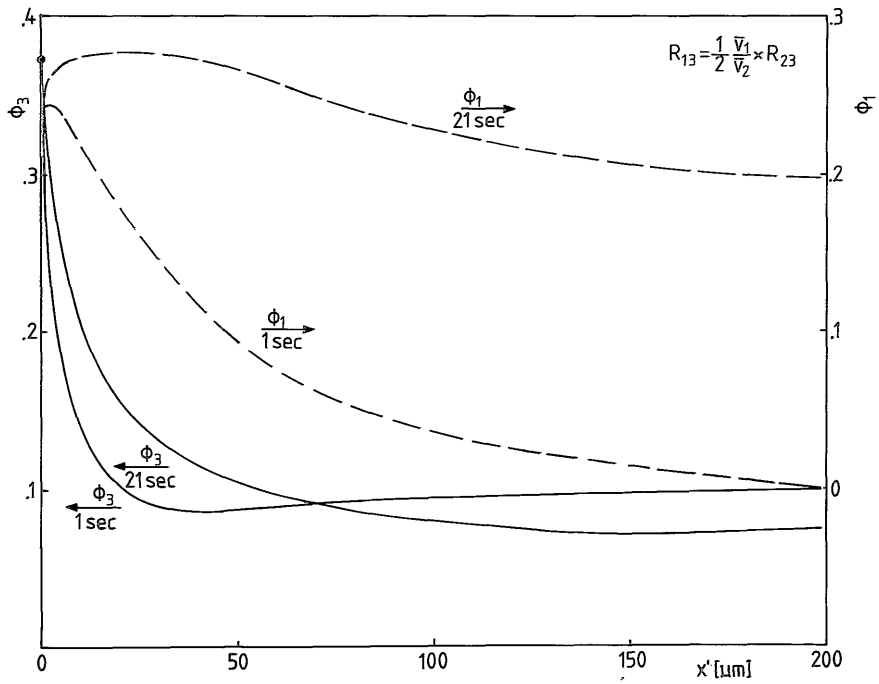

Fig. 10 Calculated composition profiles in a casting solution consisting of 10 vol.% CA in acetone immersed into a pure water bath; X' is the distance from the interfacial boundary between the bath and the film; initial film thickness: 200 µm.

The initial film thickness is 200 µm. According to the calculations, the film thickness hardly decreases during the first 21 seconds after immersion of the film. However, near the interfacial boundary the polymer concentration

increased very strongly at the very moment of contact between the polymer solution and the bath. The small region of highly concentrated solution grows out until the onset of liquid-liquid demixing (21 seconds after immersion) fixes this asymmetric polymer distribution in the film.

Thus, the asymmetric porosity distribution in the ultimate membrane is determined by the polymer distribution that results from the diffusion processes in the immersed film until the onset of liquid-liquid demixing.

Liquid-liquid demixing by means of nucleation of the diluted phase cannot take place at the interface between the bath and the film because the film composition at the interface remains situated on the binodal during the coagulation process. This is independent on the position of the composition path relative to the position of the binodal in the ternary diagram.

The porosity induced by liquid-liquid demixing in the film just beneath the interface however, depends strongly on the initial position of the composition path relative to the position of the binodal in the ternary diagram:

I. When the composition path does not cross the binodal before the bottom composition of the film has changed, which is the case for the ternary system considered in Figure 10, the region of highly concentrated polymer solution just beneath the interface increases considerably until the onset of liquid-liquid demixing. The delay time for the onset of demixing and thus the thickness of this intermediate layer at the moment of onset of liquid-liquid demixing, depend on the initial position of the composition path relative to the position of the binodal and on the rate of shifting of the composition path towards the binodal in the ternary diagram.

It is interesting that the thickness of the intermediate layer at the moment of onset of liquid-liquid demixing, must also depend on the initial thickness of the cast film.

Because the polymer concentration in the intermediate layer is relatively high at the moment of onset of liquid-liquid demixing, the porosity induced by this demixing process will be relatively low while the chance that the ultimate pores will be interconnected is small. In Chapter 7 it will even be argued that within this intermediate layer no diluted phase at all will be nucleated. Consequently, when liquid-liquid demixing is the only demixing process that is responsible for pores in the ultimate membrane, this intermediate layer will influence the transport behavior of the membrane very strongly. According to this reasoning the transport behavior of this type of

membrane is influenced by the thickness of the cast film.

Beneath this effectively dense intermediate layer with a thickness of a few micrometers (see Figure 10) a thick sublayer is formed which is highly porous because the initial polymer concentration has increased only slightly until the onset of liquid-liquid demixing in this layer.

II. When already the initial composition path crosses the binodal, the onset of liquid-liquid demixing will not be delayed and nuclei of the diluted phase will be formed just beneath the toplayer in a region where the initial polymer concentration has hardly changed. Consequently, the induced porosity and the interconnectivity of the pores will be high. In the Appendix of this thesis we will show that the nuclei of the diluted phase formed in this region of the film can even grow out to form macrovoids in the ultimate membrane. The ultimate transport behavior of this type of membranes is only determined by the very thin dense layer formed at the interface between bath and film.

For both types of membrane formation processes the viscosity of the skin layer at the interface immediately becomes so high that the nuclei of the diluted phase, formed beneath this skin layer cannot grow through this layer. In our opinion the process of liquid-liquid demixing can only yield a microporous skin layer if the formation of an interfacial boundary between the solution film and the coagulation bath is prohibited by the presence of an excess amount of solvent in the coagulation bath (see Figures 4 and 5). This assumption is in accordance with experimental results of Wijmans [9], concerning the formation of microporous skin layers.

During the immersion process the exchange of solvent and nonsolvent in the demixed film continues, causing an increase of the polymer concentration in the concentrated phase surrounding the pores. When the concentrated phase crosses the glass transition in the isothermal phase diagram the ultimate structure of the membrane is fixed.

Membranes formed by the mechanism of delayed onset of liquid-liquid demixing will be called type I membranes. Membranes formed by the mechanism of instantaneous onset of liquid-liquid demixing will be called type II membranes.

For type II membranes the thickness of the thin skin layer is very import-

ant for the transport properties of the membrane. This thickness is determined by the distance to the interface of the position where the first nuclei of the diluted phase are being formed. Unfortunately our model only predicts that the composition in the film just beneath the interface becomes metastable immediately after immersion of the film. The prediction of the exact position where the first nuclei of the diluted phase are being formed is beyond the scope of this model.

4.12. Discussion

In the previous sections we have considered liquid-liquid demixing by means of nucleation and growth of the diluted phase as the pore forming mechanism during membrane formation. According to this consideration and our model calculations we can distinguish between two types of membranes:

- Type II membranes consisting of two layers: i) a very thin skin layer where no nucleation of the diluted phase could take place; ii) a thick sublayer with interconnected pores reaching until the bottom side of the membrane.
- Type I membranes consisting of three layers. In between the two layers mentioned for type II membranes an effectively dense intermediate layer has been formed with a thickness of a few micrometers. Because of the high polymer concentration at the moment of onset of demixing the formation of an interconnective pore structure in this layer has been prohibited.

Type I membranes will be formed only when the initial composition path does not cross the binodal in the ternary phase diagram. We have shown that type I membranes are formed when a CA-acetone solution is immersed into a coagulation bath consisting of water only.

In Chapter 6 we will show that the type of membrane that will be formed is strongly influenced by the degree of miscibility of the solvent and the nonsolvent. When solvents are used which are better miscible with water than acetone (for example DMSO, DMF or dioxane) type II membranes will be formed.

Besides liquid-liquid demixing, other porosity inducing processes like crystallization or aggregate formation may occur during the immersion process. Aggregate formation occurs in several ternary systems [5,10,11] at a

certain nonsolvent or polymer concentration. This demixing process, accompanying the gelation process, often results in a nodular or fibrillar structure. In a previous paper [5] we have shown that this process also occurs in CA/acetone/water solutions, the system discussed in this paper.

We think that aggregate formation will lead to much better interconnected pores than liquid-liquid demixing (above the critical point) because the solution demixes by means of nucleation and growth of a solid phase.

Especially in type I membranes the occurrence of this demixing process during the immersion of the cast film will influence the transport properties of the ultimate membrane to a large extent because it may induce interconnected pores in the dense intermediate layer beneath the skin layer.

The influence of this demixing process on the structure of the thin skin layer is hard to predict because no experimental data are available on the structure induced by aggregate formation in highly concentrated polymer solutions. The calculations presented in this paper provide the composition range in which these structure analyses should be carried out for the ternary system CA/acetone/water.

4.13. References

1. R.V. Orye and J.N. Prausnitz, Multicomponent equilibria with the Wilson equation, Ind. Eng. Chem., 57 no. 5 (1965) 18.
2. F.W. Altena and C.A. Smolders, Calculation of liquid-liquid phase separation in a ternary system of a polymer in a mixture of a solvent and a nonsolvent, Macromolecules, 15 (1982) 1491.
3. F.W. Altena, Phase separation phenomena in cellulose acetate solutions in relation to asymmetric membrane formation, Thesis, Chapter 6, Twente University of Technology, Enschede, The Netherlands (1982).
4. M.H.V. Mulder, T. Franken and C.A. Smolders, Preferential sorption versus preferential permeability in pervaporation, J. Membrane Sci., 22 (1985) 155.
5. A.J. Reuvers, F.W. Altena and C.A. Smolders, Demixing and gelation behavior of ternary cellulose acetate solutions, J. Polym. Sci., Pol. Phys. Ed., 24 (1986) 793.
6. D.K. Anderson, J.R. Hall and A.L. Babb, Mutual diffusion in non-ideal binary liquid mixtures, J. Phys. Chem., 62 (1958) 404.

7. G.S. Park, Radioactive studies of diffusion in polymer systems part 3, Trans. Far. Soc., 57 (1961) 2314.
8. C. Cohen, G.B. Tanny and S. Prager, Diffusion-controlled formation of porous structures in ternary polymer systems, J. Polym. Sci., Pol. Phys. Ed., 17 (1979) 477.
9. J.G. Wijmans, J.P.B. Baaij and C.A. Smolders, The mechanism of formation of microporous or skinned membranes produced by the immersion precipitation process, J. Membrane Sci., 14 (1983) 263.
10. J.G. Wijmans, H.J.J. Rutten and C.A. Smolders, Phase separation phenomena in solutions of poly (2,6-dimethyl-1,4- phenyleneoxide) in mixtures of trichloroethylene, 1-octanol and methanol: relationship to membrane formation, J. Polym. Sci., Pol. Phys. Ed., 23 (1985) 1941.
11. A. Labudzinska and A. Ziabicki, Effect of composition and gelation conditions on structural changes accompanying the gelation of PAN, PVA and gelatin solutions, Kolloid Z.Z. Polym., 243 (1971) 21.

5. LIQUID-LIQUID DEMIXING BEHAVIOR OF CELLULOSE ACETATE/WATER/SOLVENT SYSTEMS. COMPARISON OF EXPERIMENTAL RESULTS WITH CALCULATIONS.

By A.J. Reuvers and C.A. Smolders

5.1. Summary

Liquid-liquid demixing behavior of the quasi-ternary systems cellulose acetate (CA)/THF/water and CA/dioxane/water is examined. Both the isothermal cloud point curve and the compositions of the coexisting phases are measured. It has been found that in the area near the critical point the compositions of the coexisting phases do not coincide with the cloud point curve. This is caused by the polydispersity of the polymer.

For the calculation of the coexisting phases we use the Flory-Huggins theory for three-component systems. Experimental concentration dependent parameters are used for the thermodynamic interaction between solvent and polymer, respectively solvent and nonsolvent. Although in the calculations CA is assumed to be monodisperse, fairly good agreement has been found between the calculated and experimentally found coexisting phases.

Experimentally as well as by calculation it has been found that the positions of the demixing gaps are quite the same for both systems. However, the slope of the tielines, connecting the coexisting phases, turned out to differ considerably for both systems. Calculations show that this is caused by the poorer miscibility of water and THF compared to that of water and dioxane.

5.2. Introduction

Knowledge of the equilibrium thermodynamics of the ternary system polymer/solvent/nonsolvent is of utmost importance to understand the mechanism of formation of membranes by means of immersion precipitation.

A correct expression for the Gibbs free energy of mixing as a function of the composition for this system enables one to derive expressions for the chemical potentials of the three components in the mixture. These expressions can be used to calculate:

- The driving forces for the ternary diffusion process in the casting solution, after being immersed into a nonsolvent bath.
- The position of the binodal in an isothermal ternary phase diagram; this binodal is the boundary between stable and metastable compositions.
- The tielines which connect the compositions of the coexisting phases, situated on the binodal; after immersion of the casting solution into the coagulation bath the compositions at the interfacial boundary between the bath and the film are given by such a pair of coexisting compositions.

Thus, knowledge of the Gibbs free energy of mixing of a polymer/solvent/nonsolvent system provides almost all the necessary information to describe the diffusion and demixing behavior in the casting solution after immersion of this solution into the nonsolvent bath. The only extra information needed concerns the coefficients which describe the frictional forces between the different components during the diffusion process.

For the calculation of the binodal, the tielines and the driving forces for a certain ternary system we use an expression for the Gibbs free energy of mixing (G^E), described in Appendix A of Chapter 3 [1]. The Gibbs free energy of mixing of the ternary system is assumed to be a function of the free energy of mixing in the three limiting binary cases. One of the aims of this Chapter is to check the reliability of the expression for G^E.

For the system CA/acetone/water we have compared the calculated and the measured position of the liquid-liquid demixing gap as a check on the reliability of the expression for G^E (Chapter 4). In this Chapter we will examine the phase behavior of the systems CA/tetrahydrofuran (THF)/water and CA/dioxane/water. We will not only examine the position of the liquid-liquid demixing gap, but we will also compare the calculated and measured compositions of the coexisting phases.

Because the cellulose acetate (CA) used is a polydisperse polymer, the liq-liquid-liquid demixing process will be accompanied by a fractionation of the polymer. This effect will be examined by measuring the number ($\bar{M}_n$) and weight ($\bar{M}_w$) average molecular weight of CA in the coexisting phases.

In this Chapter we will also examine the influence of the thermodynamic interaction between the solvent and the nonsolvent on the demixing behavior of

a ternary solution. For these calculations we will use experimentally obtained concentration dependent thermodynamic interaction parameters for various solvent-water systems. In Chapter 6 it will be shown that the thermodynamic interaction between the solvent and the nonsolvent influences the membrane formation process to a large extent.

Finally, we will discuss the influence of the polymer-solvent and polymer-nonsolvent thermodynamic interaction parameters on the demixing behavior of the ternary solution.

5.3. Experimental determination of phase equilibria of quasi ternary CA/solvent/water systems

We have chosen dioxane and THF as the solvents, because for these solvents experimental data on G^E for solvent-water mixtures are available. These data are necessary for the calculation of the phase equilibria of the ternary systems.

CA/THF/water solutions do not show any gelation phenomena up to very high polymer concentrations [3]. Unfortunately, the polymer rich phase of a demixed CA/dioxane/water solution gels already at a polymer concentration of 10%, which obstructs a total separation of the polymer lean and the polymer rich phase. The gelation phenomena are still much more pronounced when solvents like acetone, DMF or DMSO are used.

5.4. Experimental

Cellulose acetate was obtained from Eastman Kodak and had an acetyl content of 39.8% and a viscosity number 3 (ASTM); $\bar{M}_n$ = 27,000; $\bar{M}_w$ = 56,000 (determined by HPLC measurements). Dioxane and THF (both solvents from Merck, analytical grade and stabilized) were used without further purification. Water was demineralized and ultrafiltrated.

All the solutions prepared (we will call them initial solutions) contained enough water to demix into two phases at 20°C. The CA weight fraction of the initial solutions was always 0.04. The water/solvent ratio of the initial solutions has been varied.

The initial solutions have been prepared in two steps. First, the polymer was dissolved in pure solvent. Second, a mixture of solvent and water was added to the solution to obtain the desired composition of the solution. The solution was homogenized by stirring in a closed vessel at moderate temperature (30-50°C). When all the gel particles were dissolved the solutions in the closed vessels were put into a thermostated bath, at 20°C. After being shaken for some time the vessels remained in the thermostated bath, at least during one week. During this time the concentrated phase could sink to the bottom of the vessel. For the system CA/THF/water two clear phases were obtained within a week. In solutions of CA/dioxane/water the concentrated phase often stayed slightly turbid, because some of the diluted phase remained included in the gelated concentrated phase.

Taking some samples of the two phases, the solvent mixture was separated from each sample by means of vacuum destillation, using an apparatus described by Mulder [4], and the CA concentration could be determined by weighting.

The composition of the distilled water-THF mixtures was determined by density measurements using a Paar Digital Precision Density Meter model DMA 50. The composition of the distilled water-dioxane mixtures was determined by refractive index measurements.

The molecular weight distributions of the polymer in the two phases were determined by size exclusion chromatography on a Waters High Performance Liquid Chromatograph (columns: micro-styragel; flow rate: 2 ml/min.). The eluent was THF.

5.5. Experimental results

The measurements performed on the phase behavior of the systems CA/dioxane/water and CA/THF/water are represented in isothermal ternary phase diagrams (Fig. 1). Figure 1(a) and 1(b) represent a small part of the phase diagram, where the relevant measurements are performed. The compositions are represented by the weight fractions.

For both systems two curves are measured. The dashed curve connects the compositions of the phases into which the initial solutions separated. The full curve is the cloud point curve, representing the compositions of solutions which start to separate into two liquid phases at 20°C, upon cooling.

The compositions of the coexisting phases and of the initial solutions are

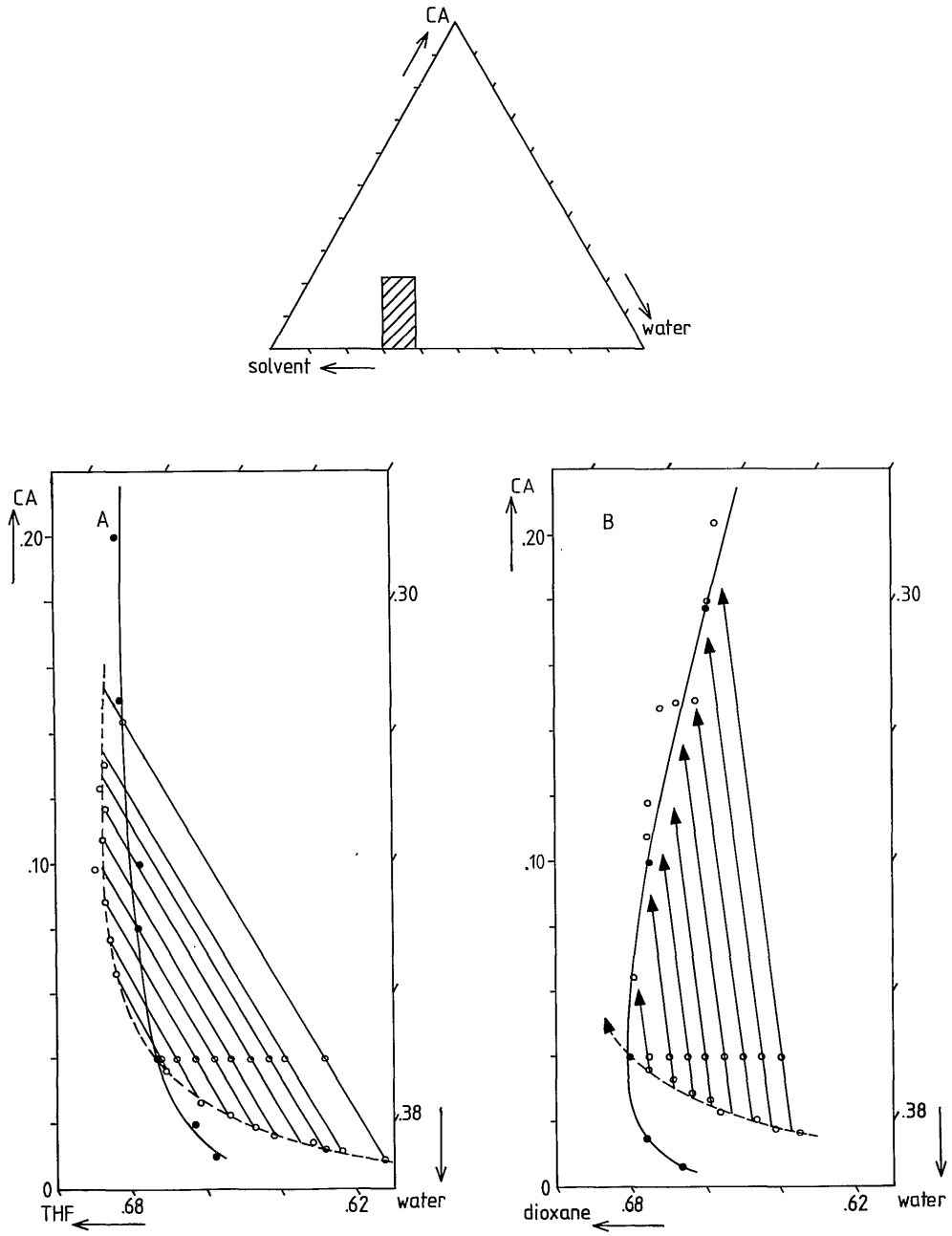

Fig. 1. Isothermal phase diagrams for the systems CA/THF/water (a) and CA/dioxane/water (b) at 20°C. —●—: measured cloud point curves; o—o—o: measured compositions of coexisting phases connected by a tieline through the composition of the initial solution.

connected by tielines.

In the CA/dioxane/water solutions the compositions of the polymer rich phases could not be determined exactly because of the incomplete separation of the diluted phase from the concentrated phase. Nevertheless, we could exactly determine the slope of the tielines in the phase diagram for this system, by connecting the compositions of the polymer lean phase and the initial polymer solution.

For both systems the cloud point curve and the curve representing the coexisting phases do not coincide as it should have been the case if the polymer components were monodisperse. The two curves cross each other at a CA weight fraction of 0.04, the CA concentration of the initial solutions.

Because of the polydispersity of the polymer, the free energy of the initial solutions is minimized when the polymer is separated into fractions with different average molecular weights in the two phases [5, 6]. We have measured the number ($\bar{M}_n$) and weight ($\bar{M}_w$) average molecular weights of the polymer in the coexisting phases of the initial solutions consisting of CA/THF/water. The results are shown in Figure 2. The polymer rich phase and the polymer lean phase contain CA with a higher, respectively lower, average molecular weight than the CA in the initial solutions. This means also that the coexisting phases contain CA with a different molecular weight than the polymer in the solutions which were used to determine the cloud point curve. This explains why the compositions of the coexisting phases do not coincide with the cloud point curve; the cloud point curve separates metastable from stable compositions for solutions, which contain CA with the initial molecular weight distribution; the curve through the compositions of the coexisting phases separates metastable from stable compositions for solutions containing CA with different molecular weight distributions.

Although we did not examine the magnitude of the effect, it must be noticed that the molecular weight distributions of CA as well as the compositions of the coexisting phases depend on the CA concentration of the initial solutions [6].

From Figure 2 it can be seen that $\bar{M}_n$ and $\bar{M}_w$ values of CA in the polymer rich phase at increasing water content of these solutions both go into the direction of $\bar{M}_n$ and $\bar{M}_w$ for the initial solutions. This is related to the fact that a larger amount of the initial polymer is partitioned in the polymer rich phase at increasing water content of the original solution. The consequence of this phenomenon is that the compositions of the polymer rich phases

will approach the cloud point curve at increasing CA concentration.

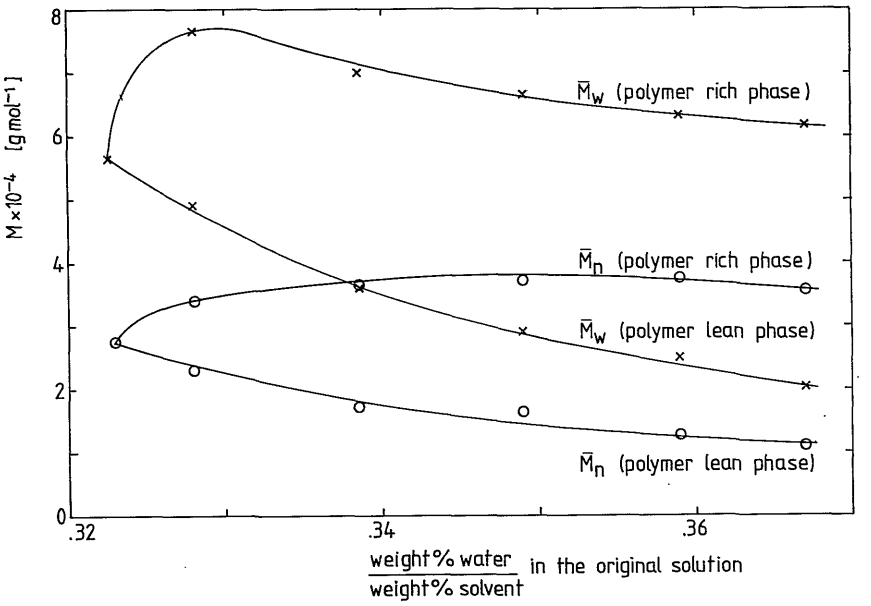

Fig. 2. Number ($\bar{M}_n$) and weight ($\bar{M}_w$) average molecular weights of CA in the coexisting phases as a function of the water/solvent ratio in the initial solutions consisting of CA/THF/water; $\bar{M}_n$ and $\bar{M}_w$ in the original solution: 27,000 respectively 56,000.

Kamide et al [7] have performed calculations on the phase behavior of quasi ternary systems that resemble the systems that we have examined. These authors have calculated coexisting phases for various molecular weight distributions of the original polymer. Unfortunately, they have not calculated the boundary in between stable and metastable compositions with the initial polymer molecular weight distribution (this boundary might be compared with the cloud point curve). Nevertheless, also their calculations show that the effect of the polydispersity of the original polymer on the phase equilibria is most pronounced at low polymer concentrations in the area near the critical point, the area where we have performed our measurements.

Figure 1 does not only show the influence of the polydispersity of CA on

the equilibrium phase behavior of the ternary systems investigated. It also shows that the choice of the solvent affects the slope of the tielines connecting the coexisting phases. This phenomenon will be discussed in the last section of this chapter.

5.6. Calculation of phase equilibria of the ternary systems CA/dioxane/water and CA/THF/water

We will calculate phase equilibria of the ternary systems CA/dioxane/water and CA/THF/water in a similar way as we have done for the system CA/ acetone/water [2]. This means that we assume the polymer to be monodisperse with molecular weight M_3.
However, unlike the expressions for the chemical potentials, used by Kamide et al [6], our expressions for the chemical potentials can be used for ternary systems with concentration dependent thermodynamic interaction parameters g_{12} (nonsolvent-solvent interaction) and g_{23} (solvent-polymer interaction).

The expressions for the chemical potentials ($\Delta\mu_i^+$) have been given in Chapter 3.

The conditions for liquid-liquid equilibrium are:

$$\Delta\mu_i^+ \text{ (polymer lean phase)} = \Delta\mu_i^+ \text{ (polymer rich phase)} \quad i = 1, 2, 3,$$

where 1, 2 and 3 refer to the nonsolvent, the solvent and the polymer respectively. The procedure used to calculate the compositions of the coexisting phases has been described by Altena [8].

In the following section the values of the interaction parameters will be given for the ternary systems we wish to examine.

5.7. The thermodynamic interaction parameters $g_{12}(\phi_2)$, $g_{23}(\phi_2)$ and χ_{13} for the systems CA/dioxane/water and CA/THF/water

The binary concentration dependent parameters $g_{12}(\phi_2)$ have been calculated from literature data [9, 10] for the excess free energy G^E of mixtures of solvent and water. These calculations have been performed using the following expressions [8]:

$$g_{12}(\phi_2) = \frac{1}{x_1\phi_2}\left[x_1 \ln(x_1/\phi_1) + x_2 \ln(x_2/\phi_2) + G^E/RT\right], \quad (1)$$

where x_i and ϕ_i represent the mole fraction, respectively the volume fraction of component i in the mixture. For the calculation of ϕ_i, we assumed the partial specific volumes of the components to be constant and equal to the values for the pure components. For the description of the concentration dependence of g_{12} we use similar expressions as have been used for the system acetone-water (Chapter 4).

THF-water (25°C):

$$g_{12} = 1.613 - 0.546\ \phi_1 + 1.096 \exp(-4.604\ \phi_1) + 0.303 \exp(-17.374\ \phi_1) \quad (2)$$

Dioxane-water (25°C):

$$g_{12} = 1.389 - 0.607\ \phi_1 + 1.050 \exp(-4.731\ \phi_1) + 0.500 \exp(-19.922\ \phi_1) \quad (3)$$

The thermodynamic interaction between water and CA is described by a constant parameter χ_{13}, measured by means of swelling experiments [4]:

$$\chi_{13} = 1.4 \ (25°C) \quad (4)$$

The concentration dependent parameter g_{23} for CA-dioxane mixtures has been obtained by Altena using osmotic pressure measurements [11]:

$$g_{23} = 0.62 - 0.11\ \phi_2 \ (25°C) \quad (5)$$

We have determined the concentration dependent parameter g_{23} for CA-THF mixtures in a way similar to that of Altena, who has examined solutions of CA in dioxane and acetone [11].

For CA concentrations above 2.5 weight % we used a high pressure osmometer [11]. For CA concentrations below 0.5 weight % we used a low pressure osmometer. The membranes used in both osmometers were Sartorius allerfeinst, catalogue number 11539.

The osmotic pressure difference (π) between the pure solvent and a polymer

solution is related to the chemical potential of the solvent in the mixture ($\Delta\mu_2^+$) in the following way:

$$\Delta\mu_2^+ + \pi\bar{v}_2M_2 = 0, \tag{6}$$

where $\bar{v}_2M_2$ is the molar volume of the solvent. For a complete list of symbols we refer to Chapter 3.

The expressions for $\Delta\mu_2^+$ for binary polymer solutions is given by (Chapter 3):

$$\Delta\mu_2^+/RT = \ln\phi_2 + \{1 - \bar{v}_2M_2 / \bar{v}_3M_3\}\ \phi_3 + \phi_3^2\ \{g_{23} + \phi_2 \frac{dg_{23}}{d\phi_2}\} \tag{7}$$

Combination of eqn. (6) and (7) yields $g_{23}(\phi_2) + \phi_2\{dg_{23}(\phi_2)/d\phi_2\}$ as a function of the osmotic pressure and ϕ_3.

For M_3 we have used $\bar{M}_n$ of CA, determined with the low pressure osmometer. This value of $\bar{M}_n$, viz. 35,000, turned out to be higher than $\bar{M}_n$ determined by HPLC measurements (27,000) because the membrane used is permeable for the very small polymer molecules. For other calculations, not connected with osmotic pressure determinations, we have used the $\bar{M}_n$ = 27,000 value.

The partial specific volume of CA in THF has been calculated from the slope of the solution density versus concentration plot and it has a value of $0.717 * 10^{-3}$ m^3kg^{-1}, within the experimental concentration range.

The results of the osmotic pressure measurements are shown in Table 1. The calculated values of $g_{23} + \phi_2\{dg_{23}/d\phi_2\}$ are shown in Figure 3. We approximate $g_{23}(\phi_2)$ for CA-THF solutions with the function:

$$g_{23}(\phi_2) = .42 - .0037\ \exp\{-50(1-\phi_2)\} \quad (25°C) \tag{8}$$

From this expression it can be seen that g_{23} is only concentration dependent for very small values of ϕ_3.

Table 1. Osmotic pressure π of CA-THF mixtures as a function of the weight and volume fraction of CA at 25°C.

w_3(weight fraction CA)	ϕ_3(volume faction CA)	$\pi * 10^{-3}[N\ m^{-2}]$
0.00099	0.00063	0.0655
0.0252	0.0161	3.1
0.0404	0.0260	5.7
0.0560	0.0363	8.6
0.0841	0.0550	17.3
0.101	0.0662	21.6
0.134	0.0891	35.0
0.202	0.138	89.2

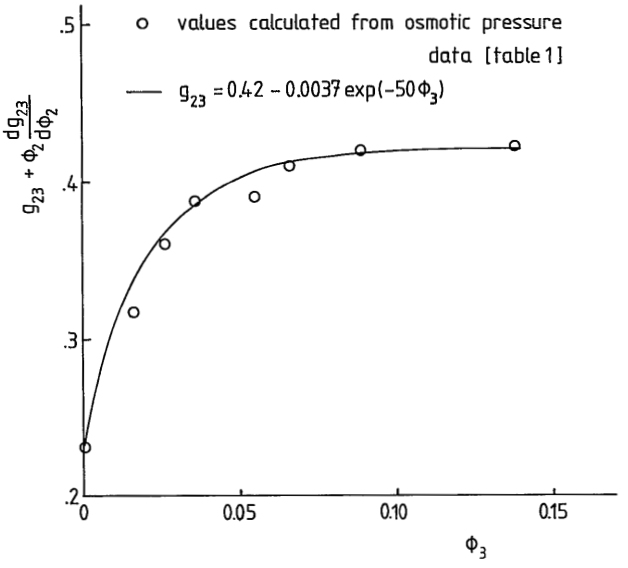

Fig. 3. $g_{23} + \phi_2 \{dg_{23}/d\phi_2\}$ (see equation (7)) as a function of CA volume fraction (ϕ_3) in a mixture of CA and THF.

5.8. Calculated phase behavior compared with experimental results

For the calculation of the phase behavior of the ternary systems, g_{12} and g_{23} were assumed to be a function of $\phi_2/(\phi_2+\phi_1)$ and $\phi_2/(\phi_2+\phi_3)$ respectively (see Appendix A, Chapter 3).

Besides the interaction parameters given in the previous section, we used the following parameters for the calculation of the phase equilibria:

- the molecular weight of CA, THF, dioxane and water: 27,000, 72.11, 88.12 and 18.0 g mol^{-1} respectively
- the partial specific volume of THF, dioxane and water: 1.130, 0.967 and 1.000 * 10^{-3} m^3kg^{-1} respectively
- the partial specific volume of CA in THF-water and of CA in dioxane-water: 0.717 and 0.725 * 10^{-3} m^3kg^{-1} respectively.

The calculated coexisting phases for the systems CA/THF/water and CA/dioxane/water are shown in the ternary phase diagrams of Figure 4. In these phase diagrams the compositions are represented by the volume fractions of the three components.

Because we assume CA to be monodisperse, the compositions of the coexisting phases (connected by tielines) are situated on a binodal curve. It can be seen that the calculated positions of the binodals are almost equal for both ternary systems. However, the slopes of the tielines differ considerably for both systems, especially in the area near the critical point.

The calculations have been performed with a molecular weight of the monodisperse polymer (M_3) equal to 27,000, the number average molecular weight of CA. We might also choose the weight average molecular weight of CA for M_3, to approximate the phase behavior of the quasi ternary system. However, an increase of M_3 from 27,000 to 56,000 has such a small effect on the position of the binodal and the direction of the tielines that the changes cannot be shown in Figure 4. Only in the area near the critical point the binodal shifts a little bit into the direction of the polymer-solvent axis. The position of the critical point itself shifts into the direction of a lower polymer concentration.

In Figure 5 the calculated phase behavior of the hypothetical ternary systems (monodisperse polymer) is shown together with the measured phase behav-

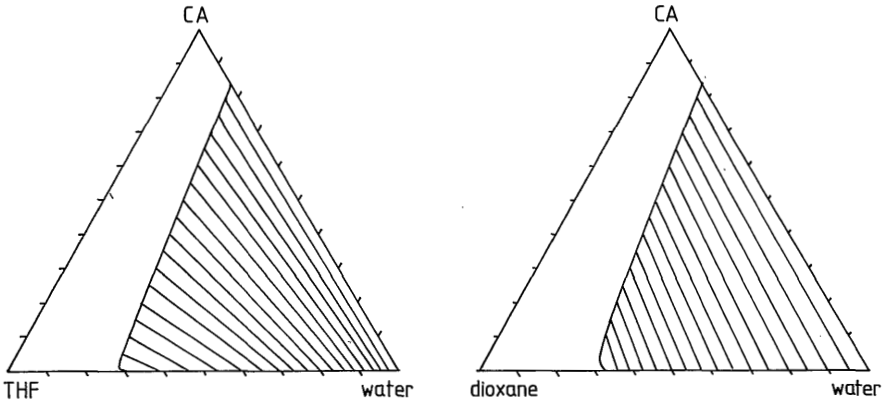

Fig. 4 Calculated binodal and tielines for the ternary systems CA/THF/water and CA/dioxane/water. The interaction parameters used are given by equations (2-5 and 8).

ior of the quasi ternary systems (polydisperse polymer). Only that part of the ternary diagram is shown where the measurements have been performed. The compositions are represented by the volume fractions of the components. Because the compositions of the coexisting phases and the cloud point curves are measured in weight fractions we have converted the compositions in volume fractions, assuming the partial specific volumes of the components to be constant:

$$\phi_i = \bar{v}_i w_i / (\bar{v}_i w_i + \bar{v}_j w_j + \bar{v}_k w_k) \quad i,j,k = 1,2 \text{ or } 3 \text{ and } k \neq j \neq i \qquad (9)$$

where w_i is the weight fraction, ϕ_i is the volume fraction and $\bar{v}_i$ is the partial specific volume of component i.

The phase behavior has been measured at a temperature of 20°C, whereas the calculations have been performed using thermodynamic data measured at a temperature of 25°C. We have observed experimentally that this temperature difference has only a small effect on the position of the cloud point curve. When the temperature is increased from 20°C onto 25°C, the cloud point curve shifts about 0.3 weight percentage into the direction of the CA-water axis for the system CA/THF/water. For the system CA/dioxane/water this value has been found to be equal to 1.0 weight percentage. Although we did not measure the compositions of the coexisting phases at a temperature of 25°C, we assume

that the positions of these compositions in the phase diagram relative to the cloud point curve hardly change at a temperature increase of 5°C.

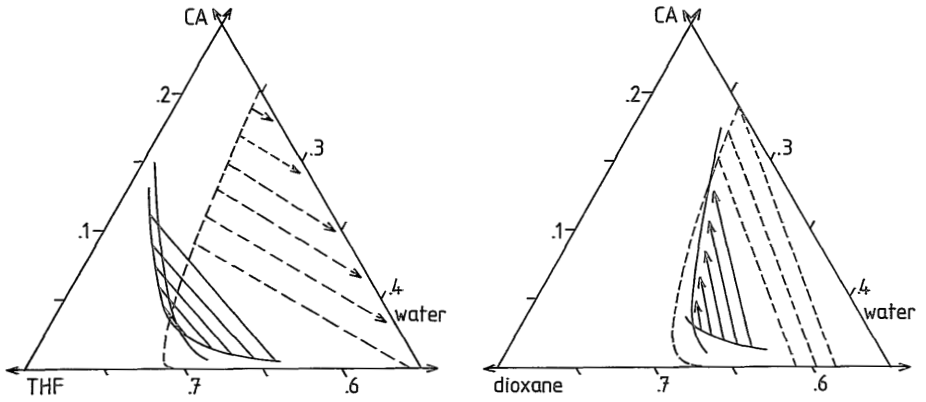

Fig. 5. Isothermal phase behavior for the systems CA/THF/water and CA/dioxane/water. The dashed curve and lines represent the calculated binodal, respectively tielines at 25°C. The full curve, connected by the tielines, represents the compositions of the coexisting phases, measured at 20°C. The other full curve is the cloud point curve measured at 20°C.

- Figure 5 shows that the slopes of the calculated tielines for the ternary systems are fairly well in agreement with the slopes of the measured tielines for the quasi ternary systems. Although the slopes of the calculated tielines are less steep than those of the measured tielines, the difference in the slopes of the tielines for the two quasi ternary systems is well approximated by the calculations.

- In this paragraph the positions of the calculated binodals are compared with the measured positions of the cloud point curves at high CA concentrations, where the influence of the polydispersity of the polymer on the phase behavior disappears (see Figure 1 and 2).

Taking into account the temperature correction for the position of the measured cloud point curve, it can be concluded that the positions of the measured cloud point curve and the calculated binodal agree very well for the system CA/dioxane/water.

For the system CA/THF/water the resemblance between the calculated and experimental results at high CA concentrations is not so good. This may be

caused by the neglected influence of the concentration dependence of the partial specific volumes of the components. Another reason may be that for this system the binary interaction parameters used are in fact only a poor approximation for the, in reality, ternary interaction parameters in the expression for the Gibbs free energy of mixing (see Appendix A, Chapter 3).

- At low polymer concentrations the polydispersity of CA causes the calculated binodal to differ from the cloud point curve and the positions of the compositions of the coexisting phases. This effect can clearly be observed from the difference of the CA concentration in the calculated and the measured polymer lean phases. The polydispersity of CA is also the reason for the difference in the measured CA concentration (3.0 vol.%) and the calculated CA concentration (1.0 vol.%) at the critical point for the system CA/THF/water (the critical point is the point in the phase diagram where the coexisting phases, connected by a tieline, coincide). When the calculations are performed with $\bar{M}_w$ instead of $\bar{M}_n$ values this difference is even larger.

Because the polydispersity influences the demixing behavior only in the area near the critical point, the assumption for the diffusion model (Chapter 3), that no polymer dissolves in the coagulation bath during the coagulation process, is also valid when polydisperse polymer is used. Only when a large amount of solvent is added to the coagulation bath, some (low molecular weight) polymer will dissolve in the coagulation bath and in the droplets of diluted phase, nucleated in the polymer solution.

From the results discussed in this section and the calculated and experimentally determined phase behavior of the system CA/acetone/water (Chapter 4), we conclude that the expression for the excess free energy, used for the calculation of the phase behavior and the diffusion behavior of ternary systems, gives a fairly good approximation of reality.

5.9. Relation between binary thermodynamic interaction parameters and the phase behavior of a ternary system.

The effect of varying the interaction parameters on the phase behavior of a polymer/solvent/nonsolvent system has been calculated by several authors [6,8,12]. Kamide [6] has calculated the phase behavior using constant inter-

action parameters. Altena [8] has used concentration dependent g_{12} (nonsolvent-solvent) parameters and Yilmaz [12] has used concentration dependent g_{12} and g_{23} (solvent-polymer) parameters. From these authors only Kamide examined the phase behavior for polydisperse polymers.

The reason for us for employing concentration dependent expressions for the interaction parameters g_{12} and g_{23} has been the examination of available experimentally determined parameters. These parameters turn out to be strongly dependent on concentration, especially g_{12} [8]. In Figure 6 the concentration dependence of g_{12} is shown for different solvent-water mixtures.

$g_{12}(\phi_2)$ for DMF-water mixtures has been calculated from data on G^E of Saphon [13]. The concentration dependence of g_{12} for DMF-water is described by the expression:

$$g_{12} = -10.619 + 2.190\ \phi_1 + 11.518\ \exp(-0.255\ \phi_1) + 0.092\ \exp(-17.962\ \phi_1)$$

The concentration dependence of g_{12} for the mixtures water-THF and water-dioxane are given by equation (2) and (3) respectively and for the mixture water-acetone by (Chapter 4):

$$g_{12} = 0.979 + 1.127\ \exp(-2.306\ \phi_1) + 0.292\ \exp(-12.564\ \phi_1)$$

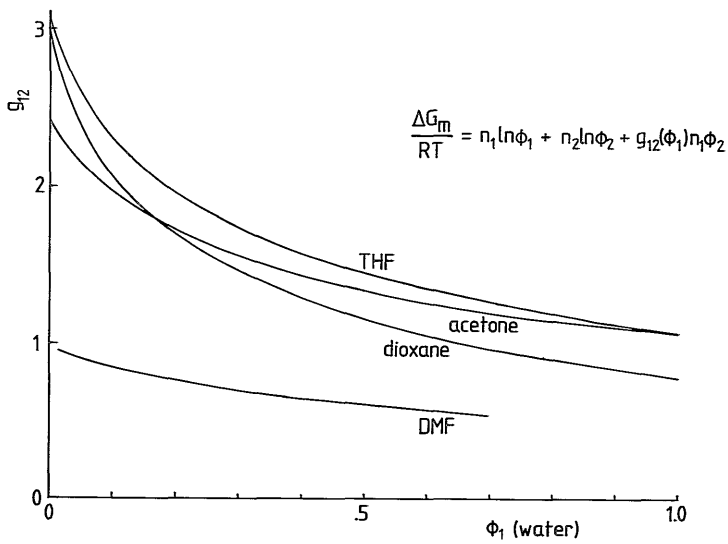

Fig. 6. Concentration dependent interaction parameters for binary solvent-water systems

We have not used the multi-order polynomials given by Altena [8] to approximate the experimental data on g_{12} because the smooth functional relation between g_{12} and ϕ_2 could be better approximated with the expressions we use; for the poorly miscible systems acetone-water and THF-water the equation used for curve fitting of $g_{12}(\phi_2)$ turned out to have a large influence on the calculated phase behavior of the ternary systems.

Kamide, Yilmaz and Altena found that an increasing value of g_{12} (poorer miscibility of solvent and nonsolvent) leads to a shift of the binodal towards the direction of the polymer-nonsolvent axis of the ternary diagram, while the slope of the tielines becomes less steep. We have examined the influence of the use of different solvents on the phase behavior of CA/solvent/water systems, assuming the solvent-polymer $g_{23}(\phi_2/\phi_2+\phi_3)$ parameter to keep the value for dioxane-CA mixtures. The solvents we have examined are THF, acetone, dioxane and DMF because the use of these solvents for the preparation of CA casting solutions leads to very different membrane structures upon coagulation of the solutions in a water bath. This will be shown in Chapter 6.

From Figure 6 one might conclude that the thermodynamic interactions between water and THF, acetone, respectively dioxane are quite the same. The value of g_{12} however, is only an indirect indication for the miscibility of a binary mixture. A better indication for the miscibility of a binary mixture is the following expression:

$$\phi_1 \frac{d\mu_1}{d\phi_1} \frac{\bar{v}_2 M_2}{\bar{v}_1 RT}$$

(the relation between μ_1 and g_{12} is given by eqn. (10) in Chapter 4).
With a decreasing value for this dimensionless expression the miscibility of the binary mixture also decreases (when the value for this expression is < 0 the binary mixture is separated into two phases). Figure 7 shows that the miscibility for the various mixtures differs considerably within a large concentration range.

The effect of the varying miscibility behavior of the binary systems on the ternary phase behavior is shown in Figure 8. It can be seen that the slope of the tielines becomes less steep when the miscibility of the solvent-water mixture becomes worse. This effect is in accordance with the calculations

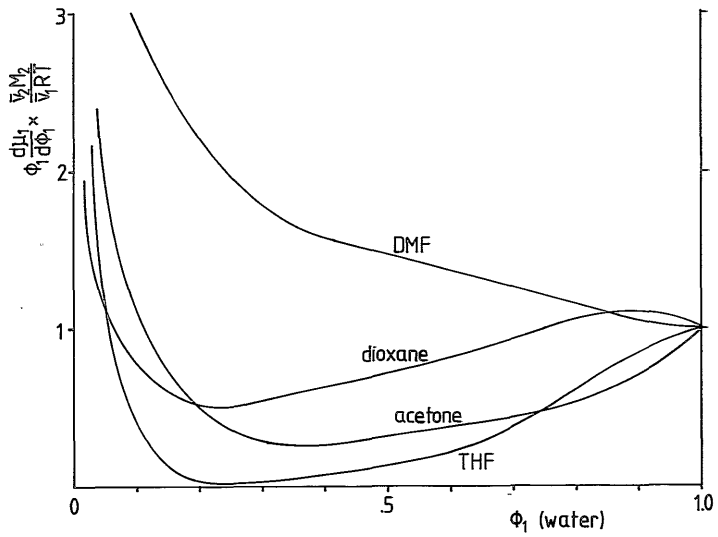

Fig. 7. The miscibility of binary solvent-water systems as a function of the composition.

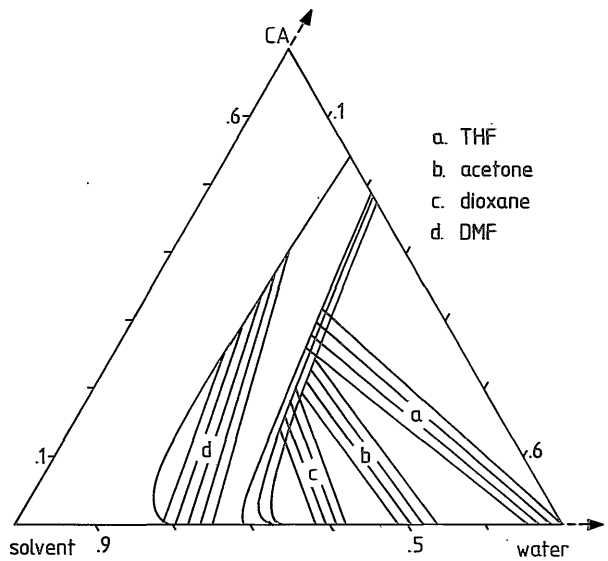

Fig. 8. Calculated binodals and tielines for ternary CA/solvent/water systems, using $g_{23}(\phi_2)$ for dioxane-CA mixtures.

reported by the previously mentioned authors [6,8,12]. The shift of the position of the binodal towards the nonsolvent-polymer axis at decreasing miscibility of the solvent-water mixture going from DMF to acetone, is also in accordance with previous calculations [8]. However, it has not yet been noticed that the binodal shifts to the left again for very poorly miscible mixtures (going from acetone to THF).

The phase behavior of the four ternary systems, shown in Figure 8, has been calculated, neglecting the influence of the varying g_{23} parameters. In a separate procedure, we have calculated the influence of this interaction parameter on the phase behavior, using the experimental g_{23} data for CA-dioxane, CA-acetone and CA-THF and an assumed value of 0.42 (this value is equal to the concentration independent part of $g_{23}(\phi_2)$ for THF-CA). The other parameters used for the calculations have been taken from the system CA/dioxane/water.

In Figure 9 the results are shown when using the appropriate g_{23} parameters of CA-dioxane and CA-THF. The calculated differences between the phase behavior for g_{23} (dioxane-CA) and g_{23} (acetone-CA), respectively, g_{23} (THF-CA) and $g_{23} = 0.42$ were so small that they could not be visualized in Figure 9. Thus the interaction parameter g_{23} has to change to a considerable extent to

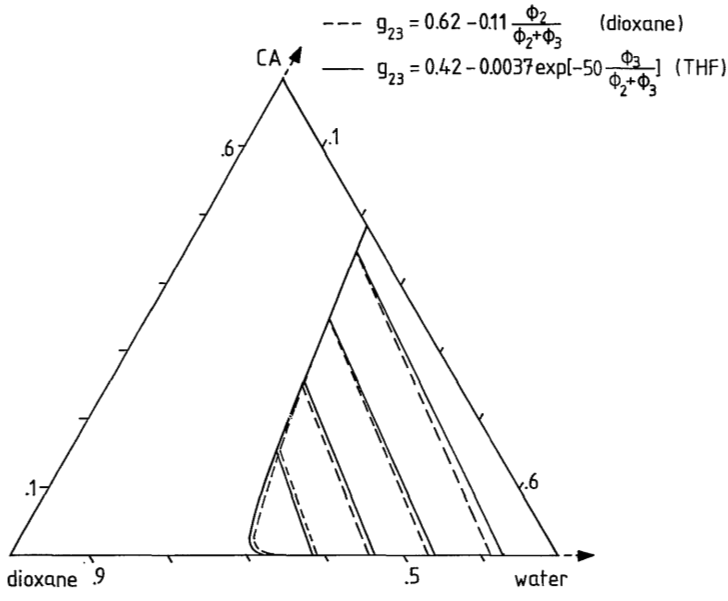

Fig. 9. Calculated binodals and tielines for the ternary system CA/dioxane/water, using $g_{23}(\phi_2)$ for dioxane-CA and THF-CA mixtures.

influence the phase behavior of a polymer/solvent/nonsolvent system, as has also been shown by Yilmaz [12]. However, it is doubtful whether the expressions for $g_{23}(\phi_2)$ chosen by Yilmaz are still realistic.

The third parameter that can influence the ternary phase behavior is χ_{13}, the parameter describing the thermodynamic interaction between the nonsolvent and the polymer. The previously mentioned authors [6,8,12] have already shown that the binodal shifts towards the polymer-solvent axis and the slope of the tielines becomes steeper for an increasing value of χ_{13}. This effect can be very large because the value of χ_{13} can vary strongly, using different nonsolvent-polymer combinations [8].

5.10. Conclusions

- Comparison of the cloud point curve with the experimentally found composition of the coexsisting phases shows that the phase behavior near the critical point is influenced by the polydispersity of the polymer, for ternary systems.
- When using the Flory-Huggins theory for three-component systems, with concentration dependent binary interaction parameters, for the calculation of the phase behavior, the neglect of the polydispersity of the polymer is responsible for only a minor part of the unaccuracy of the calculation. The neglect of ternary effects in the expression for the free energy is a larger shortcoming of our calculation procedure than the assumed monodispersity of the polymer.
- Despite the shortcomings of our calculation procedure it can be concluded that the phase behavior of ternary systems can be predicted fairly well. This indicates that the used expressions for the Gibbs free energy are also accurate enough to be used for the calculation of the driving forces for diffusion in ternary systems.
- For the solvents examined by us it is mainly the variation of their thermodynamic interaction with the nonsolvent that influences the demixing behavior of the polymer/solvent/nonsolvent system. The miscibility of the solvent and the nonsolvent especially affects the slope of the tielines.

Acknowledgement

The authors thank Mr. Van Berkel for the experimental work on the demixing behavior of the solutions and Mr. Bulten for performing the osmotic pressure measurements.

5.11. APPENDIX A. Phase equilibria of the system poly(2,6-dimethyl-1,4-phenyleneoxide)/trichloroethylene/methanol

The demixing behavior of the ternary system poly(2,6-dimethyl-1,4-phenyleneoxide/trichloroethylene/methanol (PPO/TCE/MeOH) has been examined in order to obtain the experimental data necessary to elucidate the mechanism of membrane formation for this system. Some experimental data for this system are already known: Wijmans [14] investigated the position of the cloud point curve, and the position of the liquid-liquid demixing gap has been determined in the appendix of Chapter 2 of this thesis.

In this appendix we will present some experimentally determined compositions of coexisting liquid phases. The experimental procedure followed to obtain these data has been described earlier in this chapter. (The compositions of the distilled TCE/MeOH mixtures have been determined by density measurements). Within the examined composition range, two clear liquid phases could be obtained before gelation of the concentrated phase set in. PPO has been taken from the batch used by Wijmans; $\bar{M}_n$ = 21,000; $\bar{M}_w$ = 44,000.

The compositions of the coexisting liquid phases at 25°C are represented in Figure A1, that represents a small part of the phase diagram, where the relevant measurements are performed. The compositions are represented by weight fractions of the components. The dashed curve connects the compositions of the phases into which the initial solutions, containing 4 wt.% PPO, are separated. The full curve represents the compositions of solutions which start to demix into two liquid phases at 25°C, upon quenching (at 20 wt.% PPO) or upon cooling (at PPO concentrations <10 wt.%). It can be seen that the polydispersity of PPO causes the two curves to diverge at low PPO concentrations.

In order to compare the phase diagram of the system PPO/TCE/MeOH with the phase diagrams determined for the systems CA/solvent/water, with dioxane and THF as solvent respectively, we have represented the compositions of the coexisting phases for these systems by volume fractions of the components in Figure A2.

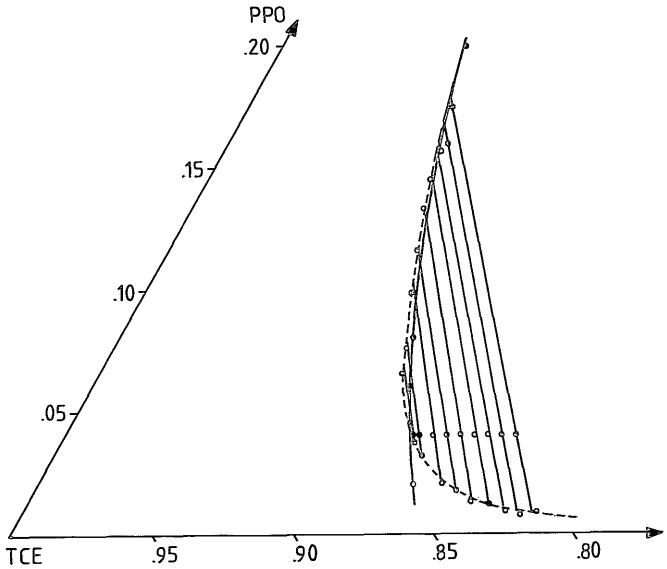

Fig. A1. Isothermal phase diagram (in wt.%) for the system PPO/TCE/MeOH at 25°C —●— : cloud point curve; o—o—o: compositions of coexisting phases connected by a tieline through the composition of the initial solution.

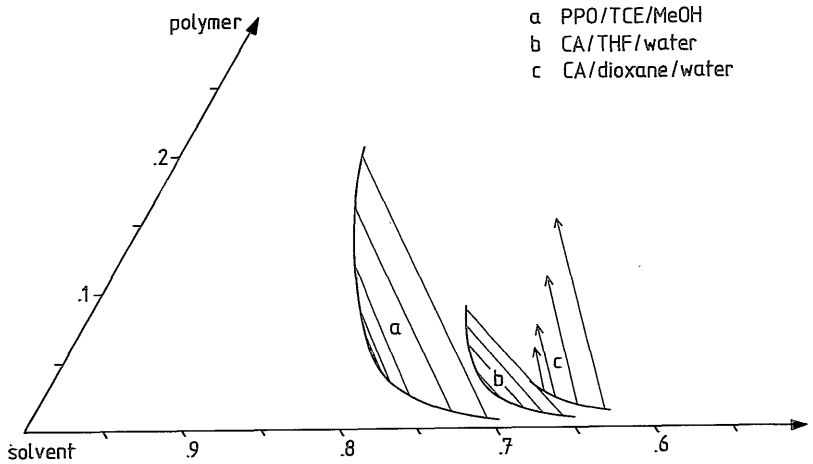

Fig. A2. Isothermal phase diagrams (in vol.%) for the indicated polymer/solvent/nonsolvent systems. The curves represent the compositions of coexisting phases, obtained from demixed, 4 wt.% polymer solutions.

Compared to the ternary CA systems, the binodal curve for the system PPO/TCE/MeOH is shifted into the direction of the polymer-solvent axis; the slope of the tielines for the PPO system has a value in between the values for the two CA systems. According to the calculations presented in this chapter, these two characteristics are correlated to a lower swelling value for PPO in MeOh compared to the swelling value for CA in water, and a lower miscibility of MeOH with TCE compared to the miscibility of water with dioxane. These conclusions can be drawn on the condition that the miscibility of PPO with TCE is, broadly speaking, equal to the miscibility of CA with dioxane or THF.

We have measured the equilibrium swelling value of PPO in MeOH to be 7.5 (±0.5) wt.% MeOH. This value corresponds with 11(±1) vol.% MeOH. The swelling value of CA in water is 17 vol.% water [4]. This means that the thermodynamic interaction between the polymer and the nonsolvent is indeed responsible for the fact that, for the PPO system less nonsolvent is needed for entering the demixing gap than for the two CA systems.

Unfortunately, no data are available on the thermodynamic interaction between TCE and MeOH. Thus we cannot verify whether the relatively flat slope of the tielines for the PPO system are related to a low tendency of mixing of MeOH with TCE.

References

1. A.J. Reuvers, J.W.A. van den Berg and C.A. Smolders, Formation of membranes by means of immersion precipitation. Part I. A model to describe the mass transfer during immersion precipitation, Submitted for publication to J. Membrane Sci.
2. A.J. Reuvers and C.A. Smolders, Formation of membranes by means of immersion precipitation. Part II. The mechanism of formation of membranes prepared from the system cellulose acetate - acetone - water, Submitted for publication to J. Membrane Sci.
3. A.J. Reuvers, F.W. Altena and C.A. Smolders, Demixing and gelation behavior of ternary cellulose acetate solutions, J. Polym. Sci., Pol. Phys. Ed., 24 (1986) 793.
4. M.H.V. Mulder, T. Franken and C.A. Smolders, Preferential sorption versus preferential permeability in pervaporation, J. Membrane Sci., 22 (1985)

155.

5. R. Koningsveld and A.J. Staverman, Liquid-liquid phase separation in multicomponent polymer solutions. I. Statement of the problem and description of methods of calculation, J. Polym. Sci., A-2, 6 (1968) 305.
6. K. Kamide, S. Matsuda and Y. Miyazaki, Phase equilibria of quasi-ternary systems consisting of multicomponent polymers in a binary solvent mix ture. I. Theoretical basis and suitable choice of solvent 1 and solvent 2, Polym. J., 16 (1984) 479.
7. K. Kamide and S. Matsuda, Phase equilibria of quasi-ternary systems consisting of multicomponent polymers in a binary solvent mixture. III. Effects of average molecular weight and molecular weight distribution of the original polymer, Polym. J., 16 (1984) 591.
8. F.W. Altena and C.A. Smolders, Calculation of liquid-liquid phase separation in a ternary system of a polymer in a mixture of a solvent and a nonsolvent, Macromolecules, 15 (1982) 1491.
9. C. Treiner, J. Bocquet and M. Chemla, Seconds coefficients du viriel des mélanges eau-tétrahydrofurane (THF). Influence sur les coefficients d'activité de l'eau et du THF a 25°C, J. Chim. Phys. Physicochim. Biol., 70 (1) (1973) 72.
10. J.R. Goates and R.J. Sullivan, Thermodynamic properties of the system water-dioxane, J. Phys. Chem., 62 (1958) 188.
11. F.W. Altena, Phase separation phenomena in cellulose acetate solutions in relation to asymmetric membrane formation, Thesis, Chapter 6, Twente University of Technology, Enschede, The Netherlands (1982).
12. L. Yilmaz and A.J. McHugh, Analysis of nonsolvent-solvent-polymer phase diagrams and their relevance to membrane formation modeling, J. Appl. Polym. Sci., 31 (1986) 997.
13. S. Saphon and H.J. Bittrich, Physikalisch-chemische Untersuchungen in binären Systemen von Dimethylformamid mit Äthylenglykol, Diäthylenglycol und Wasser, Z. Phys. Chem., 252, 113 (1973).
14. J.G. Wijmans, H.J.J. Rutten and C.A. Smolders, Phase separation phenomena in solutions of poly(2,6-dimethyl-1,4-phenyleneoxide) in mixtures of trichloroethylene, 1-octanol and methanol: relationship with membrane formation, J. Pol. Sci. Polym. Phys. Ed., 23 (1985) 1941.

6. THE CONNECTION BETWEEN NON-IDEALITY PARAMETERS OF TERNARY SYSTEMS AND THE MECHANISM OF MEMBRANE FORMATION BY MEANS OF IMMERSION PRECIPITATION

By A.J. Reuvers and C.A. Smolders

6.1. Summary

We have obtained the necessary parameters for the system CA/dioxane/water to be used in our previously derived diffusion model for membrane formation by means of immersion precipitation.

Sedimentation and diffusion measurements have been performed to obtain expressions for the frictional coefficients for diffusion in the binary mixtures dioxane-CA $[R_{23}(\phi_3)]$ and dioxane-water $[R_{12}(\phi_2)]$.

Using the frictional coefficients of the system CA/dioxane/water, model calculations have been performed in order to examine the specific influence of the three thermodynamic interaction parameters $g_{12}(\phi_2)$, $g_{23}(\phi_2)$ and χ_{13} on the moment of onset of liquid-liquid demixing in an immersed casting solution.

Light transmission measurements performed on various CA/solvent/water systems confirm the conclusion from the calculations that the thermodynamic interaction between the solvent and the nonsolvent (g_{12}) has a dominant influence on the moment of onset of liquid-liquid demixing in the immersed film.

SEM analysis clearly show the narrow connection between the moment of onset of liquid-liquid demixing and the ultimate membrane morphology.

6.2. Introduction

In Chapter 4 of this thesis we applied the diffusion model, described in Chapter 3, on the ternary membrane forming system CA/acetone/water. Composition changes in the casting solution upon immersion of this solution into a coagulation bath, have been calculated.

The calculations showed the formation of a layer highly concentrated polymer solution layer adjacent to the solution surface. The thickness of this

concentrated layer increases until the onset of liquid-liquid demixing fixes the asymmetric polymer distribution in the solution film. The moment of onset of the demixing process and, therefore, the ultimate thickness of the concentrated surface layer depends on the total thickness of the film.

However, addition of a certain minimum amount of nonsolvent, in this case water, to the casting solution results in a drastic change of the membrane formation mechanism: upon immersion of the ternary casting solution, the composition adjacent to the surface of the polymer solution instantaneously becomes metastable, which results in the formation of nuclei of a polymer lean phase, yielding a membrane with a very thin toplayer.

The existence of these two different mechanisms of membrane formation has been confirmed by light transmission measurements on coagulating casting solutions (Chapter 5).

In this chapter we will examine the connection between the choice of the solvent and the mechanism of membrane formation. The influence of the choice of the solvent on the ultimate structure of the membrane has been the subject of a few earlier investigations [1-4].

So et al. [1] and Frommer [2] measured the water content of swollen CA membranes prepared from various binary casting solutions immersed into a water bath. So proposed a correlation between the porosity of the ultimate membrane and the solvent solubility parameters: the higher the solvent solubility parameter δ, the higher the porosity of the ultimate membrane. Frommer proposed a correlation between the rate of precipitation of the casting solution and the tendency of mixing of solvent with water, indicated by the heat of mixing: the higher the heat of mixing of the solvent with water, the higher the precipitation rate.

Bloch [3] and Guillotin [4] reported pure water flow rates and salt retention values for CA membranes prepared from binary casting solutions. From their results it can be concluded that the selectivity increases and the pure water flux decreases when the CA casting solutions are prepared from solvents in the sequence: DMSO, DMF, TEP, acetic acid, dioxane and acetone.

These investigations have all in common that empirical correlations have been found between the ultimate membrane structure and the nature of the solvent used for the preparation of the casting solution. We wish to examine this correlation in a more fundamental way using the diffusion model described in Chapter 3. According to this model the nature of the solvent is

characterized by its thermodynamic and hydrodynamic interaction with the two other components.

We will first obtain expressions for the hydrodynamic interaction parameters for dioxane-water $[R_{12}(\phi_2)]$ and dioxane-CA $[R_{23}(\phi_3)]$ from diffusion and sedimentation measurements. These parameters will be compared with the hydrodynamic interaction parameters derived for the acetone-water and acetone-CA mixtures. The hydrodynamic interaction parameter for water-CA $[R_{13}(\phi_3)]$ will be determined indirectly, using light transmission measurements on CA-dioxane casting solutions immersed into various dioxane-water mixtures.

Using the hydrodynamic interaction parameters of the ternary system CA/dioxane/water we will calculate the specific influence of the thermodynamic interaction parameters of various solvent-water pairs (g_{12}) on the initial diffusion behavior in the immersed casting solution. The influence of the thermodynamic interaction between solvent and polymer (g_{23}) respectively between nonsolvent and polymer (χ_{13}) on the initial membrane formation process will be examined, using assumed values for these parameters.

Finally the model calculations will be verified by light transmission measurements on immersed CA casting solutions and by SEM analysis to observe the ultimate membrane structure obtained from these various casting solutions.

6.3. The frictional coefficients for dioxane-CA (R_{23}) and dioxane-water (R_{12}) mixtures derived from experimental data

- R_{23} derived from sedimentation measurements -

In Chapter 4 it has been shown that the concentration dependent binary frictional coefficient R_{23} can be derived from the sedimentation coefficient $s(\phi_3)$.

For the binary system dioxane-CA we have performed sedimentation experiments within a very limited concentration range because already at a fairly low CA concentration the rate of sedimentation of the polymer turned out to be too low to be measurable. In Table 1 the experimentally obtained sedimentation coefficients are presented together with the factor $F(\phi_3)$, defined in Chapter 4 of this thesis and expressing the concentration dependence of R_{23}:

$$R_{23}(\phi_3) = \frac{\bar{v}_3 RT}{M_2 F(\phi_3)} \qquad (1)$$

where $\bar{v}_3$ is the partial specific volume of the polymer and M_2 is the molecular weight of dioxane; R and T have their usual meaning.

Table 1. The sedimentation coefficient s and the factor F [eqn. (1)] as a function of the volume fraction of CA in the CA-dioxane solution, at 20°C.

ϕ_2	$s * 10^{14}$ [sec]	$F * 10^9$ [$m^2 sec^{-1}$]
.023	2.69	2.37
.040	1.93	1.70

When the values of $F(\phi_3)$ from Table 1 are compared with the values of $F(\phi_3)$ derived for CA-acetone mixtures (Chapter 4) it can be concluded that $F(\phi_3)$ for CA-dioxane mixtures is about 6 times smaller than $F(\phi_3)$ for CA-acetone mixtures, at low polymer concentration. We will assume that this ratio between the factors $F(\phi_3)$ for both mixtures remains the same at higher polymer concentrations. Therefore, we approximate the concentration dependence of $R_{23}(\phi_3)$ for CA-dioxane with an expression that resembles the expression used for CA-acetone:

$$F(\phi_3) = 2.73 * 10^{(-9-5.17\ \phi_3)} \ m^2/sec \qquad (2)$$

The large difference between the frictional coefficients R_{23} for the systems CA-acetone and CA-dioxane is in accordance with the large difference between the mutual diffusion coefficients for these systems measured by Altena [5].

It can be concluded that the choice of the solvent can have a large influence on the value of R_{23}. The effect of such a variation of R_{23} on the rate of diffusion during membrane formation however, is overshadowed by the dominant influence of R_{12} on the rate of the ternary diffusion process, as has already been shown in Chapter 4. This frictional coefficient R_{12} will be obtained from diffusion measurements performed on water-dioxane mixtures.

- The integral diffusion coefficient for dioxane-water mixtures -

The binary frictional coefficient $R_{12}(\phi_2)$ can be derived from experimental data on the mutual diffusion coefficient $D(\phi_2)$ and the chemical potential of one of the components in the binary mixture (Chapter 4).

As far as we know $D(\phi_2)$ for water-dioxane mixtures has only been measured for $\phi_2 = 0.95$ [5]. Because we wish to know the concentration dependence of D within the complete concentration range we have performed additional diffusion measurements.

Integral diffusion coefficients have been measured by the diaphragm cell technique using a Stokes type cell [6]. Two 50-cm³ cell compartments were separated by a 2-mm thick Pyrex sintered glass diaphragm (pore size 5-10 μm), and each cell was stirred magnetically (60 r.p.m). The Teflon bottom plug was of the type described by Albright [7]. The measurements were performed at 25.0°C.

The cell was calibrated by allowing 0.1 M potassium chloride to diffuse into pure water and assuming the integral diffusion coefficient to be $1.87 * 10^{-9}$ m²/sec [6].

The compartments were filled according to the procedure described by Stokes [6]. The more dense liquid was placed in the bottom compartment. The diffusion runs were stopped after 3 to 9 days.

The compositions of the dioxane-water mixtures from the diffusion runs were determined by a differential refractometer.

The integral diffusion coefficients were calculated using the formula [8]:

$$\bar{D} = \ln \left[\frac{(\Delta c_2)_o}{(\Delta c_2)_f}\right] / \beta\theta \qquad (3)$$

where $\bar{D}$ is the integral diffusion coefficient, $(\Delta c_2)_o$ and $(\Delta c_2)_f$ are the initial and the final concentration differences of dioxane between the cell compartments respectively, β is the "cell constant" and θ is the diffusion time. By calibration, β was found to be $7.53 * 10^2$ m^{-2}.

In Table 2 the values of $(c_2)_o$ in both compartments and of $(\Delta c_2)_f$ are reported together with the calculated values of $\bar{D}$.

Table 2. Integral diffusion coefficients for the system dioxane-water at 25°C, measured by the diaphragm cell technique; c_2 is the concentration of dioxane.

$(c_2)_o$ top $* 10^{-3}$ [kg m^{-3}]	$(c_2)_o$ bottom $* 10^{-3}$ [kg m^{-3}]	$(\Delta c_2)_f$ $* 10^{-3}$ [kg m^{-3}]	$\bar{D}$ $* 10^{9}$ [m^2 sec^{-1}]
0.0000	0.1003	0.0590	1.37
0.0000	0.2009	0.1555	1.35
0.1943	0.3856	0.1340	1.05
0.4039	0.6298	0.1575	0.74
0.6096	0.8191	0.1595	0.52
0.8199	0.9263	0.0760	0.61
0.9227	1.0330	0.0590	1.26

- Derivation of R_{12} from the diffusion data -

To obtain R_{12} from the diffusion data, it is necessary to rewrite the integral diffusion coefficients into "true" mutual diffusion coefficients. Assuming the partial specific volumes of dioxane and water to be constant, the integral diffusion coefficient $\bar{D}$ is approximately related to the mutual diffusion coefficient $D(\phi_2)$ via the relation [8]

$$\bar{D} = \frac{1}{(\phi_M'' - \phi_M')} \int_{\phi_M'}^{\phi_M''} D(\phi_2) d\phi_2 \qquad (4)$$

where $\phi_M = \frac{1}{2}\{(\phi_2)_o + (\phi_2)_f\}$ and the superscripts ' and " refer to the bottom and top compartments respectively; ϕ_i is the volume fraction of component i.

In Chapter 3 we have derived the following relation between the mutual diffusion coefficient D and the binary frictional coefficient R_{12},

$$D(\phi_2) = \frac{1}{R_{12}(\phi_2)} \bar{v}_2 \phi_1 \frac{d\mu_1}{d\phi_1} \qquad (5)$$

where $\bar{v}_2$ is the partial specific volume of the solvent (dioxane) and μ_1 is the chemical potential of the nonsolvent (water) in the binary mixture, given by the expression

$$\frac{M_1}{RT} * \Delta\mu_1 = \ln\phi_1 + (1-\phi_1)\{1-s+(1-\phi_1)(g_{12}+\phi_1 \frac{dg_{12}}{d\phi_1})\} \qquad (6)$$

where s is equal to $\bar{v}_1 M_1/\bar{v}_2 M_2$ and M_i is the molecular weight of component i; $\Delta\mu_1$ is equal to $\mu_1-\mu_o$, where μ_o is the chemical potential of pure water. The interaction parameter g_{12} for dioxane-water mixtures at 25°C is given by:

$$g_{12} = 1.389 - 0.607\ \phi_1 + 1.050\ \exp(-4.731\ \phi_1) + 0.500\ \exp(-19.922\ \phi_1) \qquad (6a)$$

Substitution of the equations (5) and (6) in eqn. (4) relates the measured integral diffusion coefficients $\bar{D}$ to $R_{12}(\phi_2)$. By curve fitting it has been found that the measured integral diffusion coefficients, represented in Table 2, are well approximated by eqn. (4) when using the following expression for $R_{12}(\phi_2)$:

$$\frac{1}{R_{12}(\phi_2)} = \frac{M_2}{\bar{v}_1 RT}\ (1.00 - 0.25\ \phi_2)\ D(\phi_2=0) \qquad (7)$$

where $D(\phi_2=0) = 1.20 * 10^{-9}\ m^2\ sec^{-1}$.
This is shown in Figure 1 where the integral diffusion coefficients are represented for the various intervals $\phi''_M - \phi'_M$, together with $D(\phi_2)$ calculated from eqn. (5) using the expressions (6) and (7). The diffusion coefficient $D(\phi_2=0.95)$ measured by Altena [5] is also in good agreement with the calculated diffusion coefficient.

According to the fitting procedure the frictional coefficient R_{12} is only slightly dependent on concentration and its value is about the same as for the system acetone-water. The strong concentration dependence of the calculated mutual diffusion coefficient is mainly caused by the thermodynamic factor, as is the case for the binary mixture acetone-water (Chapter 4).

Equation (7) will be used in the ternary diffusion equations, describing the mass transport in the immersed CA-dioxane casting solution, whereas equation (5) will be used in the binary diffusion equation describing the mass transport in the coagulation bath (see Chapter 3).

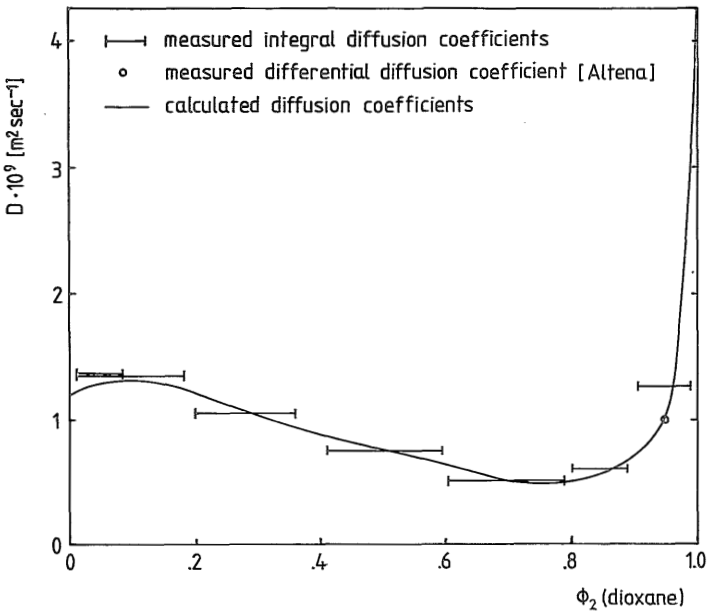

Fig. 1. Concentration dependence of the mutual diffusion coefficient D for the binary system dioxane-water at 25°C. For the calculation of $D(\phi_2)$ the equations (4-7) in the text have been used.

6.4. Determination of the frictional coefficient $R_{13}(\phi_3)$ for the ternary system CA/dioxane/water

According to the diffusion model, applied for a polymer solution immersed into a coagulation bath, the onset of liquid-liquid demixing in the polymer solution after being immersed into the bath, should either take place instantaneously or be delayed for at least the period over which the solution film can be considered as a semi-infinite medium.

For the system CA/acetone/water the existence of these different types membrane formation processes has been confirmed by light transmission measurements performed on coagulating casting solutions (Chapter 4). It has been found that addition of a certain minimal amount of water to the casting solution leads to a sharp transition from delayed to instantaneous onset of liquid-liquid demixing for this ternary system.

The same type of light transmission experiments has been performed for the system CA/dioxane/water. In contrast with CA-acetone casting solutions, it

appeared that immersion of a binary CA-dioxane casting solution into a pure water bath results in instantaneous onset of liquid-liquid demixing. Delayed onset of demixing in CA-dioxane solutions could also be obtained, but only after addition of a certain minimum amount of dioxane to the water bath.

In this section, we wish to find a reasonable expression for the still unknown frictional coefficient $R_{13}(\phi_3)$ (water-polymer interaction), for the system CA/dioxane/water. This expression will be derived in the following way:

- $R_{13}(\phi_3)$ is assumed to be related to $R_{23}(\phi_3)$ (solvent-polymer interaction) according to a specially choosen relation;
- this relation contains one unknown variable that is determined by an iterative procedure: for the optimal value of the variable, model calculations must yield the sharp transition from instantaneous to delayed onset of demixing at the same dioxane concentration in the coagulation bath as has been determined experimentally.

In a similar way, an expression for $R_{13}(\phi_3)$ has been derived for the system CA/acetone/water in Chapter 4:

$R_{13}(\phi_3)$ was assumed to be related to $R_{23}(\phi_3)$ according to the following relation:

$$R_{13}(\phi_3) = C(\bar{v}_1/\bar{v}_2)R_{23}(\phi_3) \qquad (8)$$

The iterative procedure resulted in a C-value of 0.5. Because it seems reasonable to expect that the smaller water molecules penetrate the 'polymer network' easier than the acetone molecules, the value of 0.5 for C was a satisfying result.

On physical grounds however, we expect that the ratio of $R_{13}(\phi_3)$ and $R_{23}(\phi_3)$ does not only depend on the sizes of the solvent and nonsolvent molecules, but also on the density of the 'polymer network', determined by ϕ_3. In this Chapter therefore, $R_{13}(\phi_3)$ will be assumed to be related to $R_{23}(\phi_3)$ in the following way:

$$R_{13}(\phi_3) = 10^{C\phi_3}(\bar{v}_1/\bar{v}_2)R_{23}(\phi_3) \qquad (9)$$

The procedure used to calculate the composition changes in the immersed film has been described in Chapter 4. The composition changes are calculated for the period during which the bottom composition of the film remains unchanged. Since then the composition charges are a function of $mt^{-1/2}$ only (where m is the position coordinate), the composition profile in the film during this period can be represented by a non varying composition path in the ternary diagram of the system considered (see Chapter 4). This path represents all local compositions that exist in the immersed film.

This composition path connects the initial casting solution composition (far from the interface) with the interfacial boundary composition of the film, to be found on the binodal in the ternary diagram. A tieline connects the interfacial boundary composition of the film with the interfacial boundary composition of the coagulation bath. These interfacial boundary compositions remain unchanged as long as i) the bottom composition of the film remains unchanged, ii) no convection takes place in the bath and iii) no liquid-liquid demixing occurs in the film.

The following parameters are used for the calculation of the composition changes and the moment of onset of demixing in the immersed CA-dioxane casting solution:

- the frictional coefficients $R_{23}(\phi_3)$ and $R_{12}(\phi_1/\phi_1+\phi_2)$ given by the expressions (1-2) and (7) respectively;
- the thermodynamic interaction parameters
  g_{12} given by expression (6a)
  g_{23} (dioxane-CA) = 0.62 - 0.11 $(\phi_2/\phi_1+\phi_2)$ [9],
  χ_{13} (water-CA) = 1.4 [10];
- the molecular weights of CA, dioxane and water: 27,000, 88.12 and 18.0 gram mol^{-1} respectively;
- the partial specific volume of CA, dioxane and water: 0.717, 0.967 and 1.003 * 10^{-3} m^3kg^{-1} respectively.

In Figure 2 the calculated composition paths are shown for a 15 vol.% CA-dioxane solution immersed into a coagulation bath of which the initial composition has been varied. It can be seen that the composition paths calculated for the pure water bath and the 18.5% dioxane in water bath do cross the demixing gap. This means that immediately after immersion of the casting

solution in these baths, nuclei of the polymer lean phase are formed in the film just beneath the interfacial boundary layer. The formation of these nuclei can be detected by light transmission measurements.
The calculated composition path for the casting solution immersed into the 37.5% dioxane in water bath does not cross the demixing gap, which means that the formation of nuclei of the diluted phase is delayed.

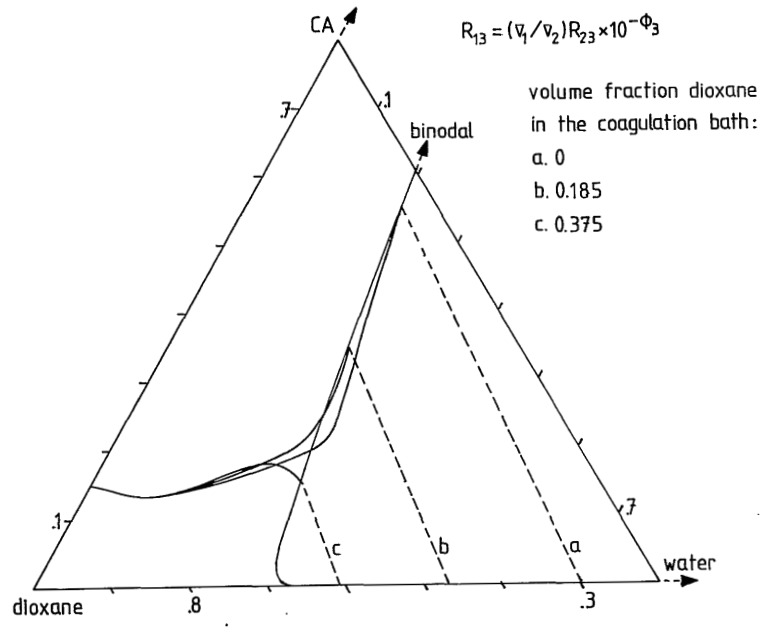

Fig. 2. Calculated initial composition paths for 15 vol.% CA-dioxane solutions immersed into a coagulation bath with a varying initial composition.

In Table 3 the calculated and measured minimum dioxane concentrations in the coagulation bath, necessary to induce delayed onset of demixing (the critical coagulation bath composition), are represented as a function of the polymer content of the casting solution. The experimental values are obtained by light transmission measurements (see Chapter 4) with an accuracy of 1 vol.% dioxane.

Table 3. The minimum dioxane content of the coagulation bath necessary to induce delayed onset of demixing at 25°C as a function of the polymer content of the casting solution. The calculations were performed, using expression (9) with C = -1.

ϕ_3 (casting solution)	ϕ_2 (coagulation bath)	
	measured	calculated
0.10	0.10	0.17
0.15	0.15	0.19
0.20	0.20	0.16

Calculations of the 'critical' coagulation bath compositions yield the best correspondence with the experimental values, using expression (9) with C = -1. This C-value means that we assume that the polymer network exerts a larger frictional force on the diffusing dioxane molecules than on the diffusing water molecules. This assumption seems reasonable because of the different sizes of the two components.

Table 4. The frictional coefficients R_{12} (water-solvent), R_{23} (solvent-CA) and R_{13} (water-CA) for the systems CA/acetone/water and CA/dioxane/water.

	CA/acetone/water	CA/dioxane/water
$\frac{\bar{v}_1 RT}{M_2 R_{12}}$	$1.25 * 10^{-9}$ m²/sec	$(1.00-0.25\ \phi_2) * 1.20*10^{-9}$ m²/sec
$\frac{\bar{v}_3 RT}{M_2 R_{23}}$	$1.66 * 10^{(-8-5.17\phi_3)}$ m²/sec	$2.73 * 10^{(-9-5.17\phi_3)}$ m²/sec
R_{13}	$0.5\ (\bar{v}_1/\bar{v}_2)R_{23}(\phi_3)$	$10^{-\phi_3}(\bar{v}_1/\bar{v}_2)R_{23}(\phi_3)$

In Table 4 a survey is given of the frictional coefficients for the system CA/dioxane/water (obtained in this Chapter) and for the system CA/acetone/water (obtained in Chapter 4). It is worth knowing that for the system CA/acetone/water the calculated composition paths are hardly affected, whether expression (9) (with C = -1) or expression (8) (with C = 0.5) is used, because the resistance for diffusion is dominated by R_{12}.

In all further calculations in this Chapter, frictional coefficients for the system CA/dioxane/water will be used.

6.5. Variation of the initial polymer concentration in the casting solution

In Figure 3 the influence of the initial polymer concentration in the CA-dioxane casting solution on the diffusion process is shown. The coagulation bath consists of pure water. For an initial CA concentration of 10%, as well as 20%, the composition path crosses the binodal which means instantaneous onset of liquid-liquid demixing.

The main intention of presenting this figure however, is to show the influence of the initial polymer concentration on the boundary compositions at the interface between the coagulation bath and the solution film. It can be seen that an increase of the initial polymer concentration yields a higher polymer concentration at the film side of the interfacial boundary during the first period after immersion of the film. The lower solvent concentration at the bath side of the interfacial boundary indicates that the rate of mass transport through the interfacial layer is lowered at increasing initial polymer concentration in the solution film.

These conclusions concerning the influence of the initial polymer concentration in the casting solution are also valid for ternary systems which yield a delayed onset of liquid-liquid demixing. In Chapter 7 it will be demonstrated that for membranes prepared according to the process of delayed onset of liquid-liquid demixing (type I membranes), the toplayer morphology and thickness are strongly influenced by the polymer concentration at the film side of the interfacial boundary during the first period after immersion of the film. Thus, for type I membranes it can be explained that the initial polymer concentration of the casting solution turns out to be an important controllable factor to optimize the selectivity and the resistance of the toplayer.

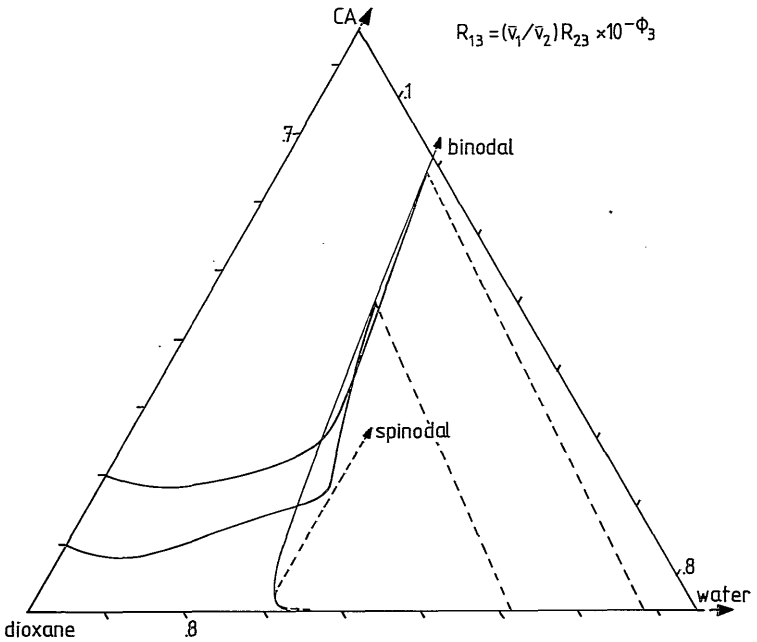

Fig. 3. Calculated initial composition paths for CA-dioxane solutions with a varying CA concentration, immersed into a pure water coagulation bath.

6.6. Influence of the three binary thermodynamic interaction parameters on the initial membrane formation process

The choice of the solvent-nonsolvent pair of components used for the preparation of asymmetric CA membranes turns out to have a large influence on the performance of the ultimate membrane [1-4]. By varying one of the components of the solvent-nonsolvent pair, two binary thermodynamic and hydrodynamic interaction parameters and the specific molar volume of the exchanged component are changed. In this section we will only examine the specific influence of the binary thermodynamic interaction parameters on the initial membrane formation process by means of model calculations. For the hydrodynamic parameters we use the expressions derived for the system CA/dioxane/water (Table 4), because in our opinion, the expression for R_{13} of this system is more realistic than the expression for R_{13} of the system CA/acetone/water.

- Influence of $g_{12}(\phi_2)$ -

First, we will examine the specific influence of the thermodynamic interaction between the solvent and the nonsolvent components $[g_{12}(\phi_2)]$ on the initial diffusion process. For $g_{12}(\phi_2)$ experimental expressions for various solvent-water combinations are used which have been described in Chapter 5. For the interaction parameters $g_{23}(\phi_2)$ and χ_{13} the experimental data for dioxane-CA, respectively water-CA are used. The molar volume of the solvent, used for the calculations, is changed together with the examined solvent-water combination.

The calculated composition paths (together with the binodals and the tie-lines connecting the interfacial boundary compositions) are shown in Figure 4, for the solvent-water combinations using dioxane, acetone and THF as solvent respectively. The composition paths have been calculated, assuming the coagulation bath to consist of pure water.

For the DMF-water combination no composition path could be calculated because the partial differential equations describing the diffusion process became intractable. This is related to the fact that the composition path tends to enter the unstable spinodal region of the composition diagram.

From Figure 7 in Chapter 5 it has been concluded that the tendency of mixing of the examined solvent-water combinations decreases in the following sequence of solvents: DMF, dioxane, acetone and THF. From Figure 4 and the calculations performed with g_{12} (DMF-water) it can be concluded that in the same sequence of solvents the parameter g_{12} causes the position of the composition path to shift from the demixing gap, in the direction of the solvent-polymer axis of the composition diagram (a shift from instantaneous to delayed onset of demixing).

For the solvents acetone and THF we have also (approximately) calculated the change of the position of the composition path from the moment the diffusion front reaches the bottom of the immersed solution film. These calculations have been performed assuming the interfacial boundary composition of the film to remain constant (see Chapter 4): for an initially 200 μm thick film the composition path crosses the binodal after 25 and 60 seconds for g_{12} (acetone-water) and g_{12} (THF-water) respectively. Thus, according to the calculations the delay time for the onset of liquid-liquid demixing increases with decreasing tendency of mixing of the solvent with the nonsolvent.

It is difficult to understand the results of the calculations as to their

physical background, because the positions of the binodal and the composition path are related to the interaction parameter g_{12} in a very complex way.

Nevertheless, from the calculations it can be concluded that a small variation of g_{12} can have a large influence on the moment of onset of liquid-liquid demixing in the immersed polymer solution and, consequently, on the ultimate membrane structure, as has been explained in Chapter 4.

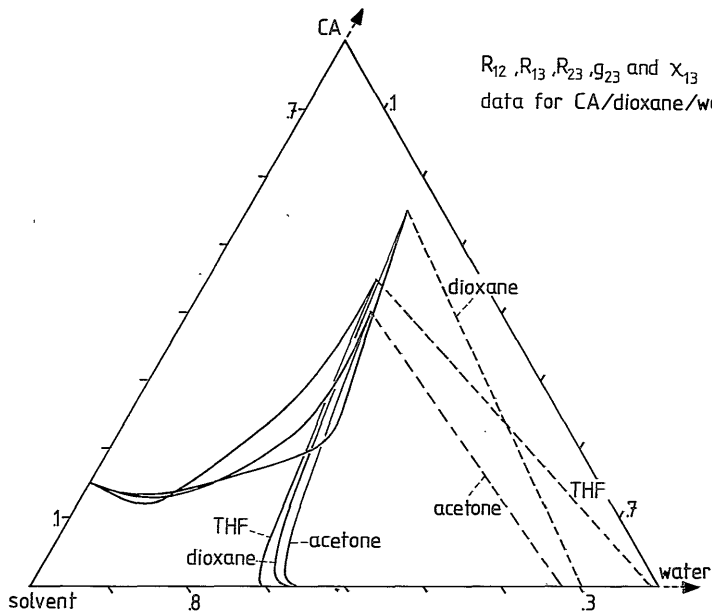

Fig. 4. Calculated influence of $g_{12}(\phi_2)$ on the initial position of the composition path for a film immersed into a pure water bath. Expressions for $g_{12}(\phi_2)$ have been chosen, which describe the thermodynamic interaction of the indicated solvents with water.

- Influence of $g_{23}(\phi_2)$ -

When the solvent component of the ternary system is varied, not only g_{12} changes, but also g_{23}. For the systems CA-dioxane, CA-acetone and CA-THF the expressions for $g_{23}(\phi_2)$ are known (see Chapter 5). The difference between these expressions is too small to have a significant influence on the positions of the composition path and the binodal. Nevertheless, the value of g_{23} may vary to a larger extent when still another solvent is chosen. Therefore,

we have calculated the influence of a larger variation of g_{23} on the positions of the composition path and the binodal.

The results, with g_{23} = 0.0 and g_{23} = 0.4, are represented in Figure 5 for a film immersed into a pure water bath. For the other thermodynamic parameters, necessary for the calculations, we have used the data for the system CA/dioxane/water. From Figure 5 it can be seen that the position of the binodal hardly changes; the direction of the tielines becomes less steep and the position of the composition path shifts towards the polymer-solvent axis when the value of g_{23} decreases. This means that the tendency towards delayed onset of liquid-liquid demixing increases when the tendency of mixing of the solvent with the polymer increases.

Thus, according to these calculations the effect of a decreasing g_{23} value on the initial membrane formation process is equal to the effect of an increasing g_{12} value. However, a rather large variation of g_{23} is necessary to obtain a significant effect.

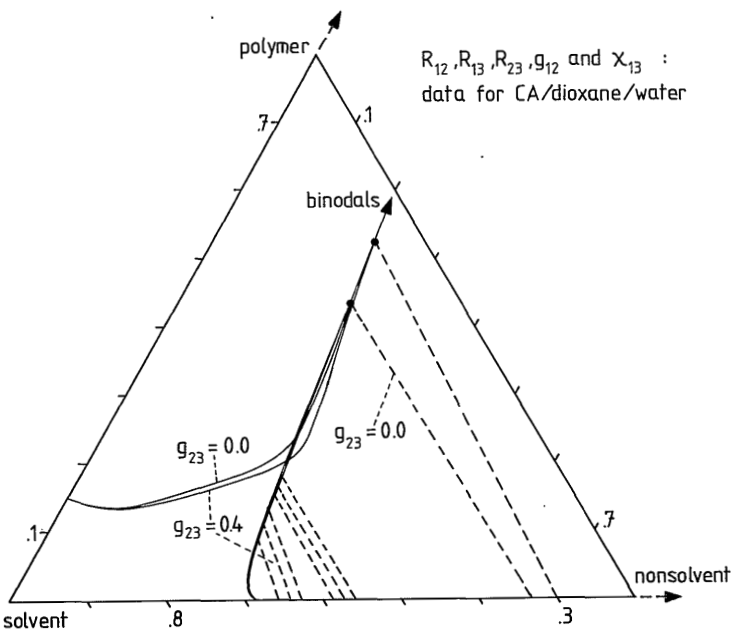

Fig. 5. Calculated influence of g_{23} on the initial position of the composition path for a film immersed into a pure water bath.

- Influence of χ_{13} -

When the nonsolvent or the polymer component in the system is varied, not only $g_{12}(\phi_2)$ or $g_{23}(\phi_3)$ but also χ_{13} (nonsolvent-polymer interaction) changes. The specific influence of χ_{13} on the initial diffusion process has been examined by comparing model calculations for χ_{13} = 1.4 and 2.0. The value of 2.0 for χ_{13} has been chosen because this interaction parameter may have a considerably higher value than 1.4, the value for CA-water interaction. Together with the other parameters used, the results of the calculations for a film immersed into a pure water bath are shown in Figure 6.

From Figure 6 it can be seen that the positions of the binodal as well as that of the composition path shift towards the polymer-solvent axis when the value of χ_{13} increases. Nevertheless, the tendency of the ternary system towards delayed onset of demixing decreases with increasing χ_{13} value. This can be concluded from the calculated delay time for the onset of demixing (assuming the interfacial boundary composition to remain constant during this delay time): for χ_{13} = 1.4 one finds 25 seconds; for χ_{13} = 2.0 a period of 10 seconds is found (initial film thickness: 200 µm).

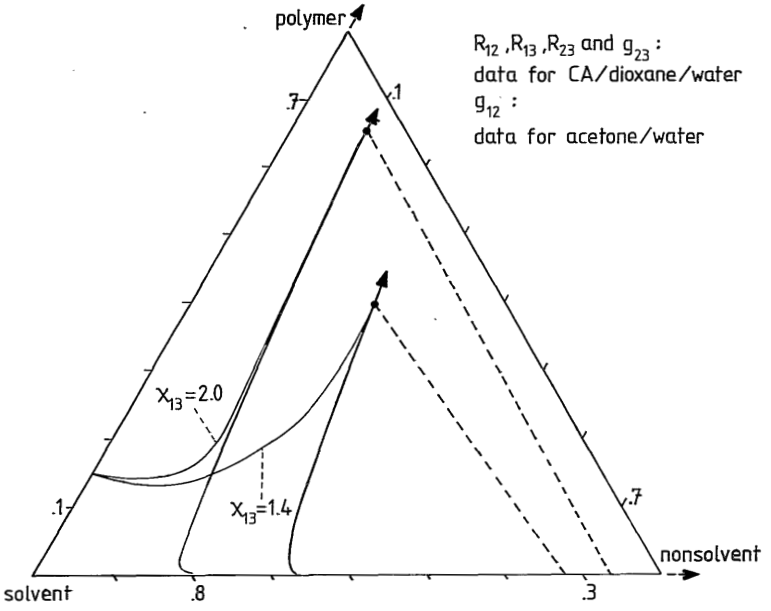

Fig. 6. Calculated influence of χ_{13} on the initial position of the composition path for a film immersed into a pure water bath.

The main results of the calculations on the specific influence of the three thermodynamic interaction parameters on the initial diffusion process can be summarized as follows:

- Decreasing values of g_{23} and χ_{13} promote the tendency towards delayed onset of liquid-liquid demixing upon immersion of a solution film into a nonsolvent bath, whereas a decreasing value of g_{12} promotes the opposite effect, viz. instantaneous demixing.
- When the solvent or nonsolvent component is varied, especially the change in the g_{12} parameter may have a large infuence on the early phenomena during the membrane formation process.

6.7. Light transmission experiments performed on CA/solvent/water systems

Light transmission experiments have been performed on various immersed CA-solvent casting solutions to obtain the delay time for the onset of liquid-liquid demixing as a function of the solvent used and of the solvent concentration in the coagulation bath. By measuring these experimental delay times the model calculations can be tested. Besides, these delay times will be correlated with the ultimate membrane structure examined with the scanning electron microscope.

The experimental set up for the light transmission experiments has been described in Chapter 4 of this thesis. For solvents with a higher density than water, the cast film has been positioned at the upper side of the immersed glass plate. For solvents with a lower density than water the opposite has been done to prevent gravitationally induced convection currents in the coagulation bath.

The results of the measurements on binary 15 vol.% CA casting solutions are represented in Figure 7. It can be seen that upon immersion into a pure water bath only THF and acetone yield a finite delay time for the onset of liquid-liquid demixing. When the solvents dioxane, DMF or DMSO are used, a minimum solvent concentration in the coagulation bath is necessary for a delayed onset of demixing.

It is very remarkable that, according to the light-transmission measurements, the tendency towards delayed onset of demixing increases in the sequence DMSO, DMF, dioxane, acetone and THF. In exactly the same sequence the tendency of the solvents to mix with water decreases. This correlation is in

accordance with the calculations in the previous section, where only g_{12} has been varied.

Obviously, variations in the frictional interaction parameters have only a slight influence on the initial diffusion processes in the film. This may also be concluded from the calculated delay times for the onset of demixing, using the frictional parameters for CA/dioxane/water, compared with the experimental delay times for THF-CA and acetone-CA solutions immersed into pure water:

CA-THF: 67 seconds (measured); 60 seconds (calculated)

CA-acetone: 19 seconds (measured); 25 seconds (calculated).

It is very striking to see the large influence of the equilibrium thermodynamic parameter $g_{12}(\phi_2)$ on the kinetics of the membrane formation process. This shows that equilibrium thermodynamic properties not only determine the phase behavior of a ternary membrane forming system (which is obvious) but also and to a large extent, the diffusion processes in the immersed casting solution.

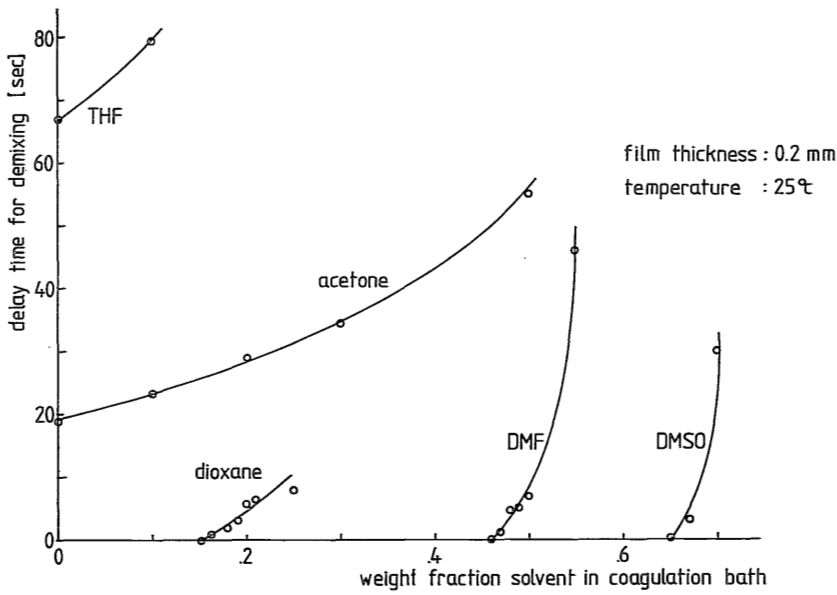

Fig. 7. Experimental delay time for the onset of liquid-liquid demixing after immersion of a 15 vol.% CA solution, prepared from the indicated solvent, into a coagulation bath with a varying initial solvent/water ratio.

6.8. SEM analysis

In Figure 8 micrographs of cross sections of the ultimate membranes are shown, which have been obtained by immersion of the 15 vol.% CA solution films into pure water baths.

The most remarkable effect that can be observed is the absence of the so called macrovoids (or finger shaped cavities) in the membranes formed by means of delayed onset of demixing. In the Appendix of this thesis it will be shown that this relation between the moment of onset of liquid-liquid demixing and the formation of macrovoids is not accidental.

A second effect that follows from the SEM analyses is the large difference between the toplayer thickness of the membranes formed by means of delayed and instantaneous onset of liquid-liquid demixing, if we define the toplayer as that surface region where no droplets of diluted liquid phase have been formed during membrane formation. It is clear that a thick toplayer is due to an extended delay time for the onset of liquid-liquid demixing (viz. for THF and acetone, Fig. 8(c) and 8(d)).

It can also be seen that during the delay time for the onset of liquid-liquid demixing the polymer film thickness decreases considerably, which causes a decrease of the porosity of the sublayer and which may prevent the formation of an interconnective pore structure. Due to this effect, the membrane prepared from the CA-THF casting solution has the performance of a homogeneous, dense membrane. However, for the membrane prepared from the CA-acetone casting solution (Fig. 8(c)) the pores in the sublayer are interconnected, due to the formation of aggregates accompanying the gelation of the sublayer. Therefore, the resistance of the sublayer of this membrane is much lower than that for the membrane prepared from the CA-THF solution.

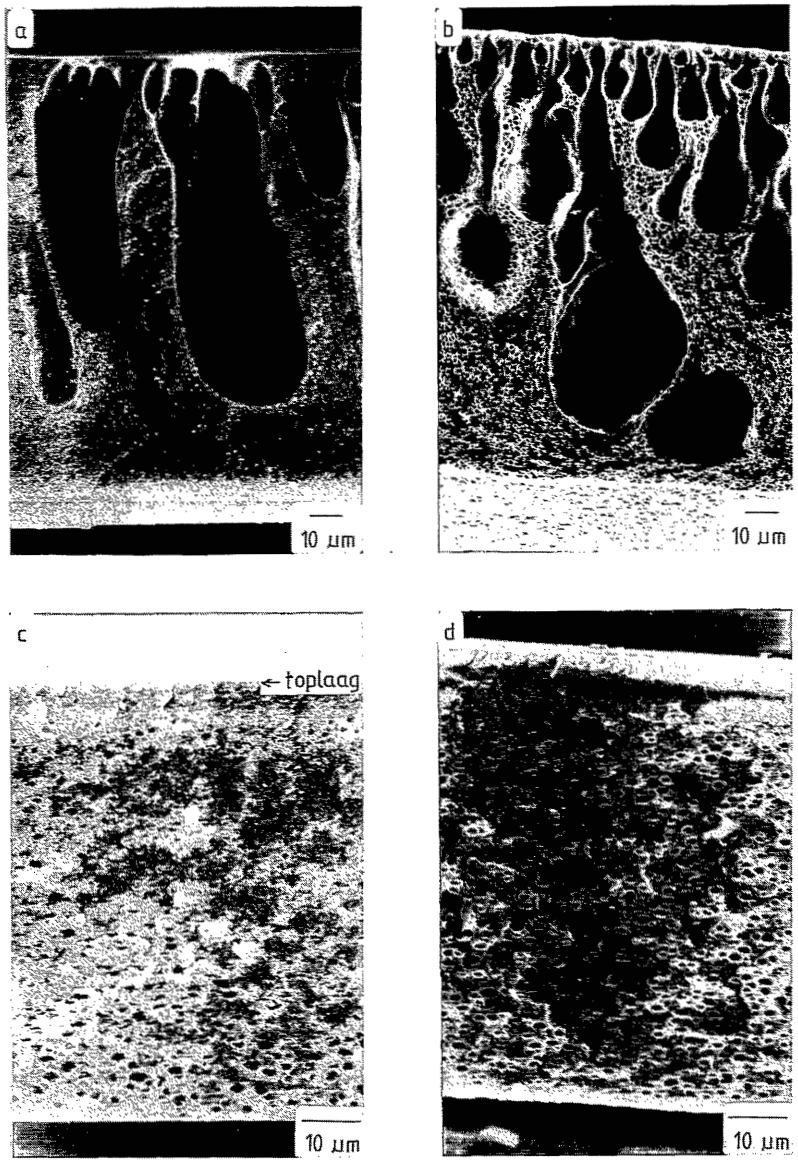

Fig. 8. Micrographs of the cross sections of membranes prepared from 15 vol.% CA casting solutions immersed into a pure water bath. Solvents used for the preparation of the casting solution: a. DMF; b. dioxane; c. acetone; d. THF (The magnification factor for a. and b. differs from that for c. and d.).

6.9. Conclusions

The diffusion model for membrane formation has been applied for the system CA/dioxane/water.

Sedimentation and diffusion measurements performed on dioxane-CA, respectively dioxane-water mixtures yielded a frictional coefficient $R_{23}(\phi_3)$ which is about six times higher than for CA-acetone, and a frictional coefficient $R_{12}(\phi_2)$ which is about the same as for acetone-water.

Light transmission measurements showed that a minimum dioxane concentration in the coagulation bath is necessary to obtain delayed onset of liquid-liquid demixing upon immersion of a CA-dioxane solution in the bath. An expression for $R_{13}(\phi_3)$ has been determined which makes the model calculations to predict delayed onset of liquid-liquid demixing in an immersed CA-dioxane film to occur at the same minimum dioxane concentration in the coagulation bath as has been measured with light transmission experiments.

Model calculations on the system CA/dioxane/water showed that an increase of the polymer concentration of the casting solution yields a strong increase of the polymer concentration at the interfacial boundary of the film upon immersion of the film. In the next chapter it will be shown for type I membrane forming systems that this effect may have a large influence on the morphology and the thickness of the ultimate toplayer.

Model calculations, performed using the frictional coefficients of the system CA/dioxane/water, further showed that decreasing values of the thermodynamic interaction parameters g_{23} and χ_{13} promote the tendency towards delayed onset of liquid-liquid demixing in an immersed film, whereas a decreasing value of g_{12} promotes the opposite effect.

Light transmission experiments performed on various immersed CA-solvent systems confirmed the conclusion from the model calculations that the value of g_{12} has a dominant influence on the moment of onset of liquid-liquid demixing in the immersed film.

With SEM analysis the influence of the delay time for the onset of liquid-liquid demixing on the ultimate membrane morphology could clearly be demonstrated.

6.10. References

1. M.T. So, F.R. Eirich, H. Strathmann and R.W. Baker, Preparation of asymmetric Loeb-Sourirajan Membranes, J. Polym. Sci. Polym. Lett., 11 (1973) 201.
2. M.A. Frommer and D. Lancet, The mechanism of membrane formation: membrane structures and their relation to preparation conditions, Reverse Osmosis Membrane Research, H.K. Lonsdale and H.E. Podall, Eds., Plenum Press New York (1972) 85.
3. R. Bloch and M.A. Frommer, The mechanism for formation of "skinned" membranes. I. Structure and properties of membranes cast from binary solutions, Desalination, 7 (1970) 259.
4. M. Guillotin, C. Lemoyne, C. Noel and L. Monnerie, Physicochemical processes occurring during the formation of cellulose diacetate membranes. Research of criteria for optimizing membrane performance. IV. Cellulose diacetate-acetone-organic additive casting solutions, Desalination, 21 (1977) 165.
5. F.W. Altena, J. Smit, J.W.A. van de Berg, J.G. Wijmans and C.A. Smolders, Diffusion of solvent from a cast cellulose acetate solution during the formation of skinned membranes, Polymer, 26 (1985) 1531.
6. R.H. Stokes, An improved diaphragm-cell for diffusion studies, and some tests of the method, J. Am. Chem. Soc., 72 (1950) 763.
7. J.G. Albright and R. Mills, A study of diffusion in the ternary system, labeled urea-urea-water, at 25° by measurements of the intradiffusion coefficients of urea, J. Phys. Chem., 69 (1965) 3120.
8. R.L. Robinson, W.C. Edmister and F.A.L. Dullien, Calculation of diffusion coefficients from diaphragm cell diffusion data, J. Phys. Chem., 69 (1965) 258.
9. F.W. Altena, Phase separation phenomena in cellulose acetate solutions in relation to asymmetric membrane formation, Thesis, chapter 6, Twente University of Technology, Enschede, The Netherlands (1982).
10. M.H.V. Mulder, T. Franken and C.A. Smolders, Preferential sorption versus preferential permeability in pervaporation, J. Membrane Sci., 22 (1985) 155.

7. CONTROL OF MEMBRANE MORPHOLOGY

By A.J. Reuvers and C.A. Smolders

7.1. Summary

Membrane formation by means of immersion precipitation can occur according to two distinctly different mechanisms, characterized by the moment of onset of liquid-liquid demixing in the immersed film. A survey is given of the way in which the mechanism of membrane formation can be controlled.

Type I membranes (formed by the mechanism of delayed onset of liquid-liquid demixing) are characterized by a relatively thick toplayer. It is shown in which way the toplayer is affected by the diffusion processes and the kinetics of liquid-liquid demixing.

Type I membranes are mostly characterized by a hyperfiltration, gas separation or pervaporation type of performance. It is reasoned that the morphology of the toplayer depends on a possible rearrangement of the polymer distribution through aggregate formation in the nascent toplayer.

Type II membranes (formed by the mechanism of instantaneous onset of liquid-liquid demixing) are characterized by a very thin toplayer and, on preparation of the membrane from a moderately concentrated casting solution, by an ultrafiltration type of performance.

7.2. Introduction

The main result of the diffusion model presented in this thesis is the elucidation of two distinctly different mechanisms of membrane formation by means of immersion precipitation. The difference between the two mechanisms is characterized by the moment of onset of liquid-liquid demixing in the immersed casting solution: this moment either coincides with the very moment at which the solution film and the coagulation bath are contacted, or it is delayed for at least the period over which the composition at the bottom of the film remains constant.

The terminology type I and type II membranes has been introduced to discri-

minate between membranes formed by delayed (type I) or instantaneous (type II) onset of liquid-liquid demixing.

In Chapter 4 it has been shown that the moment of onset of liquid-liquid demixing can be determined experimentally by a simple light transmission experiment performed on an immersed casting solution.

With the help of the diffusion model, applied to the system CA/acetone/water, it has been reasoned that the (easily measurable) delay time for the onset of liquid-liquid demixing is interrelated with the thickness of the selective toplayer of the ultimate membrane: the onset of liquid-liquid demixing stops the growth of a layer consisting of a highly concentrated polymer solution adjacent to the interface between the bath and the film; from this layer the ultimate selective toplayer of the membrane will be formed.

Besides the thickness of the toplayer, also the presence of fingerlike cavities (macrovoids) in the ultimate membrane depends on the type of membrane formation process that occurs. As a rule delayed onset of liquid-liquid demixing prohibits the formation of macrovoids, whereas instantaneous onset of liquid-liquid demixing yields the formation of macrovoids. There are two exceptions: in solutions with a high polymer or nonsolvent concentration macrovoids may not be found. The process of macrovoid formation will be discussed in the Appendix of this thesis in more detail.

In this Chapter we will discuss the toplayer structure of the two different types of membranes. First of all the influence of various process parameters on the type of membrane formation process that occurs, will be summarized.

7.3. Influence of various process parameters on the type of membrane formation process

In Chapter 4 and 6 the influence of various process parameters on the moment of onset of liquid-liquid demixing has been calculated and/or measured. In terms of the type of membrane that may be expected, the results were as follows:

- The addition of nonsolvent to the casting solution promotes the formation of type II membranes (Chapter 4).

- the addition of solvent to the coagulation bath promotes the formation of type I membranes (Chapter 6).
- An increase of the polymer concentration in the casting solution promotes the formation of type II membranes for the system CA/dioxane/water (Chapter 6). It should be premature to generalize this conclusion because the measured effect and the examined concentration range are only small.
- An increasing tendency of mixing of the solvent with the nonsolvent (expressed by the minimum value of $\phi_i\{d\mu_i/d\phi_i\}$ for the binary solution) promotes the formation of type II membranes very strongly (Chapter 6).
- A higher degree of swelling of the pure polymer in the nonsolvent (for water: the hydrophylicity of the polymer) promotes the formation of type I membranes (Chapter 6).
- An increasing solubility of the polymer in the solvent promotes the formation of type I membranes (Chapter 6).

The last three parameters are determined by the choice of the three components to be used for the immersion precipitation process. It must be noticed that the choice of the solvent-nonsolvent system has a decisive influence on the type of membrane formation process that occurs (see Chapter 6, Fig. 4 and 7). An example of the influence of the solvent-nonsolvent combination is given in Figure 1, where the cross sections are shown of a type I and a type II membrane prepared from a polysulfone-DMAc casting solution immersed into i-propanol and ethanol, respectively.

The influence of the coagulation bath temperature on the membrane formation process [1] has not been examined in this thesis. Nevertheless, in our opinion this temperature will influence the membrane formation process through a change of the thermodynamic interaction between the three components. Thus, the influence of the coagulation bath temperature can only be understood when the temperature dependence of the interaction parameters is known.

Our model predicts the moment of onset of liquid-liquid demixing for the case that immersion precipitation is performed with only three components. Nevertheless, it can be reasoned that addition of extra low molecular weight components to the coagulation bath or to the casting solution also yields composition paths which remain situated at a fixed position in the composition diagram, until the composition at the bottom of the film starts to change. This means that the discrimination which can be made between type I

and type II membrane formation processes, does not depend on the number of components used.

When two or more polymer components are used for the preparation of the casting solution, the kinetics of demixing of metastable solutions may be changed considerably. This yields a formation process and a membrane morphology that may differ from the descriptions given in this thesis for ternary systems with only one polymer component. An example of the use of two polymer components is the addition of polyvinylpyrrolidone (PVP) to the casting solution [2-4].

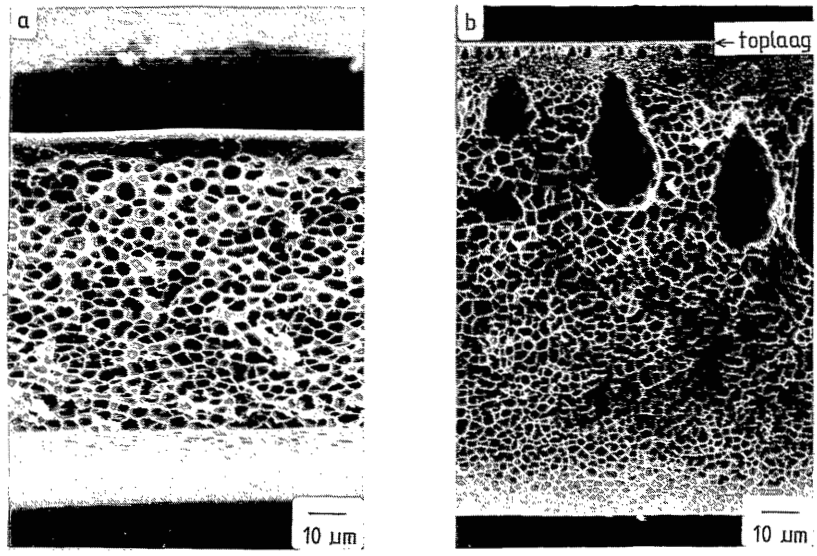

Fig. 1. Micrographs of cross sections of membranes prepared from a 25 wt.% polysulfone-DMAc casting solution immersed into:
a. i-propanol (type I membrane); b. ethanol (type II membrane).

7.4. The thickness of the selective toplayer

In the previous section we have summarized the influence of various parameters on the type of membrane formation process that will occur. This influence has been examined by calculating composition paths valid for a short period after immersion of the film and/or by light transmission experiments.

At this point the question arises what the influence of the various process parameters on the thickness of the toplayer for the two types of membranes might be. We will try to answer this question, defining the toplayer as that

surface region of the membrane cross section where no droplets of diluted liquid phase have been formed during membrane formation.

- Type I membranes -

Before the influence of the various process parameters on the thickness of the type I toplayer can be understood, the toplayer formation process should be described in more detail. Therefore, we will first discuss at which position in the immersed film the first nuclei of the diluted phase are formed. Secondly, we will reason that this position determines the ultimate toplayer thickness. Finally, the influence of various process parameters on the ultimate toplayer thickness will be shown.

a. From Figure 2 it can be concluded that, during the type I membrane formation process, crossing of the binodal by the composition path firstly occurs at the limiting composition near the interfacial boundary.

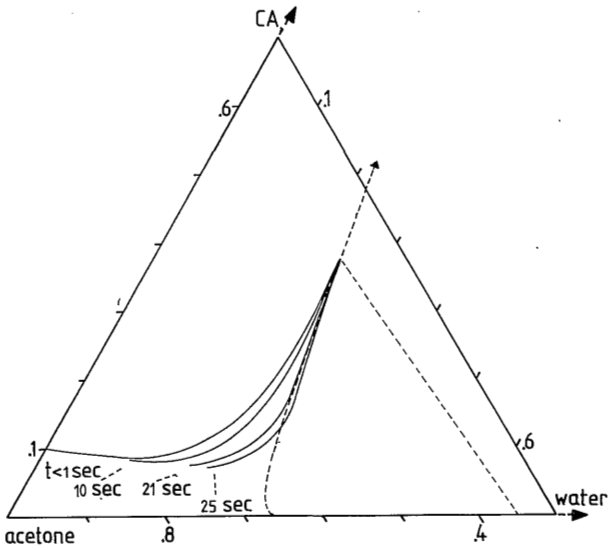

Fig. 2. Approximated change of the composition path at different immersion times for a 10 vol.% CA-acetone solution immersed into a pure water bath; initial film thickness: 200 µm (This Figure resembles Figure 9 in Chapter 4).

b. Figure 2 also shows that penetration of the composition path into the demixing gap occurs faster at compositions that lie further away from the interfacial boundary composition.
c. From kinetic measurements by Ronner [5] it can be concluded that the degree of supersaturation, necessary to induce the formation of nuclei of the diluted phase within a certain period of time, increases with increasing polymer concentration in the ternary system polymer/solvent/nonsolvent.

The phenomena mentioned at point b and c prohibit diluted phase nucleation at the limiting position near the interfacial boundary. Due to these phenomena, the degree of supersaturation necessary to induce the formation of nuclei, is reached firstly at a position on the composition path, situated at a certain distance away from the interfacial boundary composition.

Now we will try to reason that no nuclei will be formed anymore in the region in between the locus of the first formed nuclei and the surface of the polymer solution. This means that this region of the solution film constitutes the toplayer of the ultimate membrane, according to the definition of the toplayer mentioned at the beginning of this section.

At the interfacial boundary surrounding the first formed nuclei a binodal composition exists at the polymer rich side of the boundary. The exact compositions at the boundary are determined by the ends of the tieline crossing that point of the composition path where the first nuclei have been formed (see Figure 3). Thus, from the very moment the first nuclei are being formed, the region in between these nuclei and the surface of the film is enclosed by two nearly equal binodal compositions. These boundary conditions give rise to an immediate decrease of the degree of supersaturation within the top region of the film (see Figure 3), thus preventing the formation of nuclei of the diluted phase to occur within this region during the proceeding membrane formation process.

Two factors obviously determine the position in the immersed film at which the first nuclei are formed:

I. A high polymer concentration at the interfacial boundary of the film, at the very moment the composition path crosses the binodal, is accompanied by a relatively high local polymer concentration in the region near the

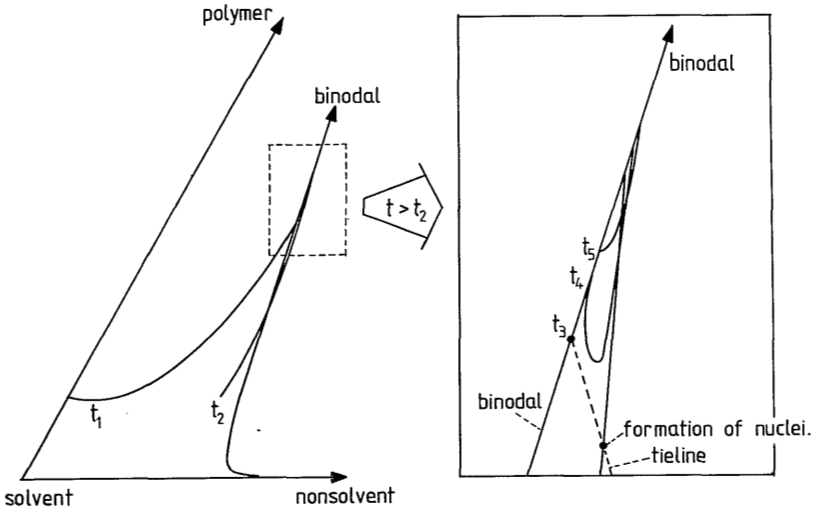

Fig. 3. Schematic representation of the change of the composition path, representing the compositions in between:
- the surface and the bottom of the immersed polymer solution film for $t < t_3$, the moment of onset of liquid-liquid demixing;
- the surface of the film and the locus of the first formed nuclei of the diluted phase, for $t > t_3$.

interfacial boundary. From this phenomenon and the kinetic measurements on nucleation by Ronner [5], it may be concluded that a higher polymer concentration at the interfacial boundary, upon immersion of the casting solution, results in a larger distance between the location of the first formed nuclei and the surface of the solution film.

II. From Figures 9-10 shown in Chapter 4 it can be seen that during the time that the composition path does not yet enter the liquid-liquid demixing gap, the local compositions in the top region of the film shift along the composition path on to the binodal boundary composition. Thus, according to the kinetics of liquid-liquid demixing [5], a longer delay time for the moment of entrance into the demixing gap also results in a larger distance between the location of the first formed nuclei and the surface of the solution film.

Keeping in mind these two factors, the influence of some process variables on the ultimate toplayer thickness will be discussed.

- The initial polymer concentration in the casting solution.

Membranes have been prepared by immersion of initially 300 μm thick CA-acetone solution films, with a CA concentration of 10 and 15 vol.%, into pure water baths. From Figure 4 it can be seen that the toplayer thickness (the region where no droplets of diluted phase have been formed) of the two ultimate membranes differ considerably. The delay times for onset of liquid-liquid demixing in the two films have been measured to be 45 and 43 seconds for the 10 vol.% CA solution and the 15 vol.% CA solution, respectively. Thus, according to the previous considerations in this subsection, the influence of the initial CA concentration in the casting solution on the CA concentration at the interfacial boundary of the immersed film (see Figure 3, Chapter 6) is solely responsible for the difference between the thicknesses of the two toplayers.

We should realize that in CA/acetone/water systems the formation of aggregates may prohibit the growth of nuclei of the diluted liquid phase (see Chapter 2). Therefore one might reason that the larger thickness of the toplayer in Figure 4(b) would be due to this effect of aggregate formation. A better example of the influence of the initial polymer concentration in the solution film on the toplayer thickness is given by Mulder [6] for membranes prepared from polysulfone-DMAc casting solutions (PSf does not readily form aggregates) immersed into an i-propanol bath: the thickness of the ultimate toplayer increases with increasing polysulfone concentration in the casting solution.

- The initial solvent concentration in the coagulation bath.

Model calculations show that the polymer concentration at the interfacial boundary of the immersed solution film decreases with increasing solvent concentration in the coagulation bath (see Figure 4 and 5, Chapter 4), whereas light transmission measurements show an increase in delay time for the onset of liquid-liquid demixing (see Figure 7, Chapter 6). Therefore, it is not possible to predict to what extent the toplayer thickness of the membrane will change with varying solvent concentration in the coagulation bath.

Wijmans [7] has observed a decrease of the toplayer thickness of membranes prepared from polysulfone-DMAc solution films with increasing DMAc concentra-

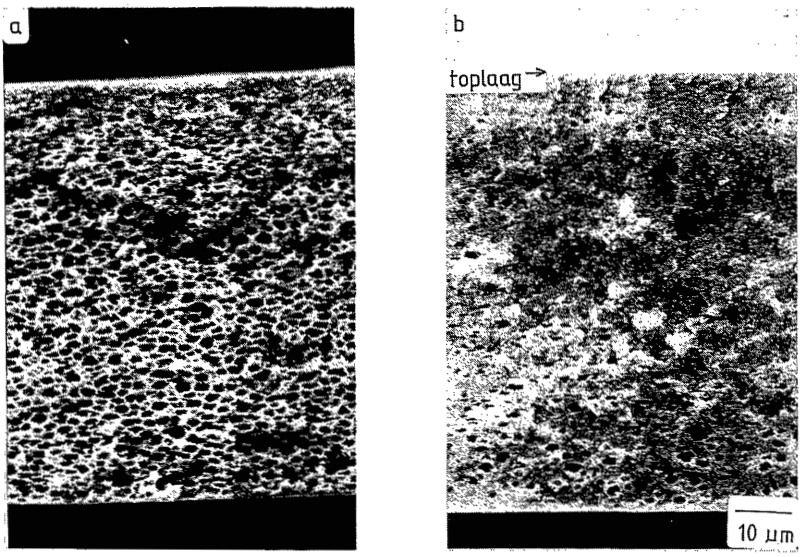

Fig. 4. Micrographs of cross sections of type I membranes prepared from CA-acetone films immersed into pure water. Initial film thickness: 300 µm; initial CA concentration in the film: a. 10 vol.%; b. 15 vol.%.

tion in the i-propanol coagulation bath. This indicates that, with increasing solvent concentration in the coagulation bath, the toplayer thickness of the ultimate membrane is mainly affected by the decreasing polymer concentration at the interfacial boundary of the immersed film.

- The initial polymer solution film thickness.

In case of type I membranes, the delay time for the onset of liquid-liquid demixing, and thus the toplayer thickness of the ultimate membrane, is affected by the film thickness of the casting solution.
This relation, predicted by the model, has never been recognized before, as far as we know. In Figure 5 this effect is demonstrated by means of micrographs of type I polysulfone membranes. It can be seen that not only the toplayer thickness, but also the dimensions of the pores in the sublayer decrease with decreasing initial film thickness. This is caused by the increasing rate at which the local compositions of the sublayer cross the binodal for smaller thicknesses, which promotes the formation of nuclei of the diluted phase.

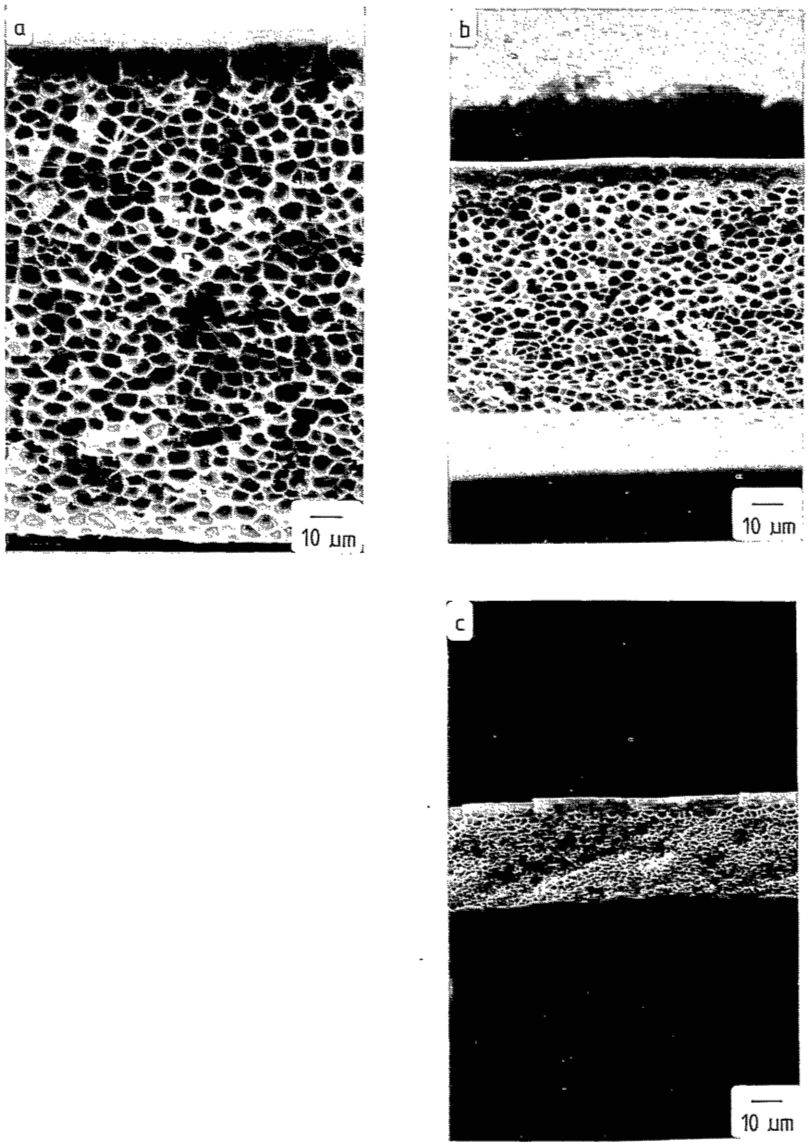

Fig. 5. Micrographs of cross sections of type I membranes prepared from 25 wt.% polysulfone-DMAc films immersed into i-propanol.
Initial film thickness: a. 0.4 mm; b. 0.2 mm; c. 0.1 mm.

- Type II membranes -

For type II membranes the model is not capable to predict the influence of the process parameters on the toplayer thickness of the ultimate membrane.

This is due to the presence of very steep concentration gradients in the region near the interface, during the initial period after immersion of the film. These steep concentration gradients cause the local free energy to depend not only on the local composition (as we have assumed in our model), but also on the local composition derivatives [8].

The steep concentration gradients do not only complicate the criteria for metastability and instability of the local composition at the interface, but they also cause the linear flow equations, used in the model, to be inadequate.

Therefore, in fact it is not yet justified to assert that the model predicts instantaneous onset of demixing for the type II membrane formation process.

For the type II membrane formation process the model rather predicts that, at least as soon as the concentration gradients are smooth enough to justify the neglect of the gradient dependent contribution to the local free energy, the system becomes metastable and nucleation will start.

Light transmission experiments show that, at process circumstances near the transition from delayed to instantaneous onset of demixing, no delay times being independent on the thickness of the casting solution could be measured. From this observation it can be concluded that the presence of steep concentration gradients during the initial period after immersion of the film does not yield measurable delay times for the onset of liquid-liquid demixing.

This conclusion justifies the assertion that the onset of liquid-liquid demixing occurs instantaneously for the type II membrane formation process. The question in which way the thickness of the toplayer of type II membranes can be influenced however, cannot be answered by the model.

7.5. The morphology of the toplayer

So far, we have only discussed to which extent the toplayer thickness of the ultimate membrane can be controlled. The toplayer thickness is an important characteristic of the membrane because jointly with the structure (i.e. packing density) of the toplayer, it determines the flux through a membrane. In this section we want to discuss the morphology of the toplayer, the characteristic that determines the selectivity of a membrane to a large extent.

The contribution of the model to a better understanding of the toplayer

morphology is substantial, but limited. The morphology cannot be explained by the model solely, because demixing processes, like crystallization and formation of aggregates, can play an important role during the formation of the toplayer [9,10], while the model calculations are only valid as long as these kinds of demixing processes do not occur.

Nevertheless, the model calculations yield the local composition of the toplayer during the first period after immersion of the casting solution, and the rate of this composition change. This information is indispensable to understand the influence of aggregate formation and crystallization on the ultimate toplayer morphology.

The formation of aggregates in supersaturated ternary systems, consisting of polymer, solvent and nonsolvent, has been examined in Chapter 2 for CA and PPO solutions. The main conclusions drawn from this work and from literature [9-12] are:

- aggregate formation is a slow process compared to liquid-liquid phase separation, probably because some orientation of the polymer molecules is required for the formation of aggregates;
- the formation of aggregates and the kinetics of this demixing process are promoted by an increase of the nonsolvent and/or the polymer concentration in a ternary solution;
- the ability of a ternary solution to form aggregates strongly depends on the choice of the three components;
- the structure induced by this demixing process depends on the composition (especially the polymer concentration) and on the type of polymer used. PPO for example, yields a nodular structure whereas CA yields a fibrillar structure.

Keeping in mind these characteristics of the process of aggregate formation, its possible impact on the toplayer morphology of the ultimate membrane will be discussed.

- Type I membranes -

According to the diffusion model the initial composition changes in the

nascent toplayer of type I membranes can be described as follows (see also Figure 6):

At the interface where the film is contacted with the coagulation bath a polymer rich binodal composition is being formed within a fraction of a second. This composition, that can be calculated with the model, remains constant during the few seconds that the bottom composition of the film remains unchanged. Thereupon, the interfacial boundary composition starts to shift upwards along the binodal. Further away from the interface between the bath and the film, the local composition of the film changes into the direction of the interfacial boundary composition at a rate that decreases with the distance to the interface. This process is suddenly disturbed by the onset of liquid-liquid demixing, which stops the increase of the toplayer thickness, but not its change in composition.

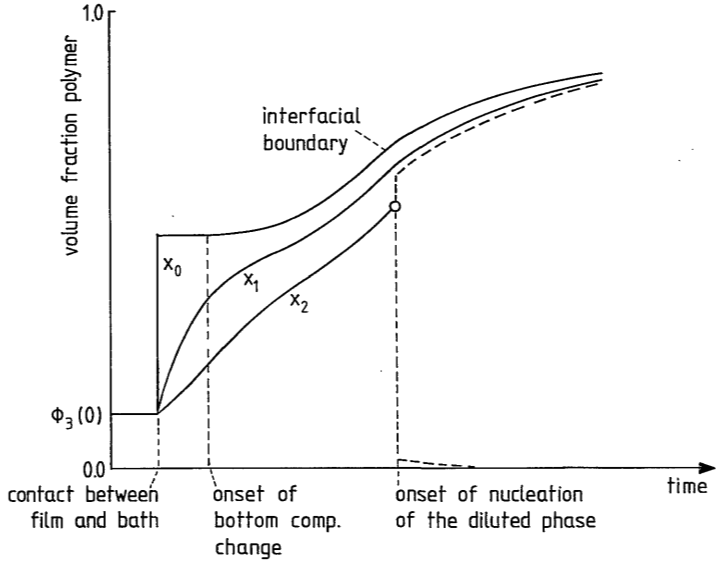

Fig. 6. Schematic representation of the initial composition changes in the nascent toplayer of a type I membrane.

Chronologically, the formation of the morphology at the interfacial boundary of the film can be classified as follows.

- During the very rapid composition change at the interfacial boundary of the film, induced by contacting the film and the bath, no orientation of polymer molecules is possible.
- During the few seconds the interfacial composition remains constant, orien-

tation of the polymer molecules is possible. Whether this will lead to aggregate formation depends on the type of ternary system considered. For the system CA/acetone/water, for example, a few seconds are enough to form an inhomogeneous structure consisting of aggregates surrounded by a diluted phase (Chapter 2). These local composition changes have not been depicted in Figure 6.

The morphology created does not only depend on the type of ternary system, but also on the number of nuclei of solid particles being formed and on the volume fraction of these solid particles in the concentrated toplayer.
It is obvious that these two characteristics are related to the composition of the supersaturated solution. A higher polymer concentration at the interfacial boundary yields a higher volume fraction of solid particles and a lower degree of porosity. A higher polymer concentration is also accompanied with a higher degree of supersaturation of the solution which may cause the number of nuclei of solid particles to increase, yielding a more finely structured toplayer.
- During the period over which the solvent is slowly depleted further from the toplayer, the changes in the morphology of this layer are completed until the glass transition is reached [13] and the ultimate structure at the interfacial boundary of the film is fixed.

The process of morphology formation in that region of the toplayer that is not directly in contact with the coagulation bath (the sub part of the toplayer) may differ from the formation process at the interfacial boundary of the film, because the rate of composition change decreases with increasing distance from the interface (see Figure 6). A lower rate of composition change enables the aggregate formation process to occur at lower polymer concentration, which may cause a density gradient in the ultimate toplayer.

The inhomogeneities formed in the (sub part of the) toplayer might be distinct enough to be measured by means of light transmission experiments during the period before the onset of liquid-liquid demixing. This has been shown by Vasarhelyi [14] for the formation of Loeb-Sourirajan-type membranes.

However, also less distinct inhomogeneities might be formed in the toplayer of type I membranes. This is for example the case for type I membranes prepared from polysulfone solutions. Formation of aggregates in concentrated ternary polysulfone solutions cannot even be detected by light scattering

experiments [5]. Nevertheless the selectivity in pervaporation processes of type I membranes, prepared from polysulfone/DMAc/i-propanol, can vary considerably as has been shown by Mulder [6]. This means that a homogeneous, amorphous toplayer is not always formed, but that the structure may vary on a molecular scale. The selectivity of the polysulfone membranes mentioned increases with increasing polysulfone concentration in the initial casting solution. According to our model a higher polymer concentration in the casting solution yields a higher polymer concentration at the interfacial boundary upon immersion of the casting solution (see Chapter 6). Consequently, the measurements performed by Mulder confirm that the polymer concentration at the onset of formation of inhomogeneities, has a large influence on the ultimate morphology of the toplayer.

Another remarkable result of the pervaporation experiments on ethanol-water mixtures performed by Mulder [6] is the higher selectivity of asymmetric CA membranes, prepared by means of immersion precipitation of a highly concentrated CA-acetone casting solution, compared to a homogeneous CA membrane prepared by evaporation of solvent from a CA-acetone solution. There are two possible explanations for this phenomenon:

- on contacting the polymer solution film with a water bath, the instantaneous increase of the CA concentration at the interfacial boundary of the film is larger than on contacting the film with air. In this way the observations of Mulder could be explained, because the formation process of aggregates results in a denser structure at higher CA concentration;
- in the presence of water (immersion precipitation) aggregate formation at the interfacial boundary leads to the formation of a more homogeneous structure compared to the situation in which no water is present (evaporation).

To verify these possible explanations, more experiments and calculations have to be performed.

The formation of aggregates may also have a large influence on the sublayer porosity. In general, the porosity of the sublayer of type I membranes is low and the pores are badly interconnected. This is caused by the fact that during the delay time for the onset of liquid-liquid demixing the polymer concentration increases not only in the top region of the solution film, but also in the sublayer. The formation of aggregates in the sublayer of membranes prepared from certain ternary systems however, may promote the interconnectivity of the pores considerably. An example of the formation of relat-

ively large aggregates in the sublayer can be seen at the Loeb-Sourirajan-type membranes [14].

-Type II membranes -

Earlier in this chapter we have stated that the formation of the toplayer of type II membranes is a highly nonlinear process that can only be described approximately by our linear diffusion equations. Supported by light transmission experiments the diffusion model indicates that the toplayer of this type of membranes must be very thin compared to the toplayer of type I membranes. In this paragraph the toplayer morphology of type II membranes will be discussed.

The diffusion model indicates that, upon contacting the casting solution with the coagulation bath, the polymer concentration at the interfacial boundary of type II casting solutions generally increases to a higher value than the polymer concentration at the interface of type I casting solutions (see the Figures 4-6 in Chapter 6). Thus, according to the considerations mentioned in the previous section, rearrangement of the polymer distribution by aggregate formation in the nascent toplayer of type II membranes must yield a denser structure than in case of type I membranes. There are two indications however, that mostly the opposite is true:

- as far as we know, type II membranes are mostly suitable for ultrafiltration, whereas type I membranes are suitable for pervaporation, hyperfiltration or gas separation (see Table 1). Only when a type II membrane is prepared from a highly concentrated casting solution (for instance 35 wt.% polysulfone in DMAc), it is characterized by a pervaporation type of performance.

- from electron microscopy studies on the toplayer morphology evidence has been gathered that the toplayer of type II membranes often consists of so called noduli, which are spherical aggregates from 20 to 200 nm in diameter [9,18,20]. Type II membranes prepared from polysulfone solutions also possess this nodular toplayer structure [20], whereas temperature quenching of highly concentrated polysulfone solutions does not cause any kind of aggregate formation at all [5].

Table 1. Membrane properties of various type I and II membranes.

casting solution	coagulant	type of membrane	membrane properties
15% PSf in DMAc	water	II	UF internal report
35% PSf in DMAc	water	I	Pervap. [6]
15% PSf in DMAc	ethanol	II	UF [6]
10% PPO in 78/22 TCE/OcOh	methanol	II	UF [15]
CA in DMSO	water	II	UF [6,16,17]
20% CA in DMF	water	II	UF [16,17]
20% CA in dioxane	water	II	HF/UF [16,17]
PI in DMAc	water	II	UF [18]
20% PVDF in DMF	water	II	UF [19]
PSf in DMAc	i-propanol	I	Pervap. [6]
10% PPO in TCE	methanol	I	Gas sep. [15]
PPO in TCE	ethanol	I	Pervap. [6]
CA in acetone	water	I	Pervap., HF [6,16,17]
CA in THF	water	I	HF internal report
PAN in DMAc	i-propanol	I	Pervap. [6]

These considerations indicate that the toplayer structure of type II membranes cannot be explained by the phenomenon of formation of aggregates in highly concentrated polymer solutions as discussed in Chapter 2.

A better explanation of the formation of a nodular toplayer structure of type II membranes might be the instability of the thin nascent toplayer, at the very moment of onset of liquid-liquid demixing just beneath this layer. At this moment a very steep concentration gradient is present in the thin layer, which may give rise to the so called "thin film" instabilities yielding an ordered spatial structure [21]. However, the verification of this theory is beyond the scope of this thesis.

7.6. Conclusions

The influence of various process parameters on the diffusional mass transfer in the casting solution, calculated or measured in Chapter 4 and 6, has been summarized.

The model presented in this thesis shows the existence of two distinctly different mechanisms of membrane formation by means of immersion precipitation. This offers the possibility of a more structurized analysis of the formation process of the selective toplayer of the ultimate membrane than ever before.

The type I membrane formation process (characterized by delayed onset of liquid-liquid demixing) yields membranes with relatively thick toplayers. The thickness of this toplayer can be influenced in different ways. The type II membrane formation process (characterized by instantaneous onset of liquid-liquid demixing) yields very thin toplayers.

Model calculations can yield the actual composition gradient and the rate of change of this gradient in the nascent toplayer of type I membranes. The morphology of the ultimate toplayer depends on a possible rearrangement of the polymer distribution, through crystallization or aggregate formation in the nascent toplayer. These processes however, are not yet fully understood.

The morphology of type II toplayers might be determined by so called "thin film instabilities" which cannot be described by the model presented in this thesis.

A study on the performance of various membranes described in literature shows that type I membranes are suitable for hyperfiltration, pervaporation or gas separation whereas type II membranes, prepared from moderately concentrated casting solutions, exhibit ultrafiltration properties.

7.7. References

1. H. Bokhorst, F.W. Altena and C.A. Smolders, Desalination, 38 (1981) 349.
2. T.A. Tweddle, O. Kutowy, W.L. Thayer and S. Sourirajan, Ind. Eng. Chem. Prod. Res. Dev., 22 (1983) 320.
3. I. Cabasso, E. Klein and J.K. Smith, J. Appl. Polym. Sci., 21 (1977) 165.
4. P. Aptel, N. Abidine, F. Ivaldi and J.P. Lafaille, J. Membrane Sci., 22

(1985) 199.

5. J.A. Ronner, to be published.
6. M.H.V. Mulder, J. Oude Hendrikman, J.G. Wijmans and C.A. Smolders, J. Appl. Polym. Sci., 30 (1985) 2805.
7. J.G. Wijmans, J.P.B. Baay and C.A. Smolders, J. Membrane Sci., 14 (1983) 263.
8. J.W. Cahn and J.E. Hilliard, J. Chem. Phys., 28 (1958) 258.
9. L. Broens, F.W. Altena and C.A. Smolders, Desalination, 32 (1980) 33.
10. J.G. Wijmans, H.J.J. Rutten and C.A. Smolders, J. Polym. Sci., Pol. Phys. Ed., 23 (1985) 1941.
11. A. Labudzinska and A. Ziabicki, Kolloid Z.Z. Polym., 243 (1971) 21.
12. F.W. Altena and C.A. Smolders, J. Polym. Sci., Pol. Symp., 69 (1981) 1.
13. A. Ziabicki, Fundamentals of Fibre Formation, Wiley, New York, 1976.
14. K. Vasarhelyi, J.A. Ronner, M.H.V. Mulder and C.A. Smolders, submitted for publ. to Desalination.
15. H.C.W.M. Buys, A.E. Jansen, H.F. van Wijk, D. Bargeman and C.A. Smolders, paper presented at the Third Symposium on Synthetic Membranes in Science and Industry, Tübingen, 1981.
16. R. Bloch and M.A. Frommer, Desalination, 7 (1970) 259.
17. M. Guillotin, C. Lemoyne, C. Noel and L. Monnerie, Desalination, 21 (1977) 165.
18. M.N. Sarbolouki, J. Appl. Polym. Sci., 29 (1984) 743.
19. A. Bottino, G. Capannelli and S. Munari, J. Appl. Pol. Sci., 30 (1985) 3009.
20. U. Merin, J. Appl. Polym. Sci., 25 (1980) 2139.
21. R.J. Ray, Thesis, University of Colorado (1983).

FORMATION OF MACROVOIDS — APPENDIX

By A.J. Reuvers and C.A. Smolders

A.1. Introduction

The supporting substructure of asymmetric membranes prepared by means of immersion precipitation is often made up of large macrovoids. These macrovoids can weaken the membrane and result in rupture of the skin under high operating pressures.

Experimentally, it has been shown that the formation of macrovoids in membranes, prepared from a polymer/solvent/nonsolvent system, can be suppressed or even eliminated by:

- choosing a solvent-nonsolvent pair of components with a low tendency of mixing with each other (Frommer [1,2]);
- increasing the polymer concentration in the casting solution or allowing the solvent to evaporate from the cast solution before immersion into the nonsolvent bath (Frommer [2] and Strathmann [3]);
- addition of solvent to the coagulation bath (Strathmann [3] and Gröbe [4]).

It is generally concluded from these observations that macrovoid formation occurs under rapid precipitation conditions and that the formation of these voids can be suppressed by increasing the viscosity of the casting solution (Frommer [1-2], Strathmann [3], Matz [5], Cabasso [6] and Ray [7]).

Despite extensive research efforts, a generally accepted theory for the actual mechanism of formation of the macrovoids has not yet been developed. In this appendix we will derive some useful empirical rules for the occurrence of macrovoids in membranes, and we will propose a theory for the formation of macrovoids which is in accordance with these empirical rules.

A.2. Empirical rules for the occurrence of macrovoids in membranes prepared from ternary systems

Before we discuss the established theories concerning the initation and growth of the macrovoids we will present some SEM analyses, performed to study the influence of the coagulation bath and casting solution compositions on the formation of macrovoids.

Some solution films which have been used for the light transmission experiments in Chapter 4 and 6 of this thesis have also been examined for the presence of macrovoids:

- In Figure 1 the cross sections are shown of CA/acetone/water solutions immersed into a pure water bath. The, initially, 200 μm thick solution films consisted of 10 vol.% CA, dissolved in a water-acetone mixture of which the nonsolvent/solvent ratio had been varied. In Chapter 4 it has been shown that the transition from delayed to instantaneous onset of liquid-liquid demixing in these immersed films is situated in between a water/acetone volume ratio of 10/90 and 12.5/87.5 in the casting solution. From Figure 1(b) and 1(c) it can be seen that this turbidimetrically detected transition is accompanied by a transition for the occurrence of macrovoids: macrovoids are being formed in solutions which start to demix instantaneously (denoted as type II membranes), whereas no macrovoids are being formed in solutions which start to demix only after a certain delay time (denoted as type I membranes).

- By SEM we have also examined the cross sections of some membranes which were being formed during the light transmission experiments on 15 vol.% CA-dioxane solutions immersed into a coagulation bath with a varying water/dioxane ratio (Chapter 6). Figure 2 shows that the type II membranes (2(a) and 2(b)) do contain macrovoids whereas the type I membranes (2(c) and 2(d)) contain some very small macrovoids (2(c)) or no macrovoids at all (2(d)). These observations are in accordance with the results of Strathmann [3], who performed a similar study on Nomex-DMF (DMAc) casting solutions immersed into various water-DMF (DMAc) coagulation baths. Strathmann also observed that instantaneous onset of liquid-liquid demixing is accompanied by formation of macrovoids, whereas no macrovoids are formed if liquid-liquid demixing starts after a certain minimum delay period.

- In Figure 8 of Chapter 6 the cross sections are shown of membranes prepared from various CA-solvent casting solutions immersed into pure water.

From these micrographs and the measured periods of delay for the onset of liquid-liquid demixing (Figure 7 in Chapter 6) it can be concluded that the transition from instantaneous to delayed onset of demixing obtained by varying the type of solvent, is also accompanied by the disappearance of macrovoids. In Chapter 7 (Figure 1) the same effect can be observed for variation of the type of nonsolvent.

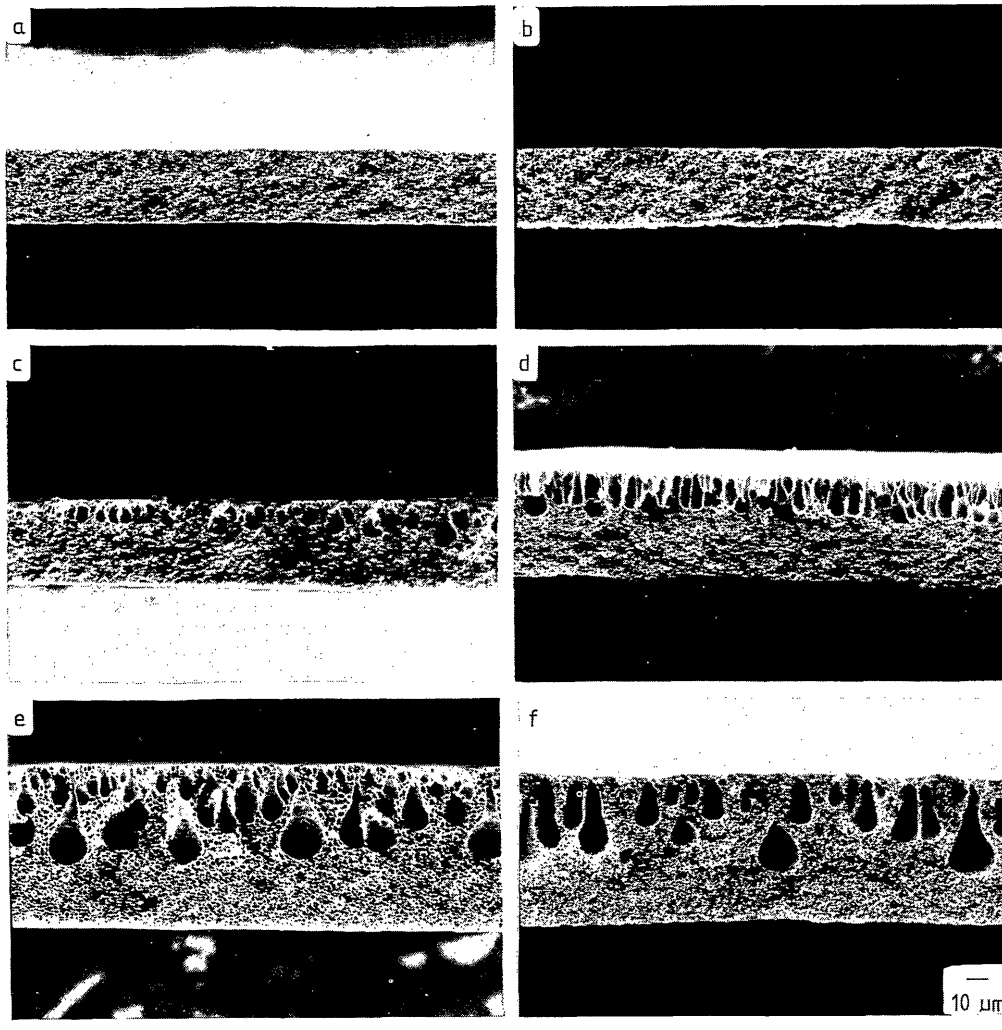

Fig.1. Micrographs of the cross sections of membranes prepared from 200 µm thick, 10 vol.% CA solution films, immersed into a pure water bath; the volume ratio water/acetone in the casting solutions has been varied: a. 0/100; b. 10/90; c. 12.5/87.5; d. 15/85; e. 21/79; f. 27/73; The enlargement factor is equal for all these micrographs.

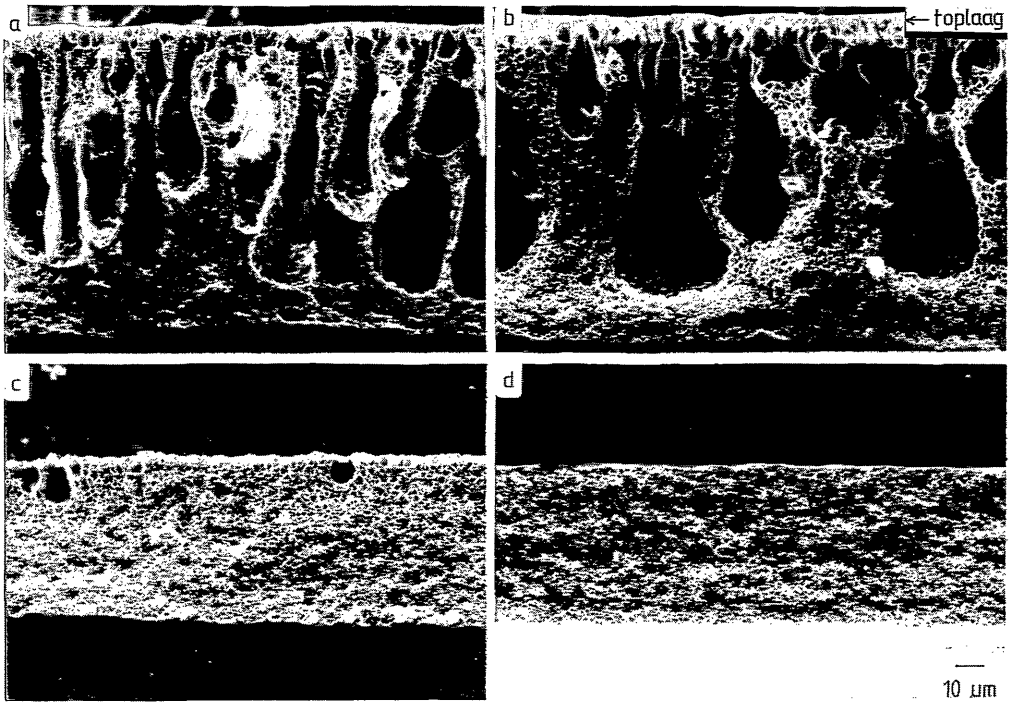

Fig.2. Micrographs of the cross sections of membranes prepared from 200 µm thick, 15 vol.% CA-dioxane solution films, immersed into a coagulation bath with a varying dioxane concentration; weight fraction of dioxane in the bath: a. 0.0; b. 0.1 c; 0.2; d. 0.3; The enlargement factor is equal for all these micrographs.

Thus, various examples show that the presence of macrovoids in the ultimate membrane is related with the delay time for the onset of liquid-liquid demixing upon immersion of the cast solution.

It is also possible to avoid the formation of macrovoids however, by changing parameters which (probably) do not effect the delay time for the onset of liquid-liquid demixing:

- Frommer [2] demonstrated that an increase of the initial polymer concentration in a CA-triethyl phosphate casting solution from 7 wt.% onto 20 wt.% prohibits the formation of macrovoids upon immersion of the casting solution into an ice-water bath. This author showed that macrovoid formation can also be eliminated in immersed CA-DMSO casting solutions, by an increase of the CA

concentration from 20 wt.% onto 30 wt.%.

Strathmann [3] observed macrovoid formation to be absent in immersed Nomex-DMAc casting solutions, upon increasing the Nomex concentration in the casting solution from 20 wt.% onto 23 wt.%.

In Chapter 6 it has been shown that the miscibility of the solvent-nonsolvent combination, used for the preparation of the membrane, has a decisive influence on the type of membrane which will be formed. The solvent-water combinations, with triethyl phosphate, DMSO or DMAc as solvent, are very good miscible systems. Therefore, it is very likely that Frommer and Strathmann prepared type II membranes and provided us with three examples of the absence of macrovoids in this type of membranes.

- Sometimes, it is also possible to avoid the formation of macrovoids in type II membranes by addition of a large amount of nonsolvent to the casting solution. This can be concluded from the micrographs in Figure 3, showing the cross sections of CA membranes prepared from homogeneous CA/dioxane/water casting solutions, immersed into a pure water bath.

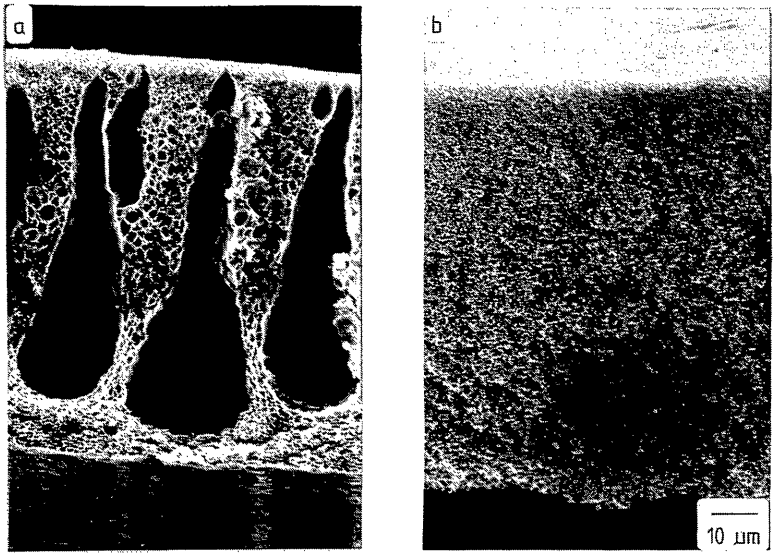

Fig.3. Micrographs of the cross sections of membranes prepared from 200 µm thick, 15 vol.% CA-dioxane solution films, immersed into a pure water bath; the volume ratio water/dioxane in the casting solution has been varied: a. 10/90; b. 25/75; the enlargement factor is equal for both micrographs.

Although more experimental evidence is necessary, we would like to propose the following empirical rules for the occurrence of macrovoids in membranes

prepared from ternary systems:

- In type I membranes no macrovoids are formed, except when the onset of demixing in the cast solution occurs within a very short period after immersion of the solution film.
- In type II membranes macrovoids are always formed, except when the polymer concentration and/or the nonsolvent concentration in the casting solution exceed a certain minimum value.

A.3. Discussion of established theories on the formation of macrovoids

The formation process of macrovoids can be split up in two parts:
- initiation of macrovoids;
- growth of the macrovoids.

Initiation of the macrovoids

Because the onset of the formation of macrovoids often occurs at the interfacial boundary between the immersed solution film and the coagulation bath, many authors propose that interfacial phenomena cause the initiation of the voids:

- Matz [5], Frommer [2] and Stevens [8] propose that surface tension gradients are the driving forces which account for the initiation of convective cells at the interfacial boundary of the film. These authors refer to Sterling [9], who showed that periodic convection cells can be generated by interfacial tension variations during the transfer of a solute across a liquid-liquid interface.
- Ray [7] proposed that excess intermolecular potential gradients, due to the steep local concentration gradient at the film side of the interfacial boundary, are responsible for the initiation of periodic convection cells.
- Strathmann [3] en Graig [10] suggested that mechanical stresses cause rupture of the thin toplayer which is formed immediately after immersion of the solution film. These rupture points should form the initiation points for the macrovoids.
- Broens [11] mentioned thinner parts or locally loose arrangement of noddules in the thin toplayer as the initiation points for the macrovoids.

We believe that it is not right to attribute the initiation of macrovoids

to interfacial phenomena, because it can be observed from cross sections of membranes that macrovoid formation sometimes starts at a large distance from the interface between the coagulation bath and the solution film.

We do agree with Gröbe [12], who proposed that the nucleation of droplets of the polymer lean phase is reponsible for the initiation of macrovoids. In the next section we will show that liquid-liquid demixing by means of nucleation of the polymer lean phase can initiate macrovoid formation under circumstances which correspond to the empirical rules for the formation of macrovoids, described in the previous section.

Growth of the macrovoids

Some different driving forces for the growth of the voids are mentioned in literature:

- Frommer [2] suggests that surface tension gradients act as the driving force for the growth of convective cells.
- Strathmann [3] proposes shrinkage of the matrix in between the growing macrovoids as the driving force for the growth of the macrovoids.
- Smolders [13] suggests that the growth of the voids is caused by solvent, expelled by the polymer solution, because the polymer molecules change to a less expanded conformation during the increase of the nonsolvent concentration in the immersed polymer solution.
- Gröbe [12] and Broens [11] propose that a diffusional flow of solvent from the polymer solution surrounding the initiated macrovoid, is responsible for the growth of the void.

The growing macrovoid can be regarded as a flow of a polymer lean phase relative to a polymer rich phase. From the enumeration given above it can be concluded that some authors suggest that the growing macrovoid represents a convective flow, while other authors suggest that the growth is a result of diffusional flows of the various components.

We will briefly comment on the possibility that the growing macrovoids represent convective flows:

- Convective flows induced by interfacial tension variations [2].

Because macrovoid formation can start at a large distance from the interface between the coagulation bath and the solution film, in our opinion not only

the initiation, but also the propagation of macrovoid formation occurs independently on possible interfacial tension variations.

Even, if interfacial tension variations should induce so called Marangoni convective cells the effects of these cells normal to the interface are nullified by the high viscosity of the solution film according to Sterling [9].

Berg [14] showed that, even in the low viscosity solution benzene chlorobenzene-water-acetic acid, stabilizing density gradients confine Marangoni cells to a narrow zone adjacent to the interface. In membrane forming systems the presence of these stabilizing density gradients depends on the way the solution film is immersed in the nonsolvent bath (i.e., the solution film lying either on top or hanging below the immersed glass plate). However, macrovoids are formed in type II membranes irrespective of the position of the solution film on the glass plate. This fact does not only rule out interfacial tension variations as the driving force for macrovoid formation, but also de-stabilizing density gradients caused by the different specific volumes of the components or by the heat of mixing in the solution film.

- Convective flows induced by shrinkage [3] or collapse phenomena [13].

In our opinion shrinkage or collapse phenomena cannot be ruled out beforehand as possible driving forces for macrovoid formation.

However, it is not evident how the empirical rules for the occurrence of macrovoids in membranes can be explained when shrinkage or collapse phenomena are the driving forces for macrovoid formation.

Matz [5] observed by microscope 'considerable convective motion' within a growing macrovoid. In our laboratory we have observed convective motion of droplets polymer rich phase in a growing macrovoid.

From these types of observations it is sometimes concluded [2,5] that the growing macrovoid itself represents a convective flow. In our opinion this conclusion may not be drawn from these observations.

It is also premature to assume that the observed convective motion within the growing macrovoid is also present under 'normal' circumstances, because this motion may easily be induced by the local strong heating of the examined sample.

In the next section we will demonstrate that the empirical rules for the occurrence of macrovoids in membranes can be explained if the growing macrovoid is considered to be a result of diffusional flows, as proposed by Gröbe [12].

A.4. Macrovoid formation as a result of liquid-liquid demixing and diffusional flows

As has been mentioned in the previous section we assume that the nucleation of droplets of the polymer lean phase in the immersed polymer solution is responsible for the initiation of macrovoids.

According to this assumption macrovoids are formed when some or all nucleated droplets expand to very large dimensions whereas a sponge-structured sublayer is formed when the growth of the droplets is rapidly stopped.

The following question has to be answered: which are the circumstances that determine whether a nucleated droplet of the diluted phase will expand or not?

This question can be answered more easily when we recognize the analogy between

- on the one hand the actual situation: a freshly formed nucleus of the diluted phase, separated from the polymer solution in front of it by an interfacial boundary;
- on the other hand the still undisturbed situation: the coagulation bath separated from the freshly immersed solution film by an interfacial boundary.

The coagulation bath will expand (and the film will shrink) as long as the diffusion process induces a 'composition path' in the film, consisting of only stable compositions (type I diffusion process). The bath will not expand however, when the diffusion process induces instantaneous onset of demixing just beneath the surface of the film (type II diffusion process). We conclude this from the different thicknesses of type I and II membranes (see Figures 1 and 2).

According to the proposed analogy, a nucleated droplet of the diluted phase will expand as long as the ternary diffusion process induces a stable composition in front of the freshly formed nucleus, whereas the droplet will not expand (or the expansion will stop) when a new nucleus of diluted phase is formed in front of the considered nucleated droplet.

In the rest of this section we shall examine the stability of the solution in front of the first formed nuclei for type II membrane formation processes because at that position, respectively in that type of membranes, macrovoid formation mainly occurs. We will examine the influence of the type of solvent

and of the casting solution composition on the solution stability in front of the first formed nuclei.

We assume that from the moment of onset of demixing, the composition changes in front of the freshly formed droplets can be described by our diffusion model applied on two homogenenous phases brought in contact with each other a fraction of time ago.

We will compare the diffusion behavior in the region near the first formed nuclei with the diffusion behavior in the film in the hypothetical situation in which no nucleation of diluted phase would have taken place. In the hypothetical situation the interfacial boundary at $t > 0$ is still situated between the coagulation bath and the solution film. In the real situation the actual interfacial boundary between the two phases under consideration is the droplet-solution interface (see Figure 4).

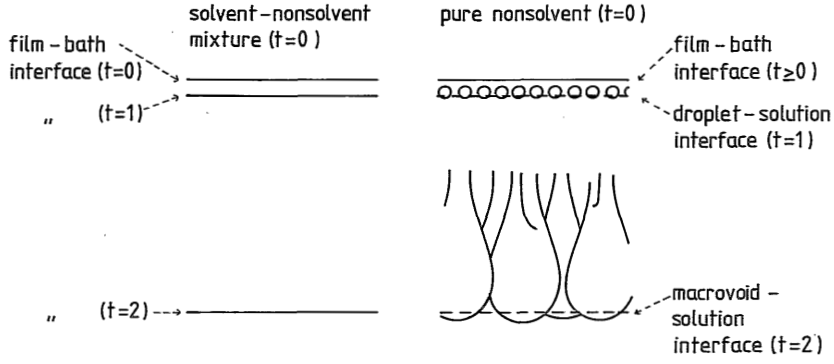

Fig.4. Schematic representation of the analogy between the growth of macrovoids in type II membranes and the movement of the interface between the solution film and the coagulation bath at the presence of a high solvent concentration in the coagulation bath.

We will now compare the interfacial compositions as a function of time at the droplet-solution interface with the interfacial composition in the hypothetical situation.

In the polymer solution in front of the droplets the resistance for diffusional exchange of solvent and nonsolvent is still the same in the hypothetical situation. However, on the bath side of the droplet-solution interface (see Figure 4) the resistance for diffusional exchange of solvent and nonsolvent is considerably higher than in the hypothetical situation where one

finds only the coagulation bath. The extra resistance is caused by the fact that the freshly formed toplayer also contributes to the diffusional resistance above the droplet-solution interface.

The result of this higher diffusional resistance is a lower nonsolvent concentration at the droplet side of the droplet-solution interface. Because the interfacial boundary compositions are binodal compositions, connected by a tie line, the polymer concentration at the solution boundary contacting the droplet will be lower than the polymer concentration at the film boundary in the hypothetical situation.

In Chapter 4 and 6 we have calculated the diffusion behavior in a freshly immersed homogeneous solution for various interfacial boundary compositions. With the aid of the interfacial boundary conditions it has been calculated that the polymer concentration at the solution boundary decreases, if solvent is added to the initial coagulation bath. Thus, the effect of the freshly formed skin layer on the diffusion process in front of the nuclei, is equal to the effect of adding a certain amount of solvent to the initial coagulation bath on the diffusion process in the immersed solution film. This has been represented schematically in Figure 4, and put on a more quantitative basis in Figure 5.

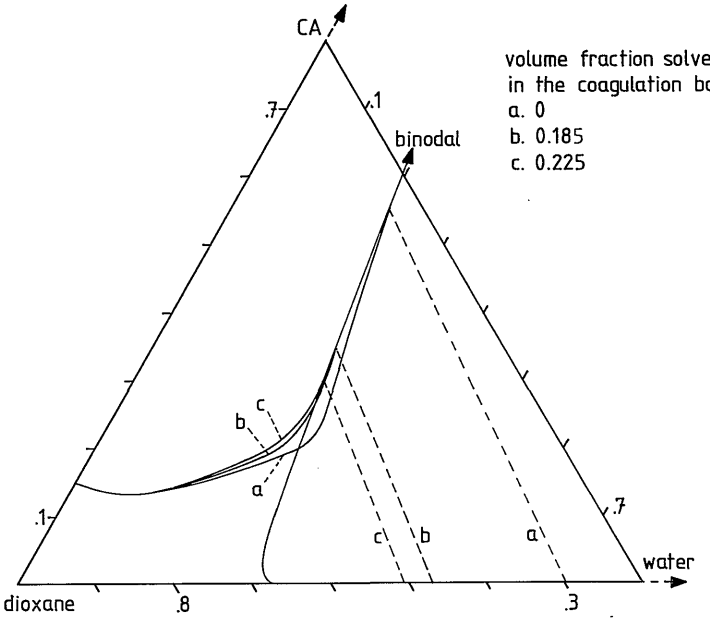

Fig.5. Calculated initial composition paths for 15 vol.% CA-dioxane solutions, immersed into a coagulation bath with a varying initial composition.

In Figure 5 the calculated composition paths are shown for 15 vol.% CA-dioxane solutions immersed into coagulation baths with a varying solvent concentration. It can be concluded that immersion of the solution film into a pure water bath results in instantaneous nucleation of the diluted phase under the surface of the film. According to the previous mentioned analogy, the compositions in front of the first formed nuclei are described by curve b or curve c, or a curve belonging to another initial solvent concentation in the coagulaton bath. If curve b describes the compositions in front of the first formed nuclei it can be concluded that new nuclei will be formed in front of the first formed droplets of diluted phase. However, if curve c describes the compositions in front of the first formed nuclei it can be concluded that the solution in front of the nuclei will remain stable, at least as long as free diffusion occurs. The nuclei will expand because the diffusional flow of nonsolvent from the nuclei into the polymer solution is smaller than the diffusional flow of solvent from the polymer solution into the nuclei. Thus, macrovoids are being formed in this case.

Although we do not know the exact diffusional resistance of the toplayer from the moment of onset of nucleation in the film, it seems reasonable to assume that this resistance increases with an increasing polymer concentration at the film boundary. This means that the chance that macrovoid formation occurs in type II membranes, increases with an increasing polymer concentration at the film boundary.

A.5. Influence of various parameters on the occurrence of macrovoids

At this point we are able to discuss the influence of an increasing nonsolvent or polymer concentration in the casting solution and the type of solvent, on the occurrence of macrovoids in type II membranes.

- Addition of nonsolvent to the casting solution.

From Figs. 1(d) and 2(a) it can be seen that in a 10 vol.% CA/water/acetone solution (water/acetone ratio: 15/85), respectively a 15 vol.% CA-dioxane solution, all the nuclei formed beneath the skin layer expanded to macrovoids by means of growth combined with coalescence. Apparently, the resistance of the freshly formed skin layers was sufficiently high to induce delayed onset of liquid-liquid demixing in front of all first formed nuclei.

From Figure 1(e) it can be seen that addition of an extra amount of water to the CA/acetone/water casting solution, resulted in a nascent skin layer of which the resistance was insufficiently high at certain spots, to induce macrovoid formation. The number of spots where macrovoid formation occurs decreases further with increasing water concentration in the initial casting solution (see Figure 1(f)). The same effect of the addition of nonsolvent to the casting solution can be observed for the membranes prepared from CA/dioxane/water solutions (see Figures 3(a) and 3(b)). Thus, there is a concentration range, within which irregularities in the nascent skin layer cause an irregular formation of macrovoids.

How can we explain that the resistance of the skin layer becomes insufficiently high to induce macrovoid formation, if a certain amount of nonsolvent is added to the casting solution?

In Chapter 4 (Figure 6) it has been calculated that the polymer concentration at the immersed film surface slightly increases, with increasing nonsolvent concentration in the casting solution. Thus, the resistance of the freshly formed skin layer will also increase. Also from Figure 6 in Chapter 4 it can easily be deduced that a higher solvent concentration is necessary in the coagulation bath, to obtain delayed onset of liquid-liquid demixing in an immersed film of which the nonsolvent concentration has been increased. According to the earlier derived connection between the top layer resistance and the solvent concentration in the coagulation bath, this means that the minimum toplayer resistance necessary to induce macrovoid formation, increases with increasing nonsolvent concentration in the casting solution.

According to our theory the elimination of macrovoids shown in the Figures 1(e), 1(f) and 3(b) can be explained by an insufficient increase of the skin layer resistance, upon addition of a certain minimum amount of nonsolvent to the casting solution.

- Variation of the polymer concentration in the casting solution and the type of solvent used.

Now we want to know in which way the process of macrovoid formation is affected by an increasing polymer concentration in the casting solution, according to our theory. Let us consider CA-dioxane casting solutions immersed into a pure water bath. From Figure 3(a) it can be seen that in the immersed 15 vol.% CA solution macrovoid formation occurs.

In Chapter 6 (Figure 3) it has been calculated that, with increasing CA

concentration in the casting solution, the polymer concentration at the immersed film surface strongly increases, promoting the formation of macrovoids according to our theory.

From Table 3 (Chapter 6) however, it can be seen that a higher solvent concentration is necessary in the coagulation bath, to obtain delayed onset of demixing in a film with an increasing polymer concentration. According to our theory, this means that the minimum toplayer resistance necessary to induce macrovoid formation, increases with increasing polymer concentration in the casting solution.

It is impossible to predict whether macrovoid formation will stop at a certain polymer concentration in the CA-dioxane casting solution:

The increase of the polymer concentration at the immersed surface will slow down when the surface composition approaches the equilibrium composition for water swollen CA; however, from the experimental values from Table 3 (Chapter 6) it cannot be derived whether the solvent concentration in the coagulation bath, necessary to obtain delayed onset of demixing, increases sufficiently to prohibit macrovoid formation at a certain CA concentration in the casting solution.

If dioxane is exchanged by a solvent, which mixes better with water, the surface composition of the immersed film approaches the composition of water swollen CA already at a relative low polymer concentration in the casting solution. This means that the resistance of the freshly formed skin layer can hardly increase any further upon raising the polymer concentration in the casting solution. Thus the absence of macrovoids in immersed CA-DMSO or CA-triethyl phosphate casting solutions, upon increasing the polymer concentration in the casting solution (observed by Frommer [2]) can be explained in our theory by the fact that the minimum amount of solvent in the coagulation bath, necessary to obtain delayed onset of demixing, increases with increasing polymer concentration in the casting solution.

Evidently, more experiments have to be performed to test our theory:

- It has to be examined at which polymer concentration in the casting solution macrovoid formation stops to occur in type II membranes. This must be examined for good and bad miscibility of solvent-nonsolvent combinations.
- For the same solvent-nonsolvent combinations, light transmission measurements have to be performed in order to obtain experimental values for the

minimum amount of solvent in the coagulation bath, necessary to obtain delayed onset of demixing in casting solutions with a varying polymer concentration.

- The initial rate of growth of marovoids must be compared with the rate of movement of the interface between the immersed polymer solution and the coagulation bath, for a solvent concentration in the coagulation bath which is high enough to prevent instantaneous onset of liquid-liquid demixing.

A.6. Conclusions

The occurrence of macrovoids in membranes prepared from ternary systems can be predicted with the following empirical rules:

- In type I membranes no macrovoids will be formed, except if the onset of demixing in the cast solution occurs within a very short period after immersion of the solution film.
- In type II membranes macrovoids will always be formed, except if the polymer concentration and/or the nonsolvent concentration in the casting solution exceeds a certain minimum value.

According to the theory proposed in this appendix:

- macrovoids are formed from freshly formed nuclei of the diluted phase if the composition in front of the nuclei remains stable for a relatively long period;
- macrovoids expand as a result of diffusional flows;
- macrovoids are formed just beneath the skin layer of a type II membrane, if the diffusional resistance of the freshly formed skin layer exceeds a certain minimum value. This conclusion is completely contrary to the widely proposed hypothese according to which macrovoids are formed at certain weak spots in the nascent skin layer;
- macrovoid formation in type II membranes is not opposed by an increase of the viscosity of the cast solution (as is generally assumed), but by an increase of the minimum solvent concentration in the coagulation bath, necessary to obtain delayed onset of liquid-liquid demixing in the immersed casting solution.

A.7. References

1. M.A. Frommer and D. Lancet, The mechanism of membrane formation: Membrane structures and their relation to preparation conditions, Reverse Osmosis Membrane Research, H.K. Lonsdale and H.E. Podall, Eds., Plenum Press, New York (1972) 85.
2. M.A. Frommer and R.M. Messalem, Mechanism of membrane formation. VI. Convective flows and large void formation during membrane precipitation, Ind. Eng. Chem. Prod. Res. Dev., 12 (1973) 328.
3. H. Strathmann, K. Kock, P. Amar and R.W. Baker, The formation mechanism of asymmetric membranes, Desalination, 16 (1975) 179.
4. V. Gröbe and G. Mann, Strukturbildung beim spinnen von Polyacrylnitrillösungen in wässerige fällbäder, Faserforsch. Textiltechn., 19 (1968) 49.
5. R. Matz, The structure of cellulose acetate membranes. I. The development of porous structures in anisotropic membranes, Desalination, 10 (1972) 1.
6. I. Cabasso, E. Klein and J.K. Smith, Polysulfone hollow fibers. II. Morphology, J. Appl. Polym. Sci., 21 (1977) 165.
7. R.J. Ray, W.B. Krantz and R.L. Sani, Linear stability theory model for finger formation in asymmetric membranes, J. Membrane Sci., 23 (1985) 155.
8. W.E. Stevens, C.S. Dunn and C.A. Petty, Surface tension induced cavitation in polymeric membranes during gelation, Paper presented at 73rd AIChE Annual Meeting, Chicago, Illinois (1980).
9. V. Sterling and L.E. Scriven, Interfacial turbulence: Hydrodynamic instability and the Marangoni effect, AIChE Jornal, 5 (1959) 514.
10. J.P. Craig, J.P. Knudsen and V.F. Holland, Textile Res. J., 32 (1962) 435.
11. L. Broens, F.W. Altena and C.A. Smolders, Asymmetric membrane stuctures as a result of phase separation phenomena. Desalination, 32 (1980) 33.
12. V. Gröbe, G. Mann and G. Duwe, Ausbildung von Strukturen bei der Koagulation von Polyacrylnitrillösungen, Fasenforsch. Textiltechn., 17 (1966) 142.
13. C.A. Smolders, in: Ultrafiltration Membranes and Applications, Ed., A.R. Cooper, Plenum Press, New York (1980) 161.
14. J.C. Berg and C.R. Morig, Density effects in interfacial convection,

Chem. Eng. Sci., 24 (1969) 937.

SUMMARY

In this thesis the mechanism of membrane formation by means of immersion precipitation is studied.

Immersion of a concentrated polymer solution film into a nonsolvent bath induces an exchange of solvent and nonsolvent in the film by means of diffusion. This process results in an asymmetric polymer distribution and leads to metastable compositions in the immersed polymer solution film. Demixing processes occur, yielding polymer rich and polymer lean entities in the film. When the exchange of solvent and nonsolvent is completed, a solidified film with a dense toplayer and a porous sublayer is obtained. The thin toplayer determines the permselectivity and the permeability of the membrane. The porous sublayer is responsible for the mechanical strength of the membrane.

The objective of this study is to gain insight into diffusional mass transport and demixing phenomena occurring during the immersion precipitation process.

In Chapter 2 the demixing behavior in cellulose acetate (CA)/solvent/water systems is studied for CA concentrations up to 40 wt.% in several solvents. Two different types of demixing processes are found to occur upon cooling: liquid-liquid demixing and aggregate formation. The rapid process of liquid-liquid demixing is clearly distinguished from the slow process of aggregate formation by examining the dependence of the cloud point position on the cooling rate and by structure analysis of quenched solutions. The appearance of aggregate formation strongly depends on the type of solvent. In the appendix of Chapter 2 it is shown that the two types of demixing processes also occur in ternary poly(2,6-dimethyl-1,4-phenyleneoxide) solutions.

In Chapter 3 equations and boundary conditions are derived for the isothermal diffusion processes that occur in the coagulation bath and in the polymer solution after immersion of a cast (ternary) polymer solution into a (binary) coagulation bath. This mass transfer is expressed in terms of thermodynamic driving forces and frictional coefficients. The frictional coefficients in the ternary system are assumed to be interrelated through the Onsager reciprocal relations and to be related to the measurable frictional coefficients defined in the three limiting binary composition ranges.

The diffusion model derived in Chapter 3 can be used to calculate concentration profiles and the moment of onset of liquid-liquid demixing in the

immersed polymer solution film. The model can be applied to a ternary membrane forming system, characterized with respect to its binary thermodynamic non-ideality parameters and its diffusion (or sedimentation) behavior in the three binary composition ranges.

In Chapter 4 the diffusion model is applied to the ternary system CA/acetone/water. Calculations show that immersion of the polymer solution into the coagulation bath results in an instantaneous increase of the polymer concentration at the surface of the solution. The thickness of this concentrated layer increases until liquid-liquid demixing starts by means of nucleation and growth of the polymer lean phase, that fixes the asymmetric polymer distribution in the film. The time lag in between the moment of immersion and the moment of onset of the demixing process is proportional to the square of the initial film thickness. Addition of a certain minimum amount of water to the casting solution results in a drastic change of the membrane formation process: liquid-liquid demixing starts instantaneously upon immersion, yielding a membrane with a very thin toplayer. The model calculations are confirmed by light transmission measurements performed on immersed casting solutions.

Chapter 5 deals with the liquid-liquid demixing behavior of quasi ternary CA/solvent/water systems. CA polydispersity causes experimentally obtained compositons of coexisting phases to deviate from the cloud point curve, at low polymer concentrations. Calculated compositons of coexisting phases and binodal curves are compared with experimentally obtained compositions of coexisting phases and cloud points, in order to verify the expression for the Gibbs free energy of a ternary system given in Chapter 3. Although in the calculations CA is assumed to be monodisperse, the calculated and experimentally found compositions of coexisting phases do agree fairly well.

In Chapter 6 the diffusion model is applied to ternary systems with different values of the thermodynamic non-ideality parameters, using experimental frictional coefficients of the system CA/dioxane/water. It is shown that the moment of onset of liquid-liquid demixing in the immersed polymer solution film is primarily affected by the miscibility of the solvent with the nonsolvent: a decreasing tendency of mixing promotes a delayed onset of liquid-liquid demixing. This conclusion is confirmed by light transmission measurements performed on several CA-solvent casting solutions immersed into a coagulation bath with a varying solvent/water ratio. With SEM analysis of membrane cross sections, the dominant influence of the delay time for the onset

of liquid-liquid demixing on the ultimate membrane morphology is clearly demonstrated.

In Chapter 7 the relation between the casting solution composition, the coagulation bath composition and the components used on the one hand, and the morphology of the ultimate membrane on the other hand, is discussed using calculated and experimental data from this thesis and from literature. The main result of the work presented in this thesis is the elucidation of two distinctly different mechanisms of membrane formation by means of immersion precipitation. These different mechanisms are characterized by the moment of onset of liquid-liquid demixing in the immersed film.

Delayed onset of liquid-liquid demixing results in membranes with a relatively thick toplayer and a relatively dense sublayer. These membranes are mostly characterized by a hyperfiltration, gas separation or pervaporation type of performance. The occurrence of aggregate formation during immersion precipitation may improve the interconnectivity of the pores in the sublayer considerably. The influence of aggregate formation on the toplayer morphology is not yet fully understood.

Instantaneous onset of liquid-liquid demixing results in membranes with a very thin toplayer and, on preparation of the membrane from a moderately concentrated casting solution, with an ultrafilration type of performance and a very porous sublayer.

In the Appendix of this thesis it is shown that the occurrence of macrovoids in membranes is also related to the moment of onset of liquid-liquid demixing in the immersed casting solution film: macrovoids may be formed, only if liquid-liquid demixing starts within a very short period after immersion of the solution film. A theory is proposed which explains why an increasing polymer or nonsolvent concentration in the casting solution opposes macrovoid formation, in the case of instantaneous onset of demixing. According to this theory, macrovoids are formed just beneath the toplayer of a membrane, if the diffusional resistance of the freshly formed toplayer exceeds a certain minimum value (at certain spots). This conclusion is in essential contradiction with current theories according to which macrovoids are formed at certain weak spots in the nascent toplayer.

SAMENVATTING

Wanneer een film geconcentreerde polymeeroplossing in contact wordt gebracht met een niet-oplosmiddelbad, vindt er een uitwisseling plaats van de twee laagmoleculaire componenten d.m.v. diffusie. Dit leidt tot een asymmetrische polymeerverdeling in de film. Bovendien induceert het diffusieproces metastabiele samenstellingen in de film die zeer snel leiden tot ontmenging van de film in polymeerarme druppeltjes, gedispergeerd in een polymeerrijke matrix. Na voltooiing van het diffusieproces resteert een vaste, poreuze film met een dichte toplaag aan het grensvlak met het coagulatiebad.

In dit poefschrift wordt het hierboven beschreven fase-inversieproces nader bestudeerd met als doelstelling deze techniek te optimaliseren voor de vervaardiging van asymmetrische membranen. De dunne toplaag dient de permselectiviteit en de permeabiliteit van het membraan te bepalen; de poreuze onderlaag moet zorgen voor de mechanische sterkte van het membraan.

In Hoofdstuk 2 wordt het ontmenggedrag in cellulose acetaat (CA)/oplosmiddel/water systemen bestudeerd. Twee verschillende typen ontmengprocessen blijken op te kunnen treden wanneer de ternaire oplossingen worden afgekoeld: vloeistof-vloeistof ontmenging en aggregaatvorming. Het zeer snelle proces van vloeistof-vloeistof ontmenging kan onderscheiden worden van de minder snelle vorming van aggregaten d.mv. troebelpuntsmetingen bij verschillende afkoelsnelheden of d.m.v. structuuranalyse van afgeschrokken oplossingen. De vorming van aggregaten blijkt sterk afhankelijk te zijn van de keuze van het oplosmiddel. In de Appendix van Hoofdstuk 2 wordt aangetoond dat de twee typen ontmengprocessen ook plaats kunnen vinden in ternaire polyphenyleenoxide (PPO) oplossingen.

In Hoofdstuk 3 worden vergelijkingen en randvoorwaarden afgeleid waarmee het isotherme diffusieproces kan worden beschreven dat plaats vindt in een polymeeroplossing die in contact is gebracht met een coagulatiebad. Het ternaire diffusieproces wordt beschreven in termen van thermodynamische drijvende krachten en wrijvingscoëfficiënten. Er wordt verondersteld dat de wrijvingscoëfficiënten samenhangen volgens de Onsager reciproke relaties, en op eenvoudige wijze gerelateerd kunnen worden aan de meetbare wrijvingscoëfficiënten, gedefinieerd in de drie binaire compositiegebieden.

Het diffusiemodel, afgeleid in Hoofdstuk 3, kan gebruikt worden om concentratieprofielen te berekenen en om het begin van vloeistof-vloeistof ontmeng-

ing in de ondergedompelde film te voorspellen. Het model kan toegepast worden op membraanvormende ternaire systemen, waarvan de thermodynamische interactieparameters en de diffusie- (of sedimentatie-)coëfficiënten in de drie binaire compositiegebieden bekend zijn.

In Hoofdstuk 4 wordt het diffusiemodel toegepast op het systeem CA/aceton/-water. Uit berekeningen blijkt dat de polymeerconcentratie aan het grensvlak van de film en het bad onmiddellijk zeer sterk toeneemt, na onderdompeling van de polymeeroplossing in het coagulatiebad. Het dunne laagje geconcentreerde oplossing verbreedt zich, totdat vloeistof-vloeistof ontmenging d.m.v. kiemvorming en groei inzet. Dit proces fixeert de op dat moment aanwezige asymmetrische polymeerverdeling in de film.

De tijdsduur tussen het moment van onderdompelen van een CA-aceton film en het begin van vloeistof-vloeistof ontmenging, is evenredig met het kwadraat van de initiële filmdikte. Wanneer meer dan een bepaalde minimum hoeveelheid water aan de polymeeroplossing wordt toegevoegd, verandert het membraanvormingsproces ingrijpend: onmiddellijk na onderdompeling van de film treedt vloeistof-vloeistof ontmenging op, hetgeen resulteert in een zeer dunne toplaag. De uitkomsten van de modelberekeningen worden bevestigd door lichttransmissie metingen aan ondergedompelde CA/aceton/(water) films.

In Hoofdstuk 5 worden metingen en berekeningen van evenwichtssamenstellingen van ontmengde, quasi-ternaire CA/oplosmiddel/water systemen gepresenteerd. De gemeten evenwichtssamenstellingen komen redelijk overeen met evenwichtssamenstellingen, berekend m.b.v. de uitdrukking voor de Gibbs vrije energie van een ternair systeem, gepresenteerd in Hoofdstuk 3. Dit kan als een aanwijzing worden beschouwd voor de betrouwbaarheid van deze uitdrukking.

In Hoofdstuk 6 wordt m.b.v. het diffusiemodel de invloed van de binaire thermodynamische interactieparameters op het membraanvormingsproces berekend. Volgens de berekeningen heeft vooral de thermodynamische interactie tussen oplosmiddel en niet-oplosmiddel een sterke invloed op het membraanvormingsproces: een toenemende mengbaarheid van deze twee componenten leidt tot een overgang van uitgestelde naar instantane ontmenging in de ondergedompelde film. Deze conclusie wordt bevestigd door lichttransmissie metingen aan ondergedompelde CA-oplosmiddel systemen. M.b.v. SEM analyses van filmdoorsnede's, wordt gedemonstreerd dat er een duidelijk verband bestaat tussen de uitsteltijd voor vloeistof-vloeistof ontmenging en de structuur van de geprecipiteerde film.

De opheldering van twee duidelijk verschillende mechanismen van membraanvorming (gekarakteriseerd door de uitsteltijd voor ontmenging) en de wijze waarop het type mechanisme dat optreedt gestuurd kan worden, vormen de essentie van dit proefschrift. In Hoofdstuk 7 wordt nader ingegaan op het verband dat bestaat tussen het type membraanvormingsmechanisme en de resulterende structuur van het membraan.

Uitgestelde vloeistof-vloeistof ontmenging leidt tot een relatief dikke toplaag op het asymmetrische membraan. Deze toplaag bezit meestal permselectieve eigenschappen die het membraan geschikt maken voor hyperfiltratie, gasscheiding of pervaporatie. Het optreden van aggregaatvorming tijdens het precipitatieproces kan de niet gewenste 'gesloten porie structuur', die in de onderlaag van dit type membranen vaak voorkomt, verhinderen.

Het optreden van instantane vloeistof-vloeistof ontmenging resulteert in membranen met een zeer dunne toplaag met ultrafiltratie eigenschappen, en een zeer poreuze onderlaag. Een uitzondering moet gemaakt worden voor membranen die bereid worden uit zeer hoog geconcentreerde polymeeroplossingen en gasscheidingseigenschappen bezitten.

In de Appendix van dit proefschrift wordt aangetoond dat ook het optreden van macrovoidvorming tijdens membraanvorming samenhangt met de uitsteltijd voor vloeistof-vloeistof ontmenging: macrovoids worden alleen gevormd wanneer vloeistof-vloeistof ontmenging zeer snel na onderdompeling van de polymeeroplossing inzet. Er wordt een theorie voorgesteld, die verklaart waarom een verhoging van de polymeer- en/of niet-oplosmiddelconcentratie in de polymeeroplossing macrovoidvorming tegenwerkt, in geval van instantane ontmenging. Volgens deze theorie worden er vlak onder de toplaag alleen dan macrovoids gevormd, wanneer de weerstand voor diffusie, uitgeoefend door de toplaag in vorming, een bepaalde minimale waarde overschrijdt. Deze conclusie is volledig in tegenspraak met heersende opvattingen m.b.t. macrovoidvorming.

LEVENSLOOP

Bart Reuvers werd op 29 juni 1956 geboren te Amersfoort. In 1974 werd het gymnasium-B diploma behaald aan het Eemland College te Amersfoort. In datzelfde jaar begon hij zijn studie Technische Natuurkunde aan de Technische Hogeschool Twente.

De baccalaureaatsstudie werd in 1979 afgerond met als hoofdrichting Chemische Fysica. In 1982 werd het doctoraalexamen Technische Natuurkunde afgelegd met als hoofdrichting Reologie bij de vakgroep Overdrachtsverschijnselen.

In october 1982 trad hij in dienst als wetenschappelijk assistent bij de werkgroep Membraanfiltratie van de afdeling Chemische Technologie aan de T.H.Twente. In de periode tot 1 october 1986 is het onderzoek verricht dat in dit proefschrift beschreven is.